

การตั้งเคราะห์ที่ควบคุมได้ของอนุภาคสังกะสีออกไซด์ในระดับนาโนเมตรด้วยปฏิกิริยาในวัฏภาคก๊าซ



นาย พัฒน์ นารถพจนานนท์

สถาบันวิทยบริการ

จุฬาลงกรณ์มหาวิทยาลัย

วิทยานิพนธ์นี้เป็นส่วนหนึ่งของการศึกษาตามหลักสูตรปริญญาวิศวกรรมศาสตรมหาบัณฑิต

สาขาวิชาวิศวกรรมเคมี ภาควิชาวิศวกรรมเคมี

คณะวิศวกรรมศาสตร์ จุฬาลงกรณ์มหาวิทยาลัย

ปีการศึกษา 2550

ลิขสิทธิ์ของจุฬาลงกรณ์มหาวิทยาลัย

CONTROLLED SYNTHESISSES OF ZnO NANOPARTICLES USING GAS PHASE REACTION




Mr. Pat Nartpochananon

สถาบันวิทยบริการ
จุฬาลงกรณ์มหาวิทยาลัย


A Thesis Submitted in Partial Fulfillment of the Requirements
for the Degree of Master of Engineering Program in Chemical Engineering
Department of Chemical Engineering
Faculty of Engineering
Chulalongkorn University
Academic Year 2007
Copyright of Chulalongkorn University

Thesis Title CONTROLLED SYNTHESSES OF ZnO
NANOPARTICLES USING GAS PHASE REACTION
By Mr. Pat Nartpochananon
Field of study Chemical Engineering
Thesis Advisor Associate Professor Tawatchai Charinpanitkul, D.Eng.
Thesis Co-advisor Assistant Professor Varong Pavarajarn, Ph.D.

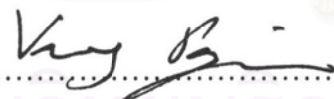
Accepted by the Faculty of Engineering, Chulalongkorn University in Partial
Fulfillment of the Requirements for the Master's Degree



..... Dean of the Faculty of Engineering
(Associate Professor Boonsom Lerdhirunwong, Dr.Eng)

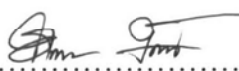
THESIS COMMITTEE


..... Chairman
(Associate Professor Prasert Pavasant, Ph.D.)


..... Thesis Advisor
(Associate Professor Tawatchai Charinpanitkul, D.Eng.)


..... Thesis Co-advisor
(Assistant Professor Varong Pavarajarn, Ph.D.)


..... Member
(Sirapat Pratontep, Ph.D.)


..... Member
(Acharawan Rattana, Ph.D.)

พัฒน์ นารตพจนานนท์ : การสังเคราะห์ที่ควบคุมได้ของอนุภาคสังกะสีออกไซด์ในระดับนาโนเมตรด้วยปฏิกิริยาในวัฏภาคก๊าซ (CONTROLLED SYNTHESIS OF ZnO NANOPARTICLES USING GAS PHASE REACTION), อ. ที่ปรึกษา: รศ.ดร. ธวัชชัย ชรินพณิชกุล, อ.ที่ปรึกษาร่วม: ผศ.ดร.วรงค์ ปวราจารย์, 93 หน้า

ปัจจุบันการสังเคราะห์อนุภาคระดับนาโนเมตรได้รับความนิยมน้อยกว่าหลายเนื่องจากคุณสมบัติที่เชื่อมโยงทั้งทางด้านการเป็นตัวเร่งปฏิกิริยา, อุปกรณ์ทางแสง, การใช้งานทางอิเล็กทรอนิกส์ และอื่นๆอีกมากมาย สังกะสีออกไซด์ระดับนาโนเมตรมีคุณสมบัติที่ดีเนื่องจาก เป็นสารกึ่งตัวนำ และมีค่าแบนด์แก๊ปกว้าง ประมาณ 3.37 อิเล็กตรอนโวล การสังเคราะห์อนุภาคสังกะสีออกไซด์ระดับนาโนเมตรนั้นสามารถทำได้หลายวิธี ซึ่งการใช้เทคนิคของการเกิดปฏิกิริยาออกซิเดชันของไอสังกะสี ในสถานะก๊าซก็เป็นอีกวิธีหนึ่ง ซึ่งมีความได้เปรียบวิธีอื่นคือ สามารถทำการผลิตได้อย่างต่อเนื่อง ผลิตภัณฑ์ที่ได้มีความบริสุทธิ์สูง นอกจากนี้วิธีนี้ยังได้มีการประยุกต์ใช้ในระดับอุตสาหกรรม

ในงานวิจัยนี้อิทธิพลของตัวแปรที่ใช้ในการสังเคราะห์ถูกทำการทดลองเพื่อหาสภาวะที่เหมาะสมในการสังเคราะห์อนุภาคสังกะสีออกไซด์ระดับนาโนเมตรที่มีขนาดและรูปร่างที่สม่ำเสมอ โดยตัวแปรที่ทำการศึกษา ได้แก่ อุณหภูมิที่ใช้ในการระเหยสังกะสี อุณหภูมิที่ใช้ในการเกิดปฏิกิริยาออกซิเดชัน อัตราการไหลก๊าซที่ทำหน้าที่นำพา (ก๊าซไนโตรเจน) และ ก๊าซที่ทำปฏิกิริยา (ก๊าซออกซิเจน) ซึ่งจากผลการทดลองพบว่า อนุภาคระดับสังกะสีออกไซด์ระดับนาโนเมตรนั้นมีรูปร่างที่น่าสนใจ คือ รูปร่างที่เป็นทรงกลมและรูปร่างที่เป็นก้านสี่เหลี่ยม โดยรูปร่างของอนุภาคสังกะสีออกไซด์เปลี่ยนจาก อนุภาคทรงกลมเป็นก้านสี่เหลี่ยม เมื่ออุณหภูมิที่ใช้ในการระเหยและอุณหภูมิที่ใช้ในการทำปฏิกิริยาออกซิเดชันเพิ่มสูงขึ้น

นอกจากนี้คณะผู้วิจัยได้ศึกษาผลของการผสมระหว่างไอสังกะสีกับก๊าซภายในเตาปฏิกรณ์ โดยการศึกษาด้วยแบบจำลองพลศาสตร์ของไหลโดยใช้คอมพิวเตอร์ แบบจำลองฟลูเอินซ์ถูกใช้เพื่อคำนวณหาความเข้มข้นของไอสังกะสีและออกซิเจนภายในเตาปฏิกรณ์ จากการเปรียบเทียบผลการทดลองพบว่า การใช้อุปกรณ์ผสมทำให้การผสมกันระหว่างไอสังกะสีและออกซิเจนเกิดได้ดีขึ้นและทำให้อนุภาคสังกะสีออกไซด์นาโนเมตรที่มีขนาดและรูปร่างที่สม่ำเสมอ

ภาควิชา.....วิศวกรรมเคมี.....ลายมือชื่อนิสิต.....พัฒน์ นารตพจนานนท์.....
สาขาวิชา.....วิศวกรรมเคมี.....ลายมือชื่ออาจารย์ที่ปรึกษา.....
ปีการศึกษา.....2550.....ลายมือชื่ออาจารย์ที่ปรึกษาร่วม.....

4870401321 : MAJOR CHEMICAL ENGINEERING

KEY WORD: ZnO NANOPARTICLES / GAS PHASE REACTION / MIXING / GROWTH MECHANISM

PAT NARTPOCHANANON: CONTROLLED SYNTHESIS OF ZnO NANOPARTICLES USING GAS PHASE REACTION, THESIS ADVISOR: ASSOC. PROF. TAWATCHAI CHARINPANITKUL, D.Eng., THESIS CO-ADVISOR: ASST. PROF. VARONG PAVARAJARN, Ph.D., 93 pp.

Today, research and development on synthesis of nanoparticles becomes of interest global because of their excellent properties in catalytic, optical and magnetic functionality. Zinc Oxide (ZnO) is one of the most promising materials due to its attractive optical function based on a wide band gap of 3.37 eV. ZnO could be synthesized by various methods. Gas phase reaction route is one of potential means being utilized, providing higher purity with low operating cost and applicable at the industrial scale.

In this research, the effects of synthesizing parameters on the size and the shape of ZnO nanoparticles were experimentally investigated. These parameters include evaporation temperature, oxidation temperature and gas flow rate. From the experimental results, it could be clearly observed that size and morphology of the ZnO nanoparticles are strongly dependent upon mixing ratio of zinc vapor and oxygen gas. ZnO nanoparticles were changed from a spherical shape to a tetrapod shape when the evaporation and oxidation temperatures were increased.

In addition, the interaction between zinc vapor and oxygen was numerically verified by computational fluid dynamic (CFD) technique. FLUENT[®] was employed for calculating the concentration of zinc vapor and oxygen inside the reactor. In comparison with the experimental results, the use of a gas mixing apparatus (orifice) enhanced the interaction between zinc vapor and oxygen, resulting in uniform size and shape of ZnO nanoparticles.

Department.....Chemical Engineering.....Student's signature. *Pat Nartpochananon*
 Field of study.....Chemical Engineering.....Advisor's signature. *V. Charinpanitkul*
 Academic year.....2007.....Co-advisor's signature. *Varong Pavrajarn*

ACKNOWLEDGEMENTS

I am very thankful to my thesis advisor and co-advisor, Assoc Prof. Tawatchai Charinpanitkul and Asst Prof. Varong Pavarajarn, Department of Chemical Engineering, Chulalongkorn University, for their introducing me to this interesting project, and for their helpful and stimulated suggestions, deep discussion and encouraging guidance throughout the course of this work. I am also very thankful to my shared advisor, Professor Yoshio Otani, Department of Chemical Engineering, Kanazawa University, for his useful guidance, hospitality, educational suggestion and his particle processing laboratory facilities. Furthermore, I am also thankful to Assoc. Prof. Prasert Pavasarn, Dr. Sirapat Pratontep and Dr. Achrawan Rattana for their stimulative comments and participation as my thesis committee.

Furthermore, I would like to acknowledge the National Nanotechnology Center (NANOTEC), National Science and Technology Development Agency for the partial financial support to this work. The present work is part of “Development of nanoparticles application with hydrogel for coating glass surface to improve its superhydrophilicity” headed by Assoc Prof. Tawatchai Charinpanitkul. Also the scholarship from Japan Student Services Organization (JASSO) for giving me a one-year fellowship at Kanazawa University is gratefully acknowledged. The thesis has also obtained a partial support from Centennial Fund of Chulalongkorn University.

Moreover, I would like to thank Mr. Takayuki Fujimoto and their particle processing lab for their kind and helpful suggestion.

I am also thankful to all members of Center of Excellence in Particle Technology for their help, suggestion and warm collaborations.

Finally, I would like to express my cordial and deep thanks to my parents for their love and encouragement.

CONTENTS

	Page
ABSTRACT IN THAI	iv
ABSTRACT IN ENGLISH	v
ACKNOWLEDGEMENTS	vi
CONTENTS	vii
LIST OF TABLES	xi
LIST OF FIGURES	xii
NOMENCLATURE	xviii
 CHAPTER	
I INTRODUCTION	1
1.1 Background.....	1
1.2 Objectives of research.....	2
1.3 Scope of research	2
1.4 Benefits to be obtained.....	3
II FUNDAMENTAL KNOWLEDGE AND LITERATURE REVIEW	4
2.1 Zinc Oxide (ZnO)	4
2.2 Wurtzite structure.....	4
2.3 Physical properties of ZnO nanostructures	5
2.4 Generation of particles by reaction	6
2.4.1 Gas-Phase techniques.....	6
2.4.2 French process	7

CHAPTER	Page
2.5 Synthesis of ZnO Nanostructures	9
2.5.1 Vapor transport synthesis.....	9
2.5.2 Other synthesis methods	10
2.6 Condensation and evaporation.....	11
2.6.1 Partial pressure.....	11
2.6.2 Homogeneous nucleation.....	12
2.6.3 Heterogeneous nucleation.....	13
2.6.4 Evaporation.....	13
2.7 Kinetics process of tetra-needle-like ZnO	14
2.8 Review of growth models of tetrapod ZnO	16
2.9 Thermophoresis force	20
2.10 Literature reviews	22
III EXPERIMENTAL	27
3.1 ZnO raw material	27
3.2 Synthesis of ZnO nanoparticles by gas phase reaction.....	27
3.3 Mixing device	29
3.4 Collecting method for synthesized ZnO nanoparticles.....	30
3.5 Experimental procedures	31
3.5.1 Effect of evaporation temperature (T_{evp})	31
3.5.2 Effect of oxidation temperature (T_{oxi}).....	31
3.5.3 Effect of air and nitrogen flow rate.....	32
3.5.4 Effect of mixing device (orifice).....	32

CHAPTER	Page
3.6 Analytical instruments	32
3.6.1 Scanning Electron Microscopy (SEM)	32
3.6.2 X-Ray Diffraction (XRD)	33
3.6.3 Scanning Mobility Particles Sizer (SMPS)	34
IV RESULTS AND DISCUSSION	35
4.1 Effect of evaporation temperature (T_{evp})	35
4.1.1 Temperature profile inside reactor	36
4.1.2 Particle size distribution of synthesized ZnO by SMPS	37
4.1.3 Morphology of ZnO nanoparticles	38
4.1.4 Effect of amount of zinc powder	41
4.1.5 Effect of air flow rate	43
4.1.6 Effect of nitrogen flow rate	44
4.2 Effect of oxidation temperature (T_{oxi}) and mixing device (orifice)	45
4.2.1 Effect of oxidation temperature (T_{oxi}) without mixing device ..	45
4.2.2 Effect of oxidation temperature (T_{oxi}) with mixing device	48
4.3 Effect of gas flow rate to the morphologies of	50
ZnO nanoparticles with mixing device and 2 nd furnace	
4.3.1 Effect of air flow rate	50
4.3.2 Effect of nitrogen flow rate	51
4.4 Study growth mechanism of ZnO nanoparticles by	53
by gas phase reaction	
4.4.1 Collecting ZnO nanoparticles by silicon wafer	53
4.4.2 Effect of orifice on morphologies of ZnO nanoparticles	56

CHAPTER	Page
4.4.3 Growth mechanism of ZnO nanoparticles in gas phase reaction	68
V CONCLUSION AND RECOMMENDATION	72
5.1 Conclusions.....	72
5.1.1 Effect of evaporation temperature (T_{evp})	72
5.1.2 Effect of oxidation temperature (T_{oxi})	72
5.1.3 Effect of gas flow rate.....	73
5.1.4 Effect of gas mixing apparatus (orifice)	73
5.2 Recommendation for future work.....	74
REFERENCES	75
APPENDICES	79
APPENDIX A Calculation of partial pressure.....	80
APPENDIX B Experimental Results.....	82
APPENDIX C International conference	89
VITA	93

สถาบันวิทยบริการ
จุฬาลงกรณ์มหาวิทยาลัย

LIST OF TABLES

	Page
Table 2.1 Physical properties of ZnO nanostructures	5
Table 2.2 Stucture of tetrapod ZnO nanostructures obtained.....	26
from different reaction parameter	



สถาบันวิทยบริการ
จุฬาลงกรณ์มหาวิทยาลัย

LIST OF FIGURES

		Page
Figure 2.1	Zinc oxide	4
Figure 2.2	ZnO wurtzite structures.....	5
Figure 2.3	Mechanisms of particles formation and growth from vapor phase.....	7
Figure 2.4	Schematic diagram of French process	8
Figure 2.5	Schematic diagram of Vapor-Liquid-Solid process.....	10
Figure 2.6	(a) a pyramid formed by three {1122} and one (0001) facets, (b) The octa-twin model composed of eight pyramidal inversion-twin crystals	19
Figure 2.7	Molecular impacts on a particle ($d < \lambda$) in a temperature gradient	21
Figure 3.1	SEM images of zinc particles (Raw material) particle diameter <10 micron	27
Figure 3.2	Experimental set up for synthesized ZnO nanoparticles..... by gas phase reaction process	28
Figure 3.3	Two electrical furnaces and quartz tube reactor	29
Figure 3.4	Mixing orifice with one hole at the center	29
	(a) front-side and (b) back-side	
Figure 3.5	Cooling tip (a) before assembly, (b) top-view and (c) side-view	30
Figure 3.6	Filter holder, (a) before assembly and (b) after assembly	31

	Page
Figure 3.7 Scanning Electron Microscopy (SEM)	33
Figure 3.8 X-Ray Diffraction (XRD).....	33
Figure 3.9 Scanning Mobility Particles Sizer (SMPS).....	34
Figure 4.1 Schematic diagram of experimental set up for	35
studying the effect of evaporation temperature (T_{evp})	
Figure 4.2 Temperature profiles inside reactor	36
Figure 4.3 Particle size distribution of ZnO nanoparticles.....	37
by varying evaporation temperature	
Figure 4.4 SEM micrographs of ZnO nanoparticles collected by filter	38
(a) T_{evp} 500 °C, (b) T_{evp} 550 °C, (c) T_{evp} 600 °C and (d) T_{evp} 700 °C	
and (d) T_{evp} 800 °C	
Figure 4.5 Partial pressure of zinc vapor and oxygen by	39
varying evaporation temperature	
Figure 4.6 Rate constant of zinc by varying evaporation temperature.....	40
Figure 4.7 Particle size distribution of ZnO nanoparticle by	41
varying amount of zinc raw material	
Figure 4.8 SEM micrographs of ZnO nanoparticles with fixed.....	42
air and nitrogen flow rate at 1 L/min, at T_{evp} 500°C (a) 2g,	
(b) 4g, at T_{evp} 600°C (c) 2g and (d) 4g	

	Page
Figure 4.9 SEM micrographs of ZnO nanoparticles with fixed.....	43
nitrogen flow rate at 1 L/min, evaporation temperature 600°C and varied air flow rate (a) 0.5, (b) 1, (c) 1.5 and (d) 2 L/min	
Figure 4.10 SEM micrographs of ZnO nanoparticles with fixed.....	44
air flow rate at 1 L/min, evaporation temperature 600°C and varied nitrogen flow rate (a) 1, (b) 1.5, and (c) 2 L/min	
Figure 4.11 Schematic diagram of experimental set up for	45
studying the effect of oxidation temperature without mixing device	
Figure 4.12 Temperature profiles inside reactor by varying oxidation temperature...	46
without mixing device	
Figure 4.13 Particle size distribution of ZnO nanoparticles.....	46
by varying oxidation temperature without mixing device	
Figure 4.14 SEM micrographs of ZnO nanoparticles collected by filter	47
(a) T_{oxi} 400 °C, (b) T_{oxi} 500 °C, (c) T_{oxi} 600 °C and (d) T_{oxi} 700 °C, without mixing device	
Figure 4.15 Schematic diagram of experimental set up for studying	48
the effect of oxidation temperature with mixing device	
Figure 4.16 Temperature profiles inside reactor by varying	48
oxidation temperature with mixing device	

	Page
Figure 4.17 SEM micrographs of ZnO nanoparticles collected by filter	49
(a) T_{oxi} 400 °C, (b) T_{oxi} 500 °C, (c) T_{oxi} 600 °C and (d) T_{oxi} 700 °C, with mixing device	
Figure 4.18 SEM micrographs of ZnO nanoparticles by varying air flow rate.....	50
(a) 0.2, (b) 1, (c) 1.5 and (d) 2 L/min, with nitrogen flow rate 1 L/min	
Figure 4.19 SEM micrographs of ZnO nanoparticles by varying nitrogen flow rate .	52
(a) 1, (b) 1.5 and (c) 2 L/min, with nitrogen flow rate 0.2 L/min	
Figure 4.20 SEM micrographs of ZnO nanoparticles by varying nitrogen flow rate .	52
(a) 1, (b) 1.5 and (c) 2 L/min, with nitrogen flow rate 1 L/min	
Figure 4.21 Partial pressure of oxygen by varying nitrogen and air flow rate.....	53
(a) vary nitrogen flow rate, (b) vary oxygen flow rate	
Figure 4.22 Silicon wafer (a) before experiment and (b) after experiment.....	54
Figure 4.23 SEM micrographs of ZnO nanoparticles in 2 nd furnace.....	55
(a) 1, (b) 10, (c) 20, (d) 30 and (e) 40 cm	
Figure 4.24 Schematic diagram of experiment set up (a) without orifice and	56
(b) with orifice	
Figure 4.25 SEM micrographs of ZnO nanoparticles collected by	58
quenched silicon wafer under any position from 2 nd furnace inlet without mixing device (a) 1, (b) 30 cm and (c) filter	

	Page
Figure 4.26 SEM micrographs of ZnO nanoparticles collected by quenched silicon wafer, under any position from 2 nd furnace inlet with mixing device (a) 1, (b) 30 and (c) filter	59
Figure 4.27 Particle size distribution of ZnO nanoparticle (a) without mixing device, (b) with mixing device	60
Figure 4.28 XRD patterns of (a) ZnO nanosphere and (b) ZnO nanotetrapod	61
Figure 4.29 Temperature profiles inside reactor	62
Figure 4.30 Particle size distribution of ZnO nanoparticle at 1 cm	62
Figure 4.31 Contours of the oxygen concentration inside reactor (a) without orifice and (b) with orifice	64
Figure 4.32 Contours of the zinc vapor concentration inside reactor (a) without orifice and (b) with orifice	64
Figure 4.33 Relation between reactant concentration inside reactor and radius direction (a) oxygen and (b) zinc vapor concentration	66
Figure 4.34 Contours of multiplication between oxygen and zinc vapor inside reactor (a) without orifice and (b) with orifice	67
Figure 4.35 Possible growth mechanism of ZnO nanoparticles in gas phase reaction	69

	Page
Figure 4.36 SEM micrographs of ZnO nanoparticles collected by 70 quenched silicon wafer, under any position from 2 nd furnace inlet with mixing device (a) 5, (b) 10, (c) 15, (d) 20 and (e) 25 cm	
Figure 4.37 SEM micrographs of ZnO nanoparticle treated at 600 °C 71 for one hour, (a) 5 and (b) 10 cm	



สถาบันวิทยบริการ
จุฬาลงกรณ์มหาวิทยาลัย

NOMENCLATURES

VLS	=	Vapor-liquid-solid
p_A	=	Partial pressure of component A
p_T	=	Total pressure of system
S_R	=	Saturation ratio
F_{th}	=	Thermal force
λ	=	Gas mean free path
∇T	=	Temperature gradient
T_{evp}	=	Evaporation temperature
T_{oxi}	=	Oxidation temperature
SEM	=	Scanning electron microscopy
XRD	=	X-Ray Diffraction
SMPS	=	Scanning mobility particle analyzer
DMA	=	Differential mobility analyzer
CPC	=	Condensation particle counter
k_{Zn}	=	rate constant of zinc
T	=	Temperature
nm	=	nanometer

CHAPTER I

INTRODUCTION

1.1 Background

Research and development on the synthesis of nanoparticles have attracted a great attention of researches and scientists because they show quantum size effect, in which the physical and chemical properties of materials are strongly dependent on particle size. Among many nanomaterials, ZnO nanoparticles have been received a great attention owing to their intriguing properties including attractive optical functions based on its wide band gap of 3.37 eV, high exciton binding energy of 60 meV and n-type semiconductor, (Huang, 2001). Many intensive research effort for its unique properties and versatile applications in transparent electronics, ultraviolet (UV) light emitters, piezoelectric devices, chemical sensors, cosmetic and photocatalytic activities have been pursued. It has been reported that size and shape of ZnO nanostructures such as nanowhisker, nanowire, nanorod, nanoshell, etc. are significantly affected by the synthesis procedure.

So far, various methods including chemical vapor deposition, aqueous solution deposition, sol-gel method, decomposition of ZnO, carbon thermal method, catalyst assisted vapor-liquid-solid (VLS) mechanism and oxidation reaction between zinc vapor and oxygen in gas phase have been developed for synthesis of ZnO nanoparticles. Gas phase reaction is one of potential means expected to provide higher yield with low operating cost. In addition, it is a direct and simple method to synthesize ZnO nanoparticles which have a uniform particle size distribution and less impurity entrainment, (Wu et-al., 2004). A typical mass production of ZnO is already known as French process which ZnO is made from zinc metal being vaporized and then oxidized in a combustion zone. However, the limitation of gas phase reaction is how to control of crystal growth. Without control, ZnO naturally grows to a size in several micrometers which in turn do not exhibit specific characteristics such as piezoelectricity and optoelectronics.

In the present work, preparation and characterization of ZnO nanoparticles via controlled syntheses of gas phase reaction were carried out. Controlling the oxidation of zinc vapor is the key issue in the synthesis of ZnO nanoparticles with a particular shape. A unique process is designed to produce ZnO nanoparticles by oxidation between zinc vapor and oxygen. This research thesis aims to control the synthesis method of ZnO nanoparticles using gas phase reaction by controlling synthesis parameters such as evaporation temperature and reaction temperature, gas flow rate (retention time and concentration of raw materials). Apply mixing device (orifice) is employed for controlling the interaction between Zn vapor and oxygen inside the reactor. Dependence of size and shapes of ZnO nanoparticles on such operating parameters was investigated and discussed. Finally, the possible growth mechanism of ZnO nanoparticles by using oxidation in gas phase method was also proposed.

1.2 Objectives of research

- 1.2.1 To develop a lab scale of production of ZnO nanoparticles from zinc powder by using gas phase reaction.
- 1.2.2 To control size and shape of ZnO nanoparticles by adjusting synthesized parameter in gas phase reaction.
- 1.2.3 To characterize the obtained ZnO nanoparticles.
- 1.2.4 To propose the growth mechanism of ZnO nanoparticles

1.3 Scope of research

- 1.3.1 Conduct lab-scale experiments for synthesizing ZnO nanoparticles via gas phase reaction.
- 1.3.2 Controlling the reaction conditions
 - Evaporation temperature
 - Oxidation temperature
 - Gas flow rate
 - Mixing device (orifice)

1.3.3 Characterization of synthesized ZnO nanoparticles

- X-ray diffraction (XRD)
- Scanning Electron Microscope (SEM)
- Scanning Mobility Particle Sizer (SMPS)

1.4 Benefits to be obtained

1.4.1 To acquire information related to synthesis of ZnO nanoparticles using gas phase reaction.

1.4.2 To apply the knowledge of gas phase reaction method for mass production of ZnO nanoparticles in Thailand's industry.



สถาบันวิทยบริการ
จุฬาลงกรณ์มหาวิทยาลัย

CHAPTER II

FUNDAMENTAL KNOWLEDGE AND LITERATURE REVIEW

2.1 Zinc Oxide (ZnO)

Zinc oxide is a chemical compound with formula ZnO. It is nearly insoluble in water but soluble in acids or alkalis. It occurs as white hexagonal crystals or a white powder commonly known as zinc white as shown in figure 2.1. It remains white when exposed to hydrogen sulfide or ultraviolet light. Crystalline ZnO exhibits the piezoelectric effect and it will be change color from white to yellow when heated, and come back to white when cooled down. ZnO will be decomposes into zinc vapor and oxygen at around 1975 °C.

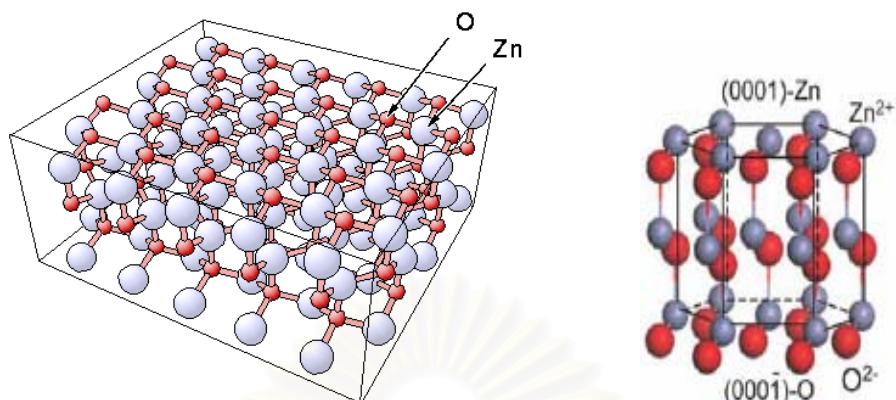


Figure 2.1 Zinc oxide

Ref.: http://en.wikipedia.org/wiki/Zinc_oxide

2.2 Wurtzite structure

The crystal structure of ZnO is wurtzite which is a member of the hexagonal crystal system and consists of tetrahedrally coordinated zinc and oxygen atoms as shown in figure 2.2. The lattice parameters of wurtzite structures is $a = 0.3249$ nm and $c = 0.5206$ nm.



ZnO (wurtzite) lattice (0001) stacking

Figure 2.2 ZnO wurtzite structures

Ref.: <http://www.fhi-berlin.mpg.de/th/personal/hermann/ZnO.gif>

2.3 Physical properties of ZnO nanostructures

Table 2.1 Physical properties of wurtzite ZnO

Properties	Value
Density	5.606 g/cm ³
Melting point	2248 K
Relative dielectric constant	8.66
Gap Energy	3.4 eV, direct
Exciton binding Energy	60 meV
Electron effective mass	0.24
Electron mobility	200 cm ² /V s

It is worth noting that as the dimension of the semiconductor materials continuously shrinks down to nanometer or even smaller scale, some of their physical properties undergo changes known as the “quantum size effects”. For example, quantum confinement increases the band gap energy of quasi-one dimensional (Q1D) ZnO, which has been confirmed by photoluminescence, X. Wang et-al. (2004).

2.4 Generation of particles by reaction

2.4.1 Gas-Phase techniques

Particles synthesis from the vapor phase involves the processes of seed generation and particle growth. The processes involved in particles synthesis from the vapor phase are summarized in figure 2.3. Seed particles are frequently produced by a burst of homogeneous nucleation of vapor phase species. Growth can involve the processes of physical vapor deposition (PVD) or chemical vapor deposition (CVD) of vapor phase species or coagulation, which is the collisional aggregation of small particles to form larger ones. The latter process dominates when large numbers of particles are formed in the nucleation burst. Because liquid particles coalesce upon coagulation, spherical particles result unless the viscosity is extremely high. Coagulation of the solid particles or of very high viscosity liquid often results in the formation of agglomerates particles comprised of the large the number of smaller primary particles. Such agglomerate formation frequently begins after a period of coalescent coagulation in high temperature regions of the reactor, leading to a relatively uniform primary particle size which is sometime misinterpreted as evidence that coalescent has ceased. Instead, coagulation accelerates once agglomerates begin to form due to the increased projected areas that result from agglomerate formation. Strong bonds can form between the primary particles by solid phase sintering, leading to hard agglomerates that are often difficult to disperse.

สถาบันวิทยบริการ
จุฬาลงกรณ์มหาวิทยาลัย

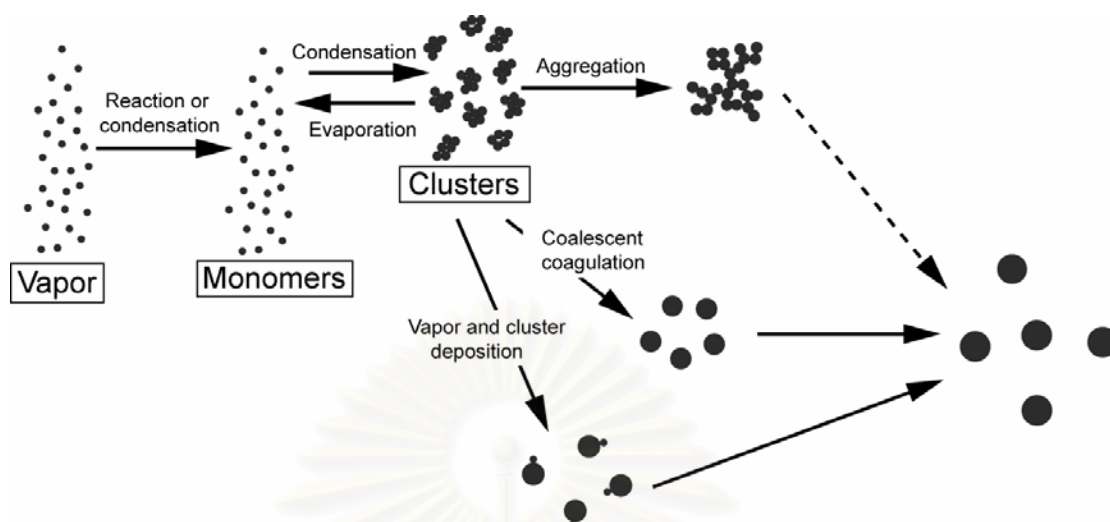


Figure 2.3 Mechanisms of particles formation and growth from vapor phase

Ref.: Powder Technology Handbook

2.4.2 French process

In the French process of producing ZnO, metallic Zn vapor drift or flows out of the mouth of the retort at low velocity and burns in the presence of an excess air. After that forming ZnO is collected in any convenient and appropriate manner. The New Jersey Zinc Company applied for a patent for a improved method of producing ZnO involves volatilizing metallic Zn and oxidizing Zn vapor, preferably by forcing the Zn vapor at relatively high velocity into an oxidizing environment to produce particle of ZnO of extreme fineness and then rapidly cooling these particles after their formation as to prevent any appreciable sublimation and growth. They found that the higher temperature or higher Zn vapor is brought the finer particles size of the resulting ZnO product. Moreover, they also used the heat absorbing capacity of the media for cooling the system after ZnO formation resulting in the finer particles size of product.

The schematic diagram was illustrated in figure 2.4, a graphite crucible adapted to contain an appropriate quantity of metallic Zn. The crucible is closed by a cover and arched roof. Heat insulating material is filled between these spaces. A discharge nozzle for Zn vapor is mounted in the top of the crucible and extends through the cover. This nozzle has an aperture of the proper size for conveying the

metallic Zn vapor at the desired velocity from the crucible to the oxidizing region or Zn combustion zone. The cover and roof are electrical insulating material, while the nozzle is electrically conductive and serves as one electrode or terminal for the application of electric energy to superheating of the metallic Zn vapor about 2000°C. A feed tube which is made electrically conductive serves for the introduction of molten Zn into crucible.

In this work, two fundamental conditions must be realized and maintained for the production of improved ZnO. First, the Zn vapor must be oxidized or burned in such a manner as to produce particles of ZnO of the desired extreme fineness. Second, the productions of oxidation or combustion must be cooled in such a interval time as to prevent appreciable sublimation and growth of the particles of ZnO after their formation.

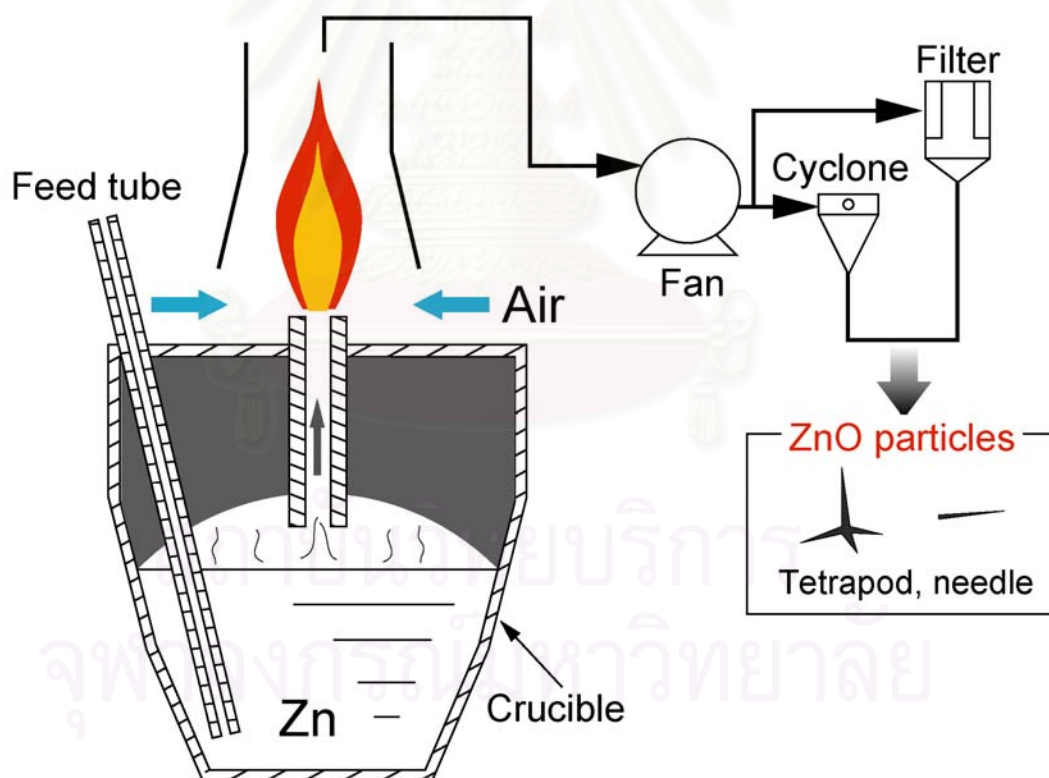


Figure 2.4 Schematic diagram of French process

2.5 Synthesis of ZnO Nanostructures

The assortment of ZnO nanostructures, such as nanowires, nano-tetrapod, nanotubes and nanorings have been successfully grown via a variety of methods including chemical vapor deposition, thermal evaporation, gas phase reaction, etc.

2.5.1 Vapor transport synthesis

The most common method to synthesize ZnO nanostructures utilizes a vapor transport process. In such a process, Zn and oxygen mixture vapor are transported and react with each other, forming ZnO nanostructures. There are several ways to generate Zn and oxygen vapor. Decomposition of ZnO is a direct and simple method; however, it is limited to very high temperature (~ 1400 °C). Another direct method is to heat up Zn powder under oxygen flow (gas phase reaction method). This method facilitates relative low growth temperature (500-700°C), but ratio between the Zn vapor pressure and oxygen pressure needs to be carefully controlled in order to obtain desired ZnO nanostructures. It has been observed that the change of this ratio contributes to a large variation on the morphology of nanostructures. Also in the widely used carbon thermal method, ZnO powder is mixed with graphite powder as source material and combustion at 800-1100 °C, graphite reduces ZnO to form Zn and CO/CO₂ vapors. Zn and CO/CO₂ later react and result in ZnO nanocrystals. The disadvantage of carbon thermal is production of ZnCO₃ which is difficult to remove from ZnO product.

According to the difference on nanostructure formation mechanism, the extensively used vapor transport process can be categorized into the catalyst free vapor-solid (VS) process and catalyst assisted vapor-liquid-solid (VLS) process.

For catalyst free vapor-solid process, The Zn atoms were continuously evaporated from the source material during the heating process. In the presence of oxygen, the Zn vapors absorbed on the surface of quartz tube and react with oxygen to form ZnO nuclei. As the reactant concentration increases, the ZnO nuclei individually grow in upward direction in the form of nanostructures. In contrast, catalyst assisted vapor-liquid-solid process; the source vapor (Zn vapor) reacted with

the metal particles, which act as catalyst and form alloy droplets. After reaching the supersaturation state, the grown droplets lead to the formation of nanostructures. The typical characteristic of VLS process is the presence of metal particles capped at the end of grown structures as shown in figure 2.5.

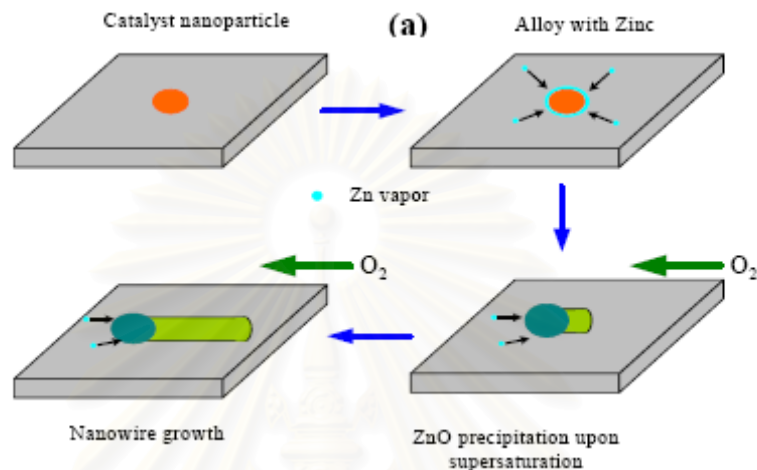


Figure 2.5 Schematic diagram of Vapor-Liquid-Solid process

2.5.2 Other synthesis methods

Although the vapor transport process is the dominant synthesis method for growing ZnO nanostructures, other growth methods such as sol-gel, electrodeposition, have been developed in parallel. These methods provide the possibility of forming ZnO nanostructures at low temperature. For example, in a sol-gel synthesis method, AAM (anodic aluminum oxide membrane) was also used as the template and immersed into a suspension containing zinc acetate for 1 minute, then heated in air at 120 °C for 6 hours. ZnO nanofibers were eventually obtained after removing the AAM template. This sol-gel process was further improved by an electrochemical method in order to obtain nanorods with diameter smaller than 50 nm, Z. Miao et al (2002). In an electrodeposition method, AAM with highly ordered nanopores was used as a template, zinc nanowires were fabricated into nanopores via electrodeposition, forming zinc nanowires array, then the nanowires array was oxidized at 300°C for 2 hours and ZnO nanowires were obtained, Y. Li et al (2000).

2.6 Condensation and evaporation

The formation and growth of aerosol particles by condensation is the principal method of aerosol production in nature and the most important mass-transfer process between the gas phase and the particulate phase. This process usually requires a supersaturated vapor and is initiated by the presence of small particles (nuclei) or ions that serve as site for particle formation.

2.6.1 Partial pressure

The partial pressure, p is the pressure that a gas (or vapor) in a mixture of gases would exert if it were to occupy, all by itself, the entire volume that is occupied by the mixture. The sum of partial pressures of the components equals the total pressure of the mixture (Dalton's law). For example, if we consider a mixture of ideal gases A and B in a container at atmospheric pressure. Gas A has a partial pressure of 1/3 atm and gas B 2/3 atm. If only gas A was in the container, the pressure in the container would be 1/3 atm. By the ideal gas law, gas A would have a volume equal to one-third of the container at atmospheric pressure. Similarly, gas B would occupy two-thirds of the container at atmospheric pressure. Thus, partial pressure is a way of defining the volume fraction of gases or vapors present in a mixture.

$$\text{Volume fraction of gas A} = \frac{p_A}{p_T}$$

Where p_A is the partial pressure of component A and $p_T = \sum p_i$ is the total pressure of the system.

The saturation vapor pressure, also called the vapor pressure, is the pressure required to maintain a vapor in mass equilibrium with the condensed vapor (liquid or solid) at a specified temperature. When the partial pressure of a vapor equals its saturation vapor pressure, evaporation from the surface of a liquid just equals condensation on that surface, and there is mass equilibrium at the surface.

The equilibrium water vapor pressure for plane surface p_s is the partial pressure p of water vapor that defines a condition of *saturation*. If, at any given temperature, the partial pressure is less than p_s , then the vapor is unsaturated, and if p

is greater than p_s , the vapor is *supersaturated*. The *saturation ratio*, S_R , is the ratio of the partial pressure of vapor in a system to the saturation vapor pressure for temperature of the system.

$$S_R = p/p_s$$

Supersaturation is usually produced by cooling a saturated vapor. Because the partial pressure of the vapor remains constant, while p_s decreases with decreasing temperature. Then a saturation ratio greater than 1.0 can be achieved.

2.6.2 Homogeneous nucleation

Homogeneous nucleation is the formation of particles from a supersaturated vapor without the assistance of condensation nuclei or ion. The process is also call *self-nucleation*. This type of particle formation is rare for water vapor in the atmosphere, but can occur for other gases and vapors, and can be produced readily in the laboratory to study the process of formation and growth. Even in unsaturated vapor, the attractive forces between molecules, such as van der waals forces, lead to the formation of molecular clusters. The clusters are form continuously, but are unstable and continuously disintegrate. When the vapor is supersaturated, the number concentration of clusters increases to the point where they collide with one another frequently. This process is similar to coagulation, except that the “agglomerates” disintegrate soon after being formed. The greater the supersaturation, the greater the number concentration of clusters and the more frequent is the formation of transient “agglomerates” having a size exceeds d^* (d^* is Kelvin diameter). Once such an “agglomerate” exceeds d^* , even momentarily, it becomes stable and grows by condensation to form a large particle. For a given vapor and temperature, the supersaturation required for this to happen occurs at a well-defined point called the *critical saturation ratio*. Certain gas phase reactions form low vapor pressure reaction products. Because of their low vapor pressure, these products exist at high supersaturations and form particle by homogeneous nucleation. When an increase in aerosol mass concentration occurs in the atmosphere by this mechanism, it is called *gas to particle conversion*.

Since a stable droplet is formed when the droplet diameter exceeds d^* for a particular saturation ratio. The droplet has passed a threshold and will grow by condensation. The rate of growth depends on the saturation ratio, particle size. Beside particle size relative to the gas mean free path. When a particle first starts to grow, its size will likely be less than the mean free path. For this condition, the rate of particle growth is governed by the rate of random molecule collisions between the particle and the vapor molecules. For particles larger than the gas mean free path, growth depends, not on the rate of random molecule collisions, but on the rate of diffusion of molecules to the droplet surface.

2.6.3 Heterogeneous nucleation

Heterogeneous nucleation or nucleated condensation is a process of particle formation and growth that is promoted by the presence of condensation nuclei or ions. Whereas homogeneous nucleation usually requires saturation ratio of 2-10, heterogeneous nucleation can occur at supersaturations of only a few percent.

Insoluble nuclei can provide a passive site for the condensation of a supersaturated vapor. At a given level of supersaturation, an insoluble nucleus with a wettable surface will have an adsorbed layer of vapor molecules on its surface. If its diameter is greater than d^* , the nucleus will behave like a droplet of that size and grow by condensation. However, the actual situation is more complicated because a particle's ability to nucleate condensation depends on many factors, including its size, shape, chemical composition, surface structure and surface charge.

2.6.4 Evaporation

It is the process whereby atoms or molecule in a liquid state (or solid state if the substance sublime) gain sufficient energy to enter the gaseous state. The thermal motion of a molecule of liquid must be sufficient to overcome the surface tension and evaporate, that is, the kinetic energy must exceed the work function of cohesion at the surface. Evaporation therefore, proceeds more quickly at high temperature, at higher flow rates between the gas and liquid phase and in liquid phase with lower surface

tension (i.e. higher vapor pressure). Because gas has less order than liquid or solid, and thus the entropy of the system is increased, which always required energy input. These mean that the enthalpy change for evaporation ($\Delta H_{\text{evaporation}}$) is always positive. So evaporation is a cooling process.

Factors that influencing rate of evaporation

- Concentration of the substance evaporating in the air. If the air already has a high concentration of the substance evaporating, then the given substance will evaporate more slowly.

- Concentration of other substances in the air. If the air is already saturated with other substances, it can have a lower capacity for substance evaporating.

- Flow rate of air or any gas. This is in part related to the concentration point above. If the fresh air is moving over the substance all the time, then the concentration of the substance in the air is less likely to go up with time, thus encouraging faster evaporation. In addition, molecules in motion have more energy than those at rest, and so the stronger the flow air, the greater the evaporating power of the air molecules.

- Temperature of the substance. If the substance is hotter, then evaporation will be faster.

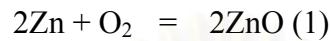
- Inter-molecular force, the stronger the forces keeping the molecules together in the liquid or solid state the more energy that must be input in order to evaporate them.

2.7 Kinetics process of tetra-needle-like ZnO

Zhou, Liu, and Hu (2005) prepared ZnO whisker (T-ZnO) using equilibrium gas controlling. ZnO whisker is the only kind of single crystal micro-fiber with peculiar three-dimension tetra-needle-like shape. They found that the growth process of T-ZnO is divided in two stages for their special crystalline morphology of the tetra-needle and radially in four directions from one central portion. Key point for the formation of single crystal is restrained crystal growth rate. Because T-ZnO with low packing density was easily carried away from reactant zinc by the heated expanding

gas which promote effective contact and continuous reaction between oxygen and zinc in the chamber was acquired.

For the growth process of T-ZnO, they suggested that the whole process consisted of three stages as oxidation of zinc, formation of nucleus and growth of needles crystal with different mechanism. From, considering the oxidation formula



The reaction ratios for the formation of the nucleus part and needle-like crystals of the whisker were successfully calculated using second-order reaction equation.

$$[\text{Zn}]^2 = kt \quad (2)$$

Because the rapid oxidation of Zn at high temperature was controlled by inadequate supply of the reactant oxygen, the associated kinetic parameters of the two crystal growth stages can be deduced from the consumption of oxygen in the first reaction stage. In addition, the oxygen near zinc would be consumed promptly once the oxidation process began, thus leading to excess of zinc and relatively inadequate supply oxygen. Accordingly, the quantity of zinc was considered as a constant while oxygen varied with the proceeding reaction. Considering the Zn content in formula [1] as constant, the kinetic process of the oxidation can be expressed as a first order reaction;

$$\ln([\text{O}_2]_0/[\text{O}_2]_t) = kt \quad (3)$$

Where $[\text{O}_2]_0$ and $[\text{O}_2]_t$ represent O_2 content at the beginning of the reaction and at the moment when the reaction had proceeded for t minutes, respectively.

The whole process of T-ZnO generation was divided into first-order reaction; the nucleus formation periods (1) for 0.5-1.5 min. and the needle crystal growth stage (2) for 2.6-6 min. with rate constant $k_1 = 0.3 \text{ min}^{-1}$ and $k_2 = 1.08 \text{ min}^{-1}$ respectively. Therefore, the weight proportion of the needles to the nuclei is approximately 20, which demonstrate predominant existence of needle-like crystals in the products. Because the reaction ratio of the nuclei generation is less than that if needle growth, so the elevation of the reaction temperature is advantageous to the second crystal growth stage of needle growth with larger k value according to the Arrhenius equation;

$$\ln k = -\frac{E}{RT} + B \quad (4)$$

Where k and E are the reaction rate constant and the activation energy of the process, respectively. R is the gas constant ($8.314 \text{ L/mol.K} = 1.987 \text{ cal/mol.K}$) and B is a constant.

The reaction rate constant is not truly a constant, but is merely independent of the concentrations of species involved in the reaction. It is almost always strongly dependent on temperature. In gas phase reaction, it depends on the catalyst and may be function of total pressure. The activation energy (E) has been equated with a minimum energy that must be possessed by reacting molecules before the reaction will occur. From the kinetic theory of gases, the factor $e^{-E/Rt}$ gives the fraction of the collision between molecules that together have this minimum energy.

2.8 Review of growth models of tetrapod ZnO

All existing models describe the growth mechanism of the tetrapod ZnO out of a seed nucleus. The main difference between these models is that they propose nuclei with different shape, geometries, and crystallographic structures, which are subsequently overgrown during the growth process along fast growing planes. However, they do not consider the earlier nucleation and the formation of the nucleus out of the gas phase.

Shiojiri and Kaito (1981) suggested a growth model in which the seed nucleus is a zinc-blende and single-crystalline ZnO nanocrystal of octahedral shape with eight $\langle 111 \rangle$ -side surfaces. Four of the surfaces are zinc terminated and act as nucleation sides for hexagonal ZnO crystals, which overgrow the nucleus resulting in tetrapod ZnO. The cubic structure of the nucleus and the interface between the two phases has not been observed directly, but the ambiguous diffraction pattern of the material after etching experiments indicates a cubic structure of the remaining material. On the other hand, cubic ZnO phases are not stable in ambient circumstances and especially the nanosized particles, should undergo a phase transformation to wurtzite ZnO.

Nishio et al. (1997) proposed such a phase transformation of a cubic tetrahedral nucleus in their growth model by a lattice plane slip resulting in multiply twinned hexagonal crystal with various elements. The number of a twin element varies between four and six in their model, depending on which specific plane slipped and induced the transformation. These suggestions are based on high-resolution transmission electron microscopy (HRTEM) investigations, where the authors observed tetrapod ZnO consisting of four or six elements. However, they also found seven element tetrapod ZnO nanostructures and the calculated angles between two legs, using such a model do not agree with the angles measured previously by Fujii et al (1993).

Iwanaga, Fujii, and Takeuchi (1993) introduced the common “octa-twin model” which has been described in detail in several publications. The main idea of this model is that the center nucleus is an octahedral multiple inversion twin made up of eight trigonal pyramidal crystals with a {0001} basal plane and three {11-22} twin planes. Such an eight trigonal pyramidal crystal cannot construct a perfect octahedral because the angle between two {11-22} planes is 85.5° and not 90° . Thus, a cracking process between twin boundaries during crystal growth was assumed to release the possibly accumulated misfit strain energy.

Dai et al. (2003) have developed a simple solid vapor approach for controlled growth of the tetraleg ZnO nanostructure at high yield. The length of the tetraleg is 2-3 μm and the edge size of its centering nucleus is 70-200 nm. From their electron microscopy studied. They proved the first evidence about the existence of the octahedral multiple twin nucleuses, which are confirmed to be responsible for the formation of the tetraleg ZnO nanostructure. They explain that the formation of T-ZnO structure has two stages: nucleation and growth. In their process, nucleation process at the initial stage might have a crucial role on the formation of T-ZnO nanostructures. The metallic Zn is in its vapor state at the high temperature (Zn has boiling point at 911°C). The gaseous Zn diffuses and immediately reoxidize in the environment of oxygen. It is known that the gaseous ZnO only exists as highly

activated species with extremely short lifetime. The oxidation reaction at their processing temperature is as follows: $Zn_{(g)} + O_2 = 2ZnO_{(s)}$. The process of the initial nucleation includes diffusion, collision of atoms and reaction between the vapor molecules (including vapor Zn and O_2). When the supersaturation increases to a level at which nuclei formed, the produced ZnO nuclei grow to sizes larger than the critical size. The ZnO nuclei formed in the alumina crucible are homogeneous as carried by the gas phase. According to the octa-twin nucleus model, ZnO nuclei formed in atmosphere containing oxygen are octa-twins nuclei which consist of eight tetrahedral-shape crystals, each consisting of three $\{11\bar{2}\}$ pyramidal facets and one (0001) basal facet (figure. 2.6a). The eight tetrahedral crystals are connected together by making the pyramidal faces contact one with another to form an octahedron. The surfaces of the octa-twin are all basal planes. An important additional condition is that every twin is of the inversion type, for example the polarities of the twinned crystals are not mirror-symmetric with respect to the contact plane but antisymmetric. Thus the eight basal surfaces of the octa-twin are alternately the plus (0001) surface (+c) and the minus surfaces (0001) (-c), as shown in figure 2.6b. The formation of the tetraleg structure has to do with the following two factors based on the octa-twin nucleus. It is known through the study of ZnO nanowires and nanobelts, [0001] is the fastest growth direction in the formation of nanostructure. The octa-twin has four positively charged (0001) surfaces. The positively charged surfaces are likely to be terminated with Zn, which may be the favorable sites to attracting vapor species, resulting in the growth of whisker along four [0001] directions. The growth mechanism is believed to be a vapor-solid process.

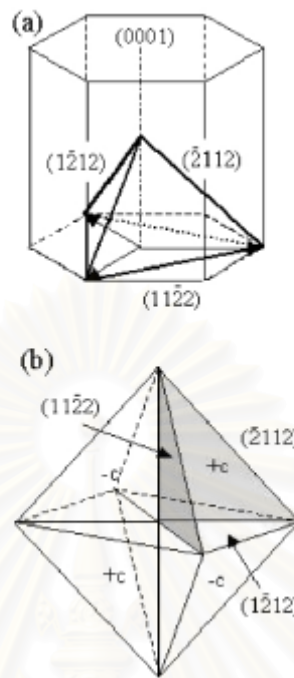


Figure 2.6 (a) a pyramid formed by three $\{11\bar{2}2\}$ and one (0001) facets, (b) The octa-twin model composed of eight pyramidal inversion-twin crystals.

Ronning et al. (2005) developed a nucleation and growth model, which covers all stages of the development from the gas phase to the final tetrapod ZnO nanostructure. Tetrapod ZnO nanorods were synthesized in a tube furnace in static air conditions. Silicon (001) substrates were cleaned in acetone and ethanol and then placed downstream in the lower temperature zone of the furnace, towards the open end of the tube. The furnace was heated up to 1100°C. They observed that the center cores of the tetrapod ZnO nanorods consist of four grains of hexagonal structure, which are directly related to the four elongated legs. It appears that the four tiny grains form a distorted tetrahedral-like structure with a large number of structural defects mediating the misfit stress between grains. Such a distorted tetrahedral configuration consisting of four rather than six or eight grains should correspond to the lowest energy state of a stable nucleus. They proposed a freestanding self-assembly nucleation and growth process, which adopts the characteristics of a phase transition proposed in the model by Nishio et al.

In the first step, Zn vapor diffused to the lower temperature zones of the furnace and condenses out of the supersaturated air into very tiny Zn clusters with

only a few atoms. Zn clusters with less than 20 atoms do not show a specific structure. These Zn clusters oxidize immediately due to the ambient conditions within this temperature zone and result in tiny ZnO clusters. The stability of small ZnO clusters has been theoretically investigated and experimentally confirmed by mass spectrometry. It was predicted that spheroid $(\text{ZnO})_i$ clusters are stable for $11 \leq i \leq 15$. This phase transition results in a structure of nanoparticles, which is determined by the interplay between the formation energies of different surfaces and grain-boundary interfaces. They consider that the (0001)-Zn and (000-1)-O surfaces have the highest surface energies for wurtzite ZnO due to their polar character. Therefore the growth of nanoparticles having a morphology for which (0001) polar surfaces are suppressed is favorable. Then that cluster collapses into a tetrahedron, which consists of four equivalent grains having triangular dipyramidal shapes. Each single-crystalline hexagonal ZnO grain is located at the apex of the tetrahedron, and the grain boundaries run along the bisector of the edges and surfaces. The proposed geometry with four grains is energetically favorable, because the tetrahedron has the minimal ratio between grain boundary areas and surface areas of $r \approx 0.2$, compared with other multiple grain formation like a cube (with six grains, $r \approx 0.71$), an octahedral (eight grains, $r \approx 0.87$). Finally, the four tiny ZnO grains overgrow the tetrahedron nucleus and form tips/legs of the tetrapod due to the fast growth rate of hexagonal ZnO along the direction of the c axis via the VS process.

2.9 Thermophoresis force

A thermal force arises from asymmetrical interaction of a particle with the surrounding gas molecules in a temperature gradient is called “Thermophoresis Force”. The movement of the particles that results from this force is called “thermophoresis”. The magnitude of the thermal force depends on the gas and particles properties, as well as the temperature gradient. The earliest studies of the thermophoresis were empirical investigations of the dust-free layer observed around a heat object, such as a metal rod immersed in smoke. The smoke particles appear to be repelled by the heated object and form a particle-free layer usually less than 1 mm thick.

The thermal force and the aerosol particle motion are always in the direction of decreasing temperature. When a cold surface is proximate to a warm gas, thermophoresis causes particles in the gas to be deposited onto the surface. We also adapted this concept for collecting synthesized ZnO nanoparticles from airborne. Therefore we tried to cool the surface of deposited substrate by water.

For a small particle ($d < \lambda$), the thermal force is result of a greater transfer of momentum from the gas molecules on the hot side of the particles, relative to those on the cold side. As shown in figure 2.7. , the gas molecules coming from the left side have a greater velocity than those coming from the right side because of the difference in temperature between the gas on the left and right side of the particles. The greater momentum received from the left caused a net force to the right, in direction of colder temperature. The exact description of this force is more complicated than that given here because it depends on the nature of molecular reflection at the particle surface (Waldmann and Schmitt, 1966) Theoretically the thermal force on a particle of diameter d is

$$F_{th} = \frac{-p\lambda d^2 \nabla T}{T} \quad \text{for } d < \lambda$$

where p is the gas pressure, λ is the gas mean free path, ∇T is the temperature gradient and T is the absolute temperature of the particle. The minus sign is required because the force is in the direction of decreasing temperature.

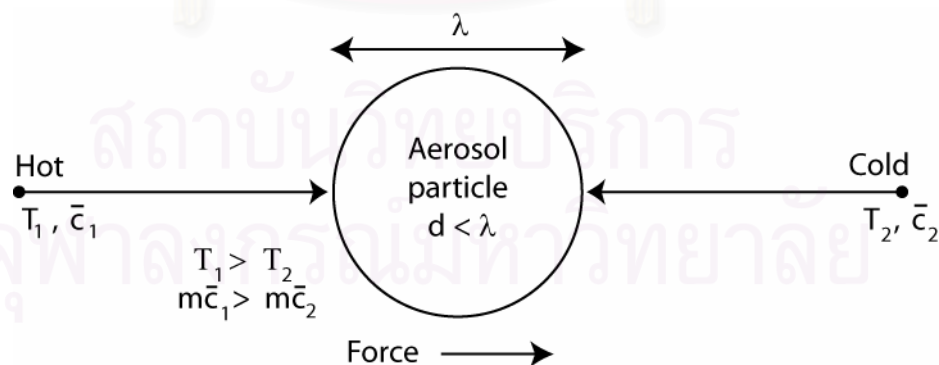


Figure 2.7 Molecular impacts on a particle ($d < \lambda$) in a temperature gradient.

2.10 Literature reviews

Wu and et al. (2002) studied about synthesis of Zn and ZnO nanoparticles by using an evaporation-condensing method in Ar or gas mixture between Ar and O₂. The high frequency induction heating was applied to evaporated pure Zn powder with a size of 15 μm, at the temperature of 1100 °C and pressure 1.6 kPa. The shape of Zn nanoparticles with an average size of about 65 nm was produced in argon gas at atmosphere. However, ZnO nanoparticles synthesized in a gas mixture of 50% Argon-50%Oxygen, at pressure 10 kPa, have the shape of ellipsoid with 90 nm in long axis and 60 nm in short axis. The tetrapod ZnO nanoparticles were synthesized at pressure 1.6 kPa and the dimension is about 8 nm in diameter and 360 nm in length.

Dai and et al. (2002) synthesized tetrapod ZnO nanoparticles using oxidation reaction between pure Zn and oxygen. Alumina boat which loaded Zn was inserted in a horizontal tube furnace. The temperature of furnace was ramped to 825-925 °C at heating rate of 50-100 °C/min. From FE-SEM images, ZnO nanoparticles were a tetrapod shape having four legs with diameter 70-150 nm and length of legs was 2-3 μm. In detailed structure of individual ZnO was characterized by using TEM. From bright-field images, there was no streaking in the nanorod. From dark-field images, single crystal nature of nanorod was observed. Therefore, ZnO nanoparticles which use oxidations in gas phase were high-quality nanocrystal.

Leung and et al. (2004) synthesized ZnO nanostructures by controlling Zn vapor release by changing the type of starting material (ZnO powder vs. ZnO nanoparticles, graphite vs. carbon nanotubes). When the single wall carbon nanotubes (SWCNTs) were used, the reaction was much faster than in the case of graphite. While ZnO nanoparticles instead of conventional ZnO powder were used, similar effect was observed due to higher reactivity of nanosized ZnO. ZnO nanostructures were synthesized in a tube furnace which was heated to 1100°C. The reaction was performed in atmosphere with no addition gas flow in an open end quartz tube.

The morphologies of synthesized ZnO nanostructure changed from tetrapod to bone-like nanorod when the starting materials were changed. This is most likely due to variation in the rate of reduction of Zn and release of Zn vapor from the source. The growth of nanostructures is strongly depend on the partial pressure of the reactant (Zn and O₂), and therefore depends on the geometry of the experimental system.

Wu and Xie (2004) studied about synthesis of ZnO nanoparticles using the oxidation reaction between Zinc vapor and oxygen at various temperatures (1050-1400 °C) and pressure (1-12 kPa). The powder Zn was vaporized by using inductive furnace. Firstly, Zn vapor contacted with argon atoms in the gas mixture because the molecular weight of argon atom is heavier than oxygen atom. Then, Zn vapor was condensed to Zn aerosol. In the same time, Zn aerosol reacted with oxygen atom to produced ZnO nanoparticles.

As-synthesis ZnO have four needle-like feet (tetrapod) with diameter of 6-45 nm and length 280-435 nm. While the temperature was raised, the diameter of ZnO increased and the length of ZnO decreased. The ZnO nanoparticles of different sizes were obtained in range of gas pressure at each evaporation temperature. For example at 1350 °C, the pressure was varied from 2.2 to 6 kPa and the nanowhiskers with longest needle-like feet were obtained at a pressure of 4 kPa. However, the spheroid nanoparticles were obtained out side this pressure range.

Park and et al. (2005) researched about synthesis of ZnO nanowires by using two-step of gas flow controlled evaporation process. The evaporation process was carried out in a quartz tube which located in the horizontal tube furnace at evaporation temperature 700 °C. The first step, high purity Ar used as a carrier gas for Zn vapor, when the temperature reached the processing temperature, high purity of oxygen gas was introduced as the second step. Zn vapor were condensed on the Si substrate coated with Au and the oxidation reaction between condensed Zn and oxygen were produced ZnO nanowires with 40-150 nm in diameter and 1.2-4.5 μm in length. Size of ZnO nanowires were increased when the evaporating temperature and the thickness of Au coat were increased.

Zhang and et al. (2005) studied about the effect of heating rate toward size and shape of ZnO nanoparticles by using thermal evaporation technique, at 700 °C in air without the present of catalyst and carrier gas. From SEM images, at heating rate 27.5 °C/min. no one-dimension nanostructure were formed but they can observed porous ZnO membrane on Zn foil. When the heating rate was increased to 68 °C/min., one-dimension nanostructure start to grow from the surface of Zn foil and when the heating rate was increased to 97 °C/min, beside the long one-dimension nanostructure were observed, some ZnO nanoflowers were observed on the surface of Zn foil. When the heating rate was more than 170 °C/min., they were observed the tetrapod morphologies.

Shen, Cho, and Lee (2005) were synthesized ZnO nanonails on silicon substrate through a simple low-temperature thermal evaporation process at atmospheric pressure. The ZnO nanonails were fabricated in a two heating zone horizontal tube furnace (Indium powders were put at first heating zone in the furnace upstream, and zinc powders at the heating zone downstream). The obtained ZnO nanonails exhibit well-defined morphologies and clean surface without amorphous contamination. The temperature of In powders are obvious the key factor to get ZnO nanonails. Without In powder, only ZnO nanorod arrays are formed.

Kong, Kim, and Cho (2006) were synthesized ZnO nanostructure via thermal evaporation under various cooling down procedures by changing the flow rate of the carrier gas (Ar) and the reaction gas (O₂). When cooled down without any gas (sample A), the remaining oxygen gas and the Zn vapor will be transported in to area of nanostructure formation which resulted in a limited reaction only the surface of nanostructures and the formation of nanonail structures with hexagon surface morphology. The reaction area between the remaining oxygen and Zn vapor transported by carrier gas will be broaden with the constant flow of the carrier gas at high temperature (sample B) and it induces the nanonail structure with a longer shaft head compared with sample A.

The pillar shape of ZnO nanostructures will be synthesized when cooled down with continuous gas flow of oxygen and Ar (sample C) because the gas flow was

evenly transported in the whole area of 1D nanostructure. When cooled down with increased carrier gas flow, 1D nanowire without a hexagonal head was formed. It originated from the enhanced growth rate into the vertical direction rather than lateral growth due to the lowest surface energy. These results imply that surface reaction occurs easily at the high temperature of 700°C, and the mass transport of source material is the dominant growth mechanism that determines the growth rate.

Liu and et al. (2006) were synthesized ZnO microhollowspheres and ZnO nanocombs by evaporation of a mixture of zinc, graphite, and zinc oxide powders. Zn powder was evaporated at a temperature of over 400 °C and transported to the low temperature zone. The flow of nitrogen then makes zinc vapor condense zinc spherical droplets on the substrate, which has lowest surface energy. On the other hand, the surface of zinc spherical droplets was subsequently oxidized to form an oxide while the core of zinc droplets was still zinc. With the temperature increase (by controlling the step of evaporation temperature), the core of zinc droplets were re-evaporated whereas zinc oxide on the surface of zinc droplets were not evaporated due to its high melting point (~1750°C)

Park and et al. (2006) were studied the synthesis of ZnO nanowire by a thermal evaporation method with very small amount of oxygen. The ZnO nanowire has grown from metal Zn granule under controlled O₂ environments at high temperature (700-1000 °C for 0.5-2 h). The oxygen contents were adjusted from 0.5 to 5 vol% by mass flow controller. The behavior of the ZnO nanowire growth with the change of oxygen content in carrier gas (N₂) shown that ZnO nanowire grew only at 1.6-2.0 vol% O₂ conditions. When the oxygen content is higher than 2.5 vol%, nanostructure was not synthesized even though metal zinc was converted ZnO. From these result, it was confirmed that oxygen content in the thermal evaporation method is an important factor for the synthesis of the ZnO nanowire.

Chen and et al. (2007) synthesized tetrapod ZnO nanostructures with three different morphologies (Rod-wire junction, dumbbell-like and cone like). Tetrapod

ZnO nanostructures were synthesized by vapor phase oxidation from Zn powder by high purity O₂ with Ar as carrier gas in Al₂O₃ crucible. The reaction conditions and the corresponding ZnO nanostructures obtained are given in Table 2.2.

Table 2.2 Structure of tetrapod ZnO nanostructures obtained from different reaction parameter.

Sample	O ₂ (sccm)	Ar (sccm)	Reaction Temperature (°C)	Reaction time (°C)	Whether O ₂ and Ar was flowed at the same time	Morphology of ZnO nanostructures
1	1	200	900	10	Yes	rod-wire junction
2	1	100	800	10	Yes	dumbbell-like
3	1	200	800	1	Yes	cone-like

From table 2.2, the change in the tetrapod shape is due to the change of the synthesis temperature and oxygen partial pressure. Base on their observation, a possible growth mechanism is proposed as follow. Since any catalysts were not used during the growth process which suggests that the growth mechanism of our ZnO nanostructures is a vapor-solid process, not a vapor-liquid-solid process. The formation of the tetrapod ZnO nanostructures may include two stages: nucleation and growth. The nuclei are octa-twins which consist of eight tetrahedral-shape crystals and the polarities of the twinned crystals are anti-symmetric, and the rods grow from the four (0001) planes. The rod morphology is determined by the competition of surface energy minimization and growth kinetics. Zn atoms adsorbed on rough surface reduce extra surface diffusion barrier, called Schwoebel barrier, and enhance the diffusion and growth along the [0001] direction. Following nucleation, the nanorods are carried out of the high temperature region by carrier gas under the limited oxygen. The second step growth process occurs in layer (0001), and then nanowires formed at the nanorods. While dumbbell-shaped structures have different growth process is caused by rich oxygen condition as the kinetics factors are dominating since the growth rate along [0001] direction depends on the oxygen partial pressure to a different extent. On the other hand, at very short synthesis time (about 1 min) and lower oxygen supply, the conical structure is formed along the growth direction.

CHAPTER III

EXPERIMENTAL

3.1 ZnO raw material

Zinc, which is used as raw materials in this work, was bought from Sigma-Aldrich. Type of Zinc is Zinc dust and average particles size is smaller than 10 micron. The purity of Zinc is 98+%. From SEM images, morphology of Zinc is spherical shape and smooth surface as shown in figure 3.1.

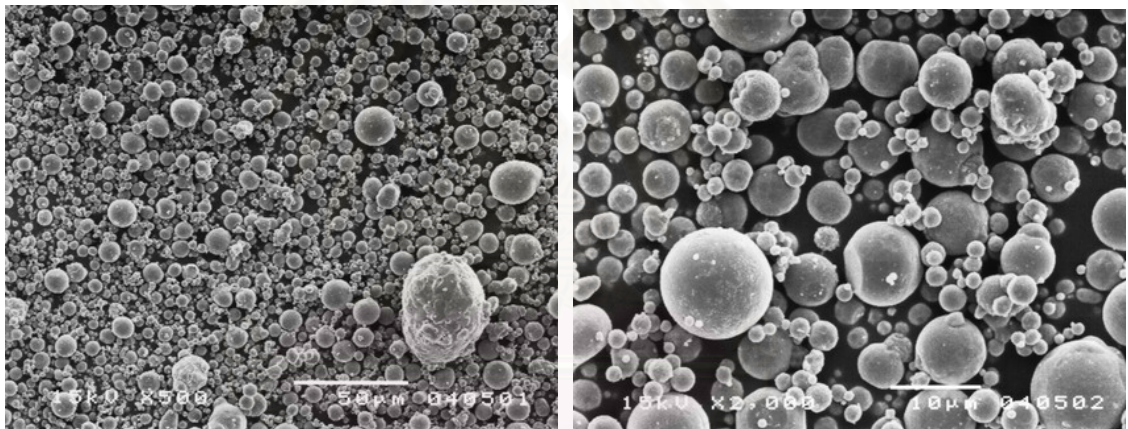


Figure 3.1 SEM images of zinc particles (Raw material) particle diameter <10 micron.

3.2 Synthesis of ZnO nanoparticles by gas phase reaction

High densities of ZnO nanoparticles were synthesized by oxidation of zinc vapor in the gas phase reaction without using any catalyst and additives. The gas phase reaction process, as shown in figure 3.2, was done in a horizontal quartz tube furnace (150 cm in length, 2.7 cm in diameter) which contains two electrical heating zones as shown in figure 3.3. Cleaned silicon wafer quenched with cold water was used as a deposition substrate in order to enhance the deposition flux by thermophoresis as well as avoiding the growth of collected particles on the substrate. The silicon wafer was placed 1 and 30 cm downstream of the second furnace which

aim to observe the growth mechanism of ZnO. In addition, synthesized ZnO in the airborne were collected by glass filter at the outlet of the quartz tube. About 2 g of metallic Zn powder (Zinc dust, <10micron, Sigma Aldrich) was loaded into an alumina boat placed at the center of the first electrical furnace which is an evaporation zone. High purity nitrogen gas and clean air were used as a carrier gas and oxygen source, respectively, during the whole reaction process. An orifice was placed downstream direction from the center of the alumina boat in order to enhance the interaction between zinc vapor and air. After that zinc vapor react with oxygen to form ZnO nanoparticles in the second heating zone as a reaction zone. Prior to the heating, the system was purged with nitrogen for 10 min. Then 1 L/min of nitrogen gas and clean air, which was controlled by mass flow controller, were introduced into the reactor after purging step. The gas phase reaction for growth of ZnO nanoparticles was conducted at 600°C for a period of 80 min. After the growth process, the reactor furnaces were allowed to cool down at ambient temperature. The white colored products were observed on the surface of silicon substrate and glass filter.

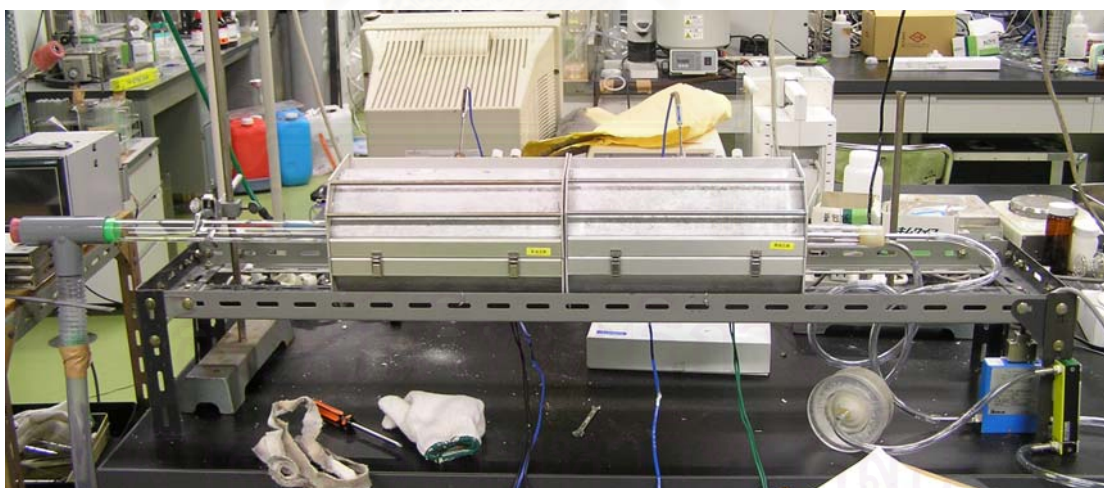


Figure 3.2 Experimental set up for synthesized ZnO nanoparticles by gas phase reaction process.

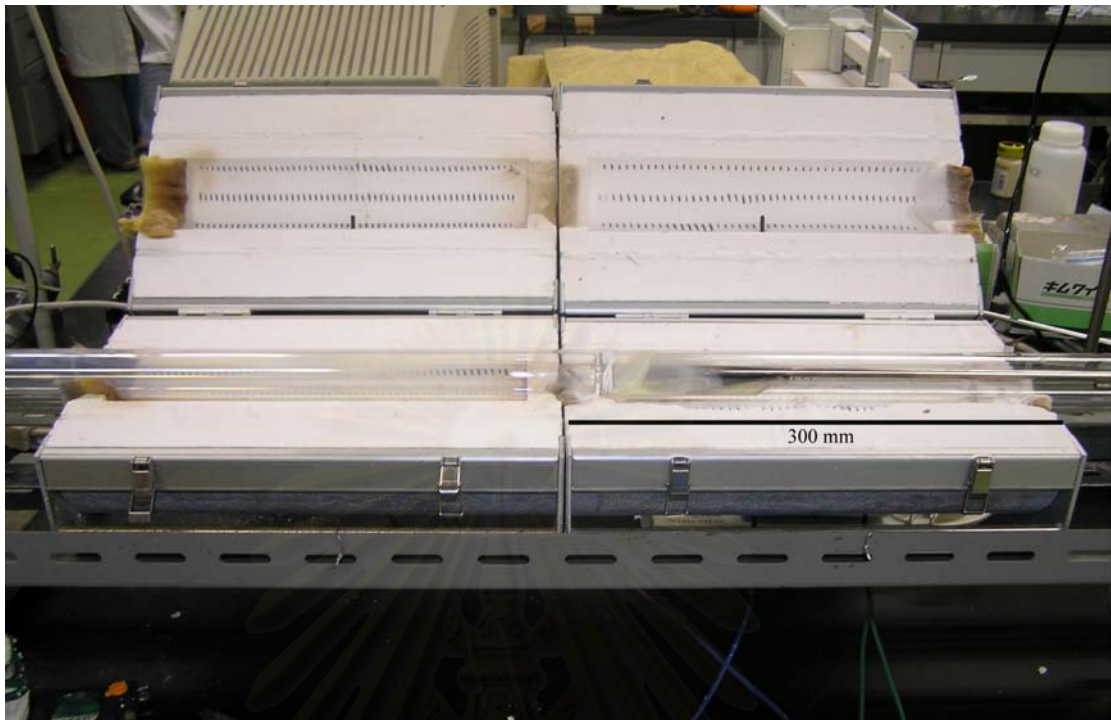


Figure 3.3 Two electrical furnaces and quartz tube reactor.

3.3 Mixing device

In this work, Orifice was used as a mixing device for enhancing the interaction between zinc vapor and oxygen. It was made from brass and it has one hole at the center of orifice as shown in figure 3.4. The effects of orifice toward morphology of ZnO nanoparticles were investigated by SEM.

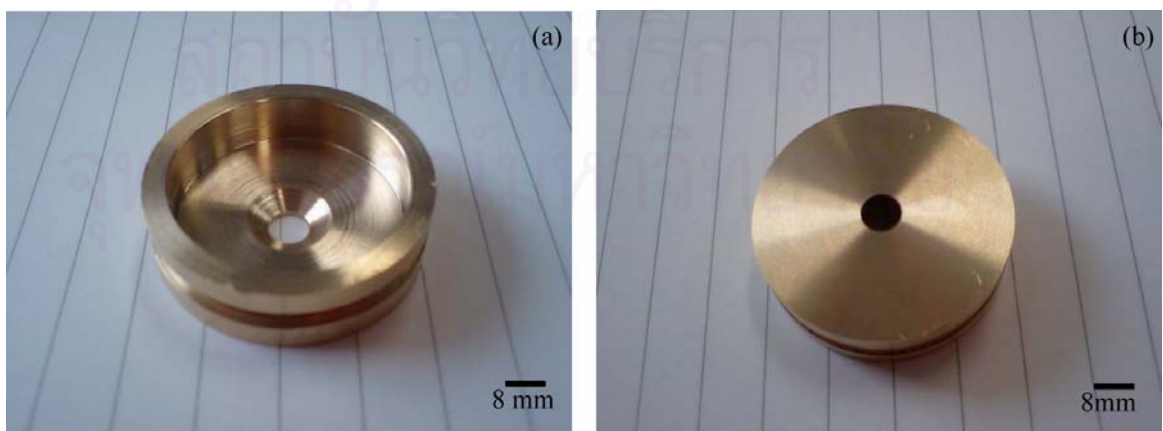


Figure 3.4 Mixing orifice with one hole at the center (a) front-side and (b) back-side.

3.4 Collecting method for synthesized ZnO nanoparticles

In our work, Synthesized ZnO nanoparticles were collected by using silicon wafer and filter. Generated ZnO were collected by cleaned silicon wafer ($1 \times 1 \text{ cm}^2$) at any position inside the quartz tube reactor which aims to study the growth mechanism of ZnO. Silicon wafer was held on the cooling tip, which make from brass as shown in figure 3.5. Silicon wafer was quenched by cooled water in order to enhance the collected efficiency and avoiding the growth of collected ZnO on the substrate. Moreover, Filter with diameter 4.9 mm was used for collect synthesized ZnO from the airborne at downstream process. Filter was held inside the holder filter as shown in figure 3.6.

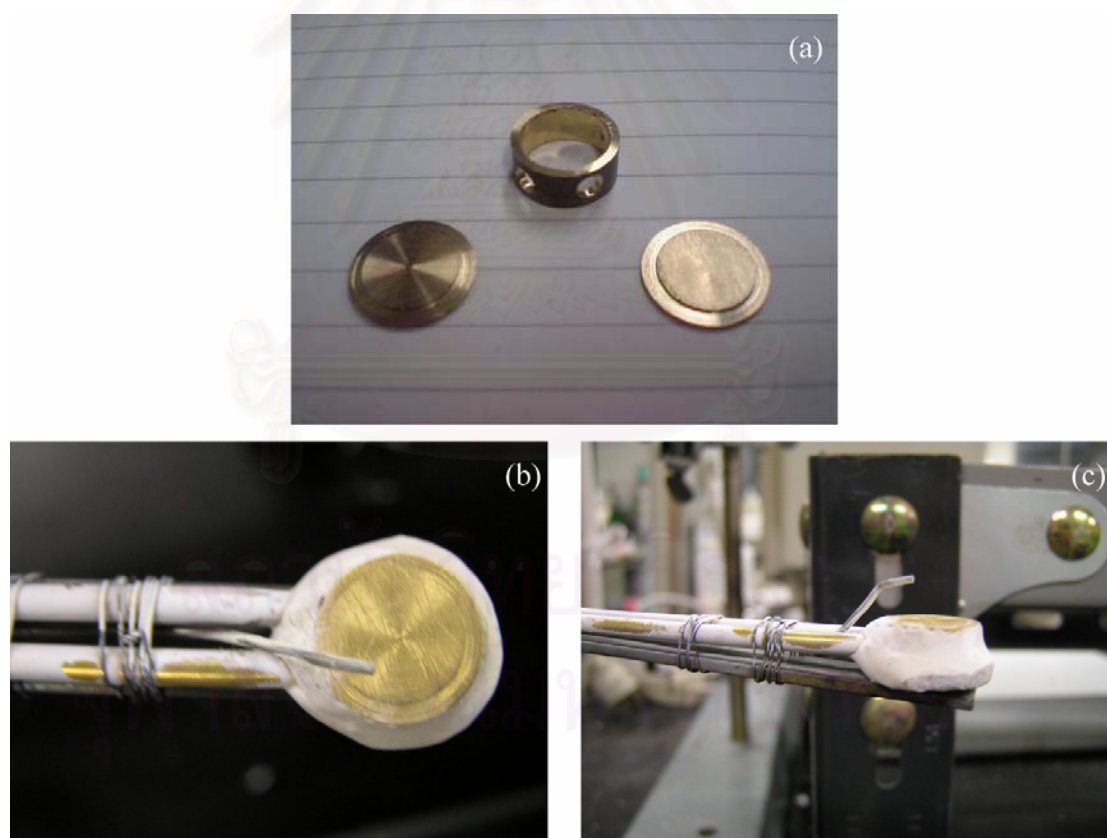


Figure 3.5 Cooling tip (a) before assembly, (b) top-view and (c) side-view.

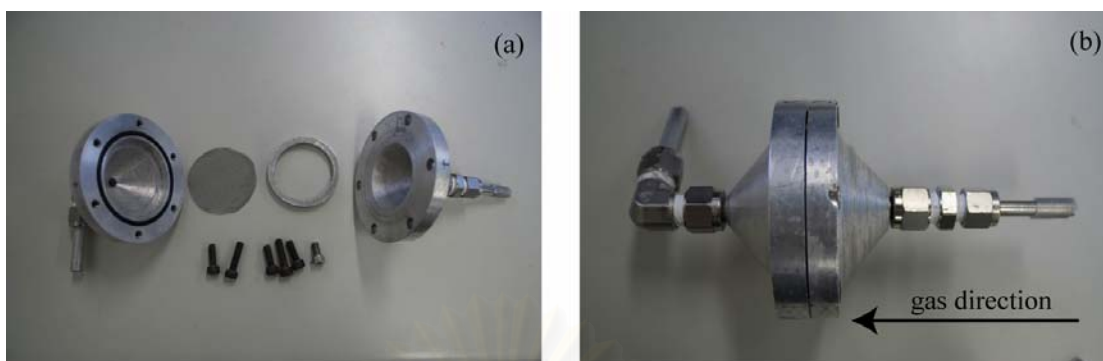


Figure 3.6 filter holder, (a) before assembly and (b) after assembly.

3.5 Experiment procedures

The experiment procedures of this work were separated into 4 parts as follow

3.5.1 The effect of evaporation temperature (T_{evp})

In this part, the effects of T_{evp} were studied toward the morphology, size and particle size distribution of synthesized ZnO. Therefore one electrical furnace was used for synthesized ZnO nanoparticles by varying evaporation temperature (500, 550, 600, 700 and 800°C). Synthesized ZnO nanoparticles were characterized by SEM and scanning mobility particle sizer (SMPS).

3.5.2 The effect of oxidation temperature (T_{oxi})

We studied the effect of T_{oxi} by using two electrical furnaces. First furnace was used for controlling evaporation temperature while the second furnace was used for controlling oxidation temperature. In this part, T_{evp} was set at 600°C and T_{oxi} was varied, 400, 500, 600 and 700°C. Nitrogen and air flow rate were also fixed at 1 L/min.

3.5.3 The effect of air and nitrogen flow rate

From literature reviews, partial pressure of reactant could effect to the morphology of synthesized ZnO. Therefore air and nitrogen flow rate were varied in our experimental set up. Both reactants flow rate were controlled by mass flow controller. However the maximum and the minimum flow rate were 2 and 0.1 L/min, respectively.

3.5.4 Studying the effect of mixing device (orifice)

Mixing device (orifice) was applied into experimental set up for studying the effect of interaction between zinc vapor and air at the initial stage. In this part, one and two electrical furnaces were used. Beside we also varied oxidation temperature because we want to study the main parameter that effect to the morphology of synthesized ZnO.

3.6 Analytical instruments

The instruments used to characterize the properties of synthesized ZnO are SEM (Hitachi, S 4500), XRD (Bruker AXS model D8 discover) and SMPS (model 3081) for finding the morphology and size, phase and particle size distribution respectively, while the concentration of both reactant inside the reactor were calculated by FLUENT simulation.

3.6.1 Scanning Electron Microscopy (SEM)

The deposition of ZnO nanoparticles on the surface of filter and silicon substrate were observed using SEM images. SEM specimens were prepared by cutting out a small piece of filter or ZnO formed on the surface of silicon substrate, and then directly placing the piece onto a conductive gold coated microscope grid. The specimens were loaded into a sample chamber, and observations were immediately

started using image catcher scanner for taking the photos. A photo of the Scanning Electron Microscopy (SEM) machine is shown in figure 3.7



Figure 3.7 Scanning Electron Microscope (SEM)

3.6.2 X-Ray Diffraction (XRD)

The XRD (Bruker AXS model D8 discover) was used to analyze phase of the investigated zinc oxide. Figure 3.8 shows the XRD analysis system used in this work. The ZnO sample was spread on the glass slide and then set in the equipment which provide x-ray beam for the analysis.



Figure 3.8 X-Ray Diffraction (XRD)

3.6.3 Scanning Mobility Particles Sizer (SMPS)

The SMPS (Model 3081, TSI) was used to analyze particle size distribution of ZnO nanoparticles in the airborne as shown in figure 3.9. SMPS consists of electrostatic classifier which has to use with differential mobility analyzer (DMA) as the main component for generating or sizing aerosol. For example given a polydisperse input aerosol, the instrument output can be a stream of monodisperse aerosol of known particle size. The number of monodisperse aerosol was counted by condensation particle counter (CPC).



Figure 3.9 Scanning Mobility Particles Sizer (SMPS)

สถาบันวิทยบริการ
จุฬาลงกรณ์มหาวิทยาลัย

CHAPTER IV

RESULT AND DISCUSSION

Referring to many experimental results reported in other previous works, this research has set its aim to study effect of synthetic parameters on the morphology of ZnO nanoparticles synthesized from gas phase reaction method. Effect of evaporation and oxidation temperature, gas flow rate and orifice variable on the morphologies and size of synthesized ZnO nanoparticles were thoroughly investigated and then reported and discussed in this chapter.

4.1 Effect of evaporation temperature (T_{evp})

At the beginning, we tried to study about the effect of evaporation temperature on the morphology and size of synthesized ZnO nanoparticles. The schematic diagram of experimental set up for studying the effect of evaporation temperature is shown in figure 4.1. The evaporation temperature was varied from 500 to 800°C. Air and nitrogen gas were introduced into the reactor at fixed flow rate 1L/min. Synthesized ZnO nanoparticles were collected at the outlet of the system for characterized by SEM and SMPS.

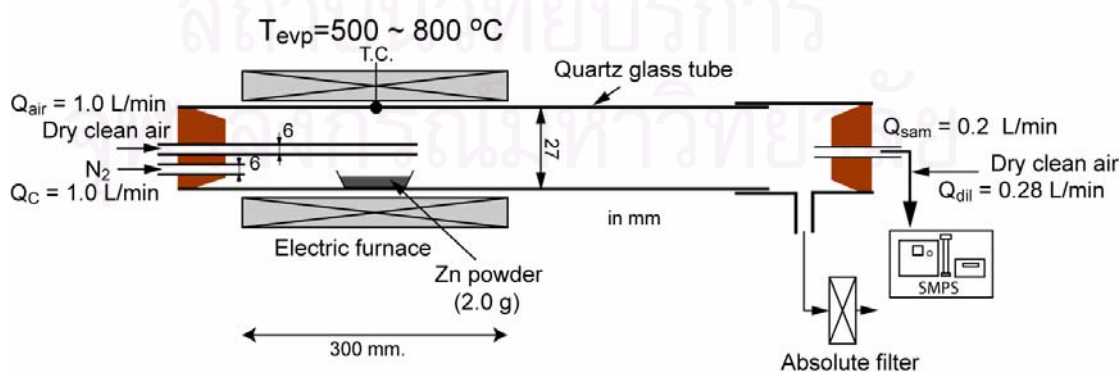


Figure 4.1 Schematic diagram of experimental set up for studying the effect of T_{evp} .

4.1.1 Temperature profile inside reactor

Temperature profile inside the reactor were mapped, as shown in figure 4.2. We found that temperature inside the reactor reached the desired temperature from 150 mm to 200 mm. Base on this data, the effective reaction zone for oxidation reaction is supposed to lay in the zone of 150 to 200 mm.

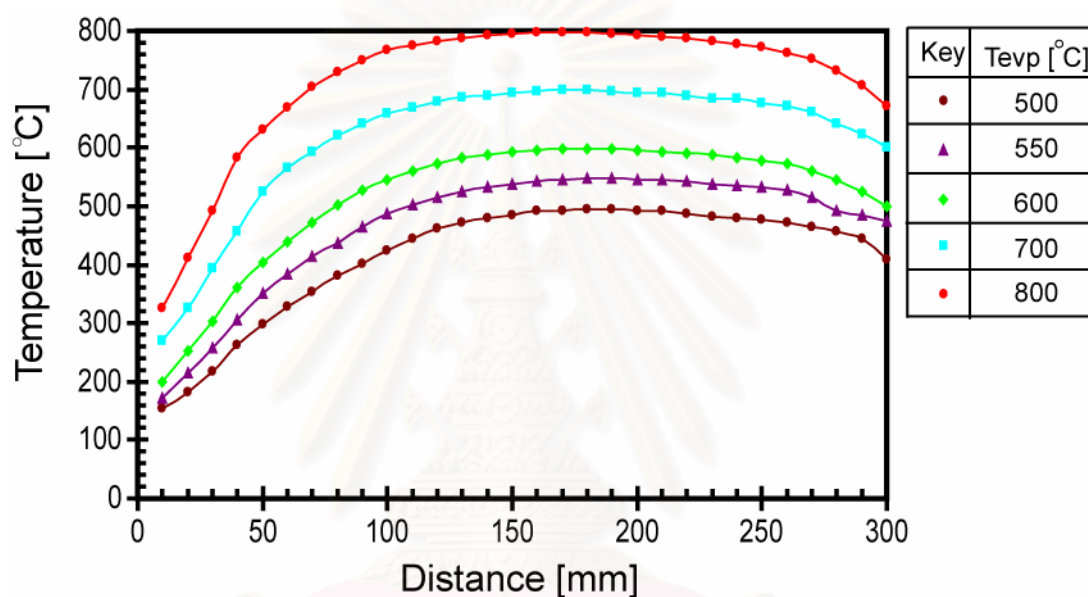


Figure 4.2 Temperature profiles inside reactor.

4.1.2 Particle size distribution (PSD) of synthesized ZnO by SMPS

The particle size distribution (PSD) of synthesized ZnO nanoparticle was collected at the outlet of experimental set up and then analyzed by scanning mobility particle sizer (SMPS). Figure 4.3 shows particle size distribution of synthesized ZnO nanoparticles, all of particle size distributions are normal size distribution curve. We found that particles size of synthesized ZnO nanoparticles was larger when evaporation temperature was increased. At evaporation temperature 500, 550, 600, 700 and 800°C, the average size of ZnO nanoparticles is 41, 127, 279, 514 and 573 nm respectively.

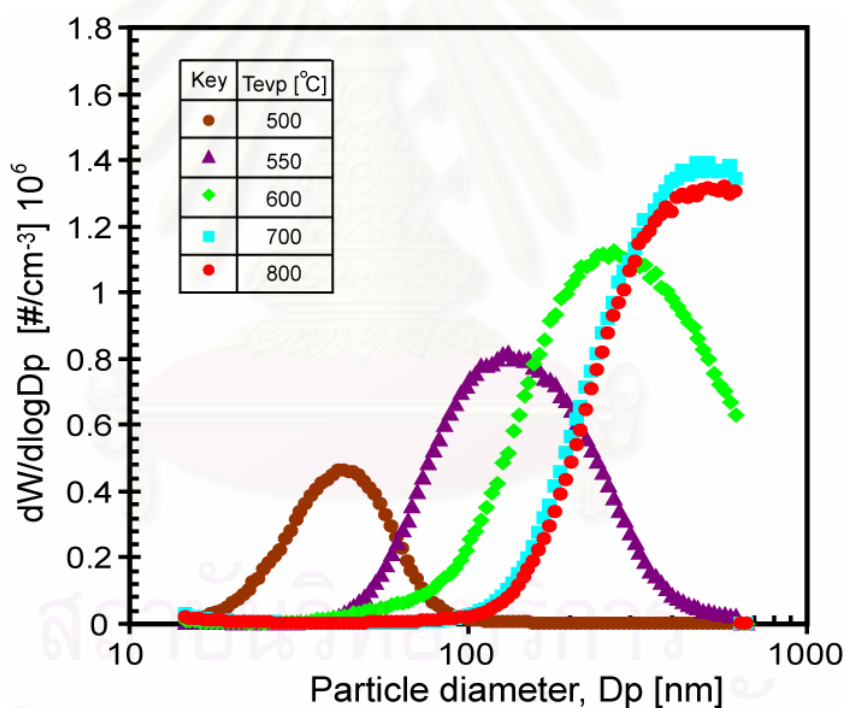


Figure 4.3 Particle size distribution of ZnO nanoparticle by varying evaporation temperature.

4.1.3 Morphology of ZnO nanoparticles

Morphology of synthesized ZnO nanoparticles were also characterized by scanning electron microscopy (SEM). SEM micrographs in figure 4.4 show that morphology of ZnO nanoparticles was rather spherical shape when evaporation temperature was varied from 500 to 600 °C. However at evaporation temperature of 700 and 800 °C, morphology of ZnO nanoparticles turned to spherical and tetrapod shapes.

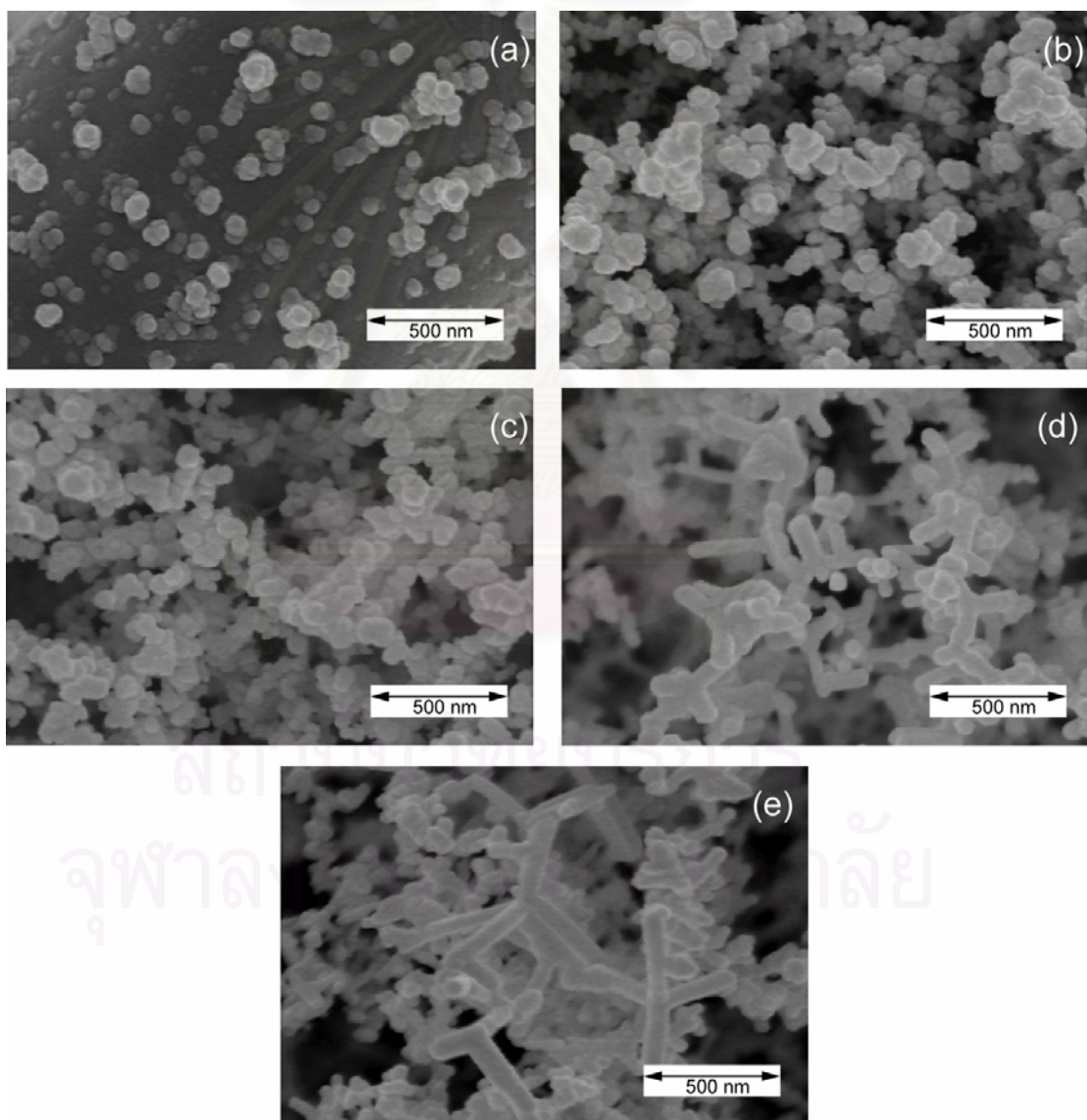


Figure 4.4 SEM micrographs of ZnO nanoparticles collected by filter (a) T_{evp} 500 °C, (b) T_{evp} 550 °C, (c) T_{evp} 600 °C and (d) T_{evp} 700 °C and (e) T_{evp} 800 °C.

Partial pressure of zinc vapor and oxygen were calculated as shown in figure 4.5. We found that partial pressure of zinc vapor increased when evaporation temperature was increased.

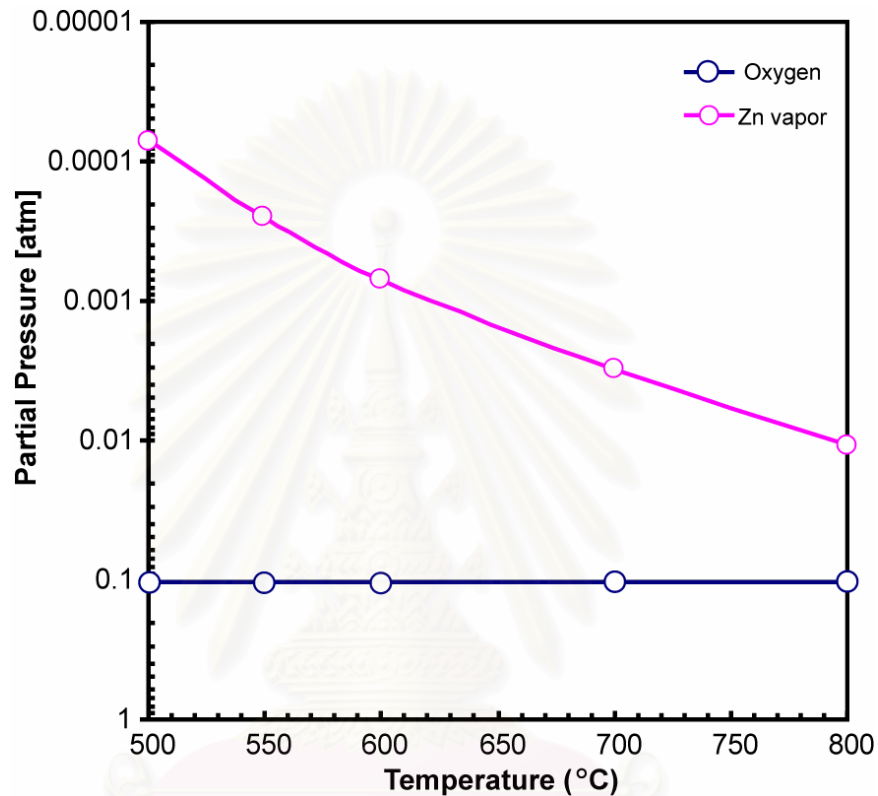


Figure 4.5 Partial pressure of zinc vapor and oxygen by varying evaporation temperature.

We also calculated the rate constant of zinc oxidation as shown in equation 4.1

$$-\ln k_{Zn} = -10.3 + 1.56 \times \frac{10^4}{T} \quad (4.1)$$

k_{Zn} is rate constant of zinc oxidation [min^{-1}] and T is temperature of reactor [K]

This equation was proposed by Delalu et al. (2000) who investigated the kinetics of the complete oxidation of zinc powder by oxygen and air. It could be observed that rate constant of zinc increased when evaporation temperature was increased as shown in figure 4.6. The increasing temperature could promote the reaction rate of ZnO formation which in term affected the morphology and size of ZnO.

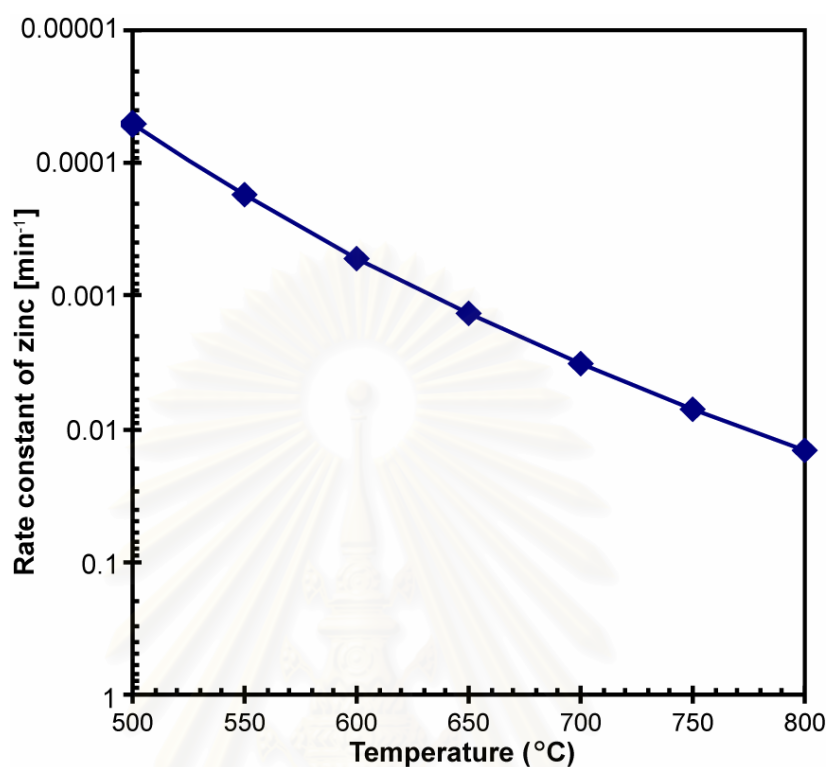


Figure 4.6 Rate constant of zinc by varying evaporation temperature

From above results, morphology of synthesized ZnO nanoparticles changed from spherical to tetrapod shape when evaporation temperatures were increased. Therefore morphology and size of ZnO nanoparticles relate with partial pressure of zinc vapor and kinetic reaction of ZnO.

สถาบันวิทยบริการ
จุฬาลงกรณ์มหาวิทยาลัย

4.1.4 Effect of amount of zinc powder

From the above results, it could be implied that evaporation temperature and zinc partial pressure could affect morphology and size of ZnO nanoparticles. However zinc vapor partial pressure also depends on evaporation temperature because more zinc powder can be vaporized when the system temperature was increased. It is necessary to find out the dominating factor that affects morphology and size of ZnO nanoparticles. Therefore amount of zinc raw material was changed from 2 to 4 g at same evaporation temperature.

Particle size distribution in figure 4.7 shows that average size of ZnO nanoparticles changed from 41 to 102 nm and from 250 to 359 nm when amount of zinc powder was increased from 2 to 4 g at evaporation temperature 500 and 600°C, respectively.

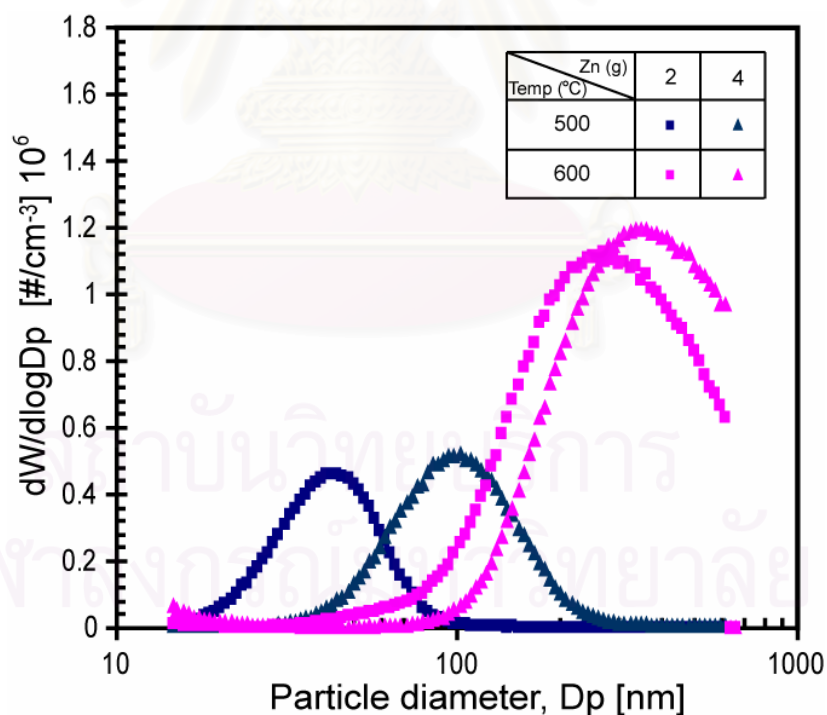


Figure 4.7 Particle size distribution of ZnO nanoparticle by varying amount of zinc raw material.

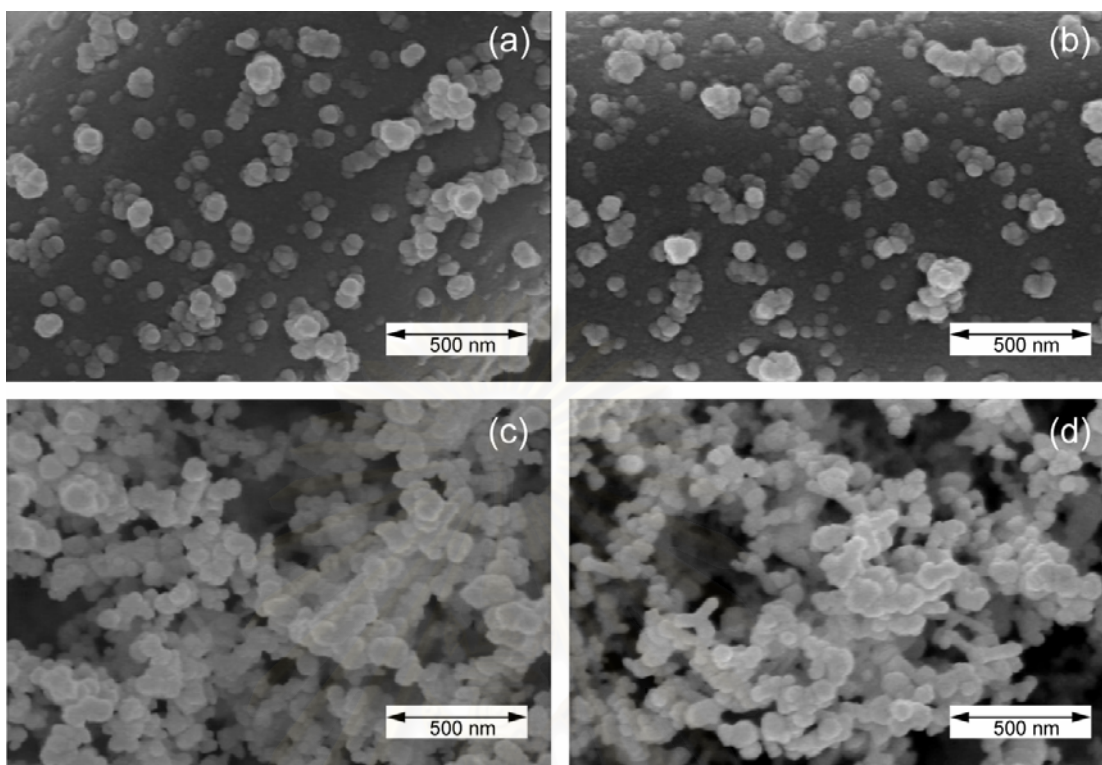


Figure 4.8 SEM micrographs of synthesized ZnO particles with fixed air and nitrogen flow rate at 1 L/min, at $T_{evp}500^{\circ}\text{C}$ (a) 2g, (b) 4g, at $T_{evp}600^{\circ}\text{C}$ (c) 2g and (d) 4g.

SEM micrographs in figure 4.8 reveal that morphology of ZnO nanoparticles in all conditions is only spherical shape. Zinc vapor partial pressure inside the reactor was also calculated. We found that partial pressure of zinc vapor increased twice when amount of zinc raw material was increased from 2 to 4g. From this result, zinc partial pressure affected significantly the size of ZnO nanoparticles and affected slightly the shape of ZnO nanoparticles.

จุฬาลงกรณ์มหาวิทยาลัย

4.1.5 Effect of air flow rate

The effect of air flow rate was studied by changing from 0.5 to 2 L/min and nitrogen flow rate was fixed at 1 L/min. Evaporation temperature was fixed at 600°C. SEM micrographs in figure 4.9 reveal that all ZnO nanoparticles were spherical shape, although air flow rate was changed.

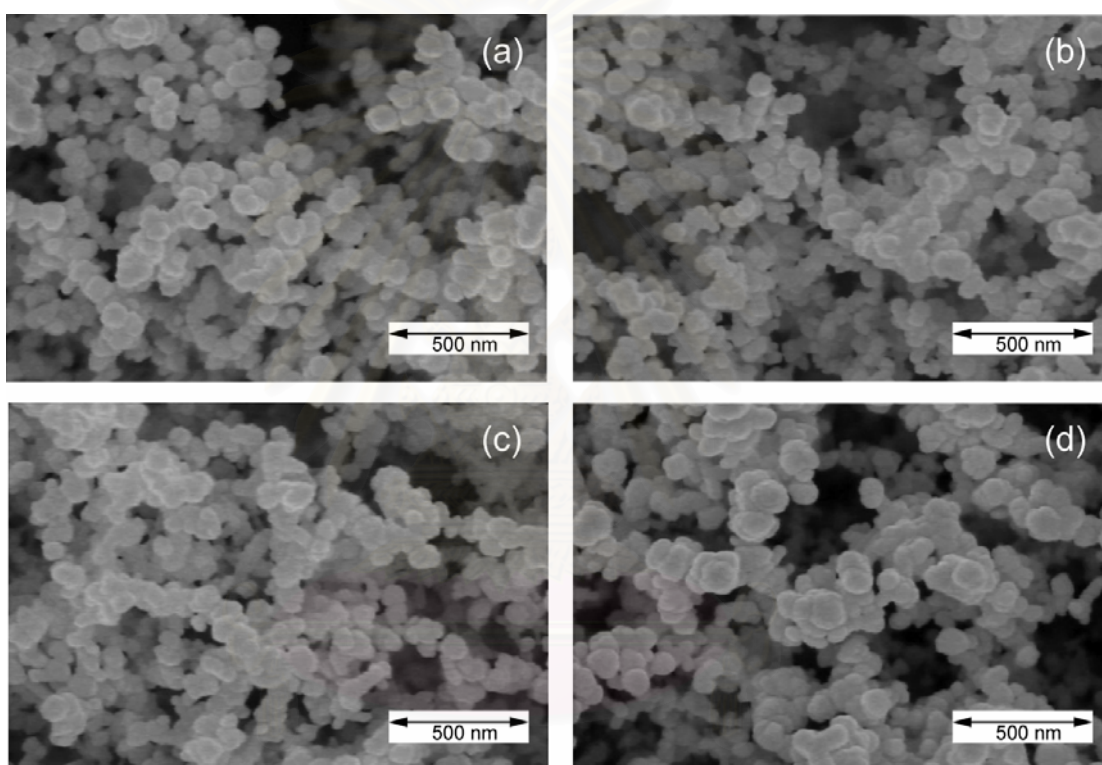


Figure 4.9 SEM micrographs of ZnO nanoparticles with fixed nitrogen flow rate at 1 L/min, evaporation temperature 600°C and varied air flow rate (a) 0.5, (b) 1, (c) 1.5 and (d) 2 L/min.

4.1.6 Effect of nitrogen flow rate

Nitrogen flow rate was changed from 1 to 2 L/min, while air flow rate was kept constant at 1 L/min in all experiments. Figure 4.10 shows that all synthesized ZnO nanoparticles were still spherical shape even though nitrogen flow rate was changed from 1 to 2 L/min.

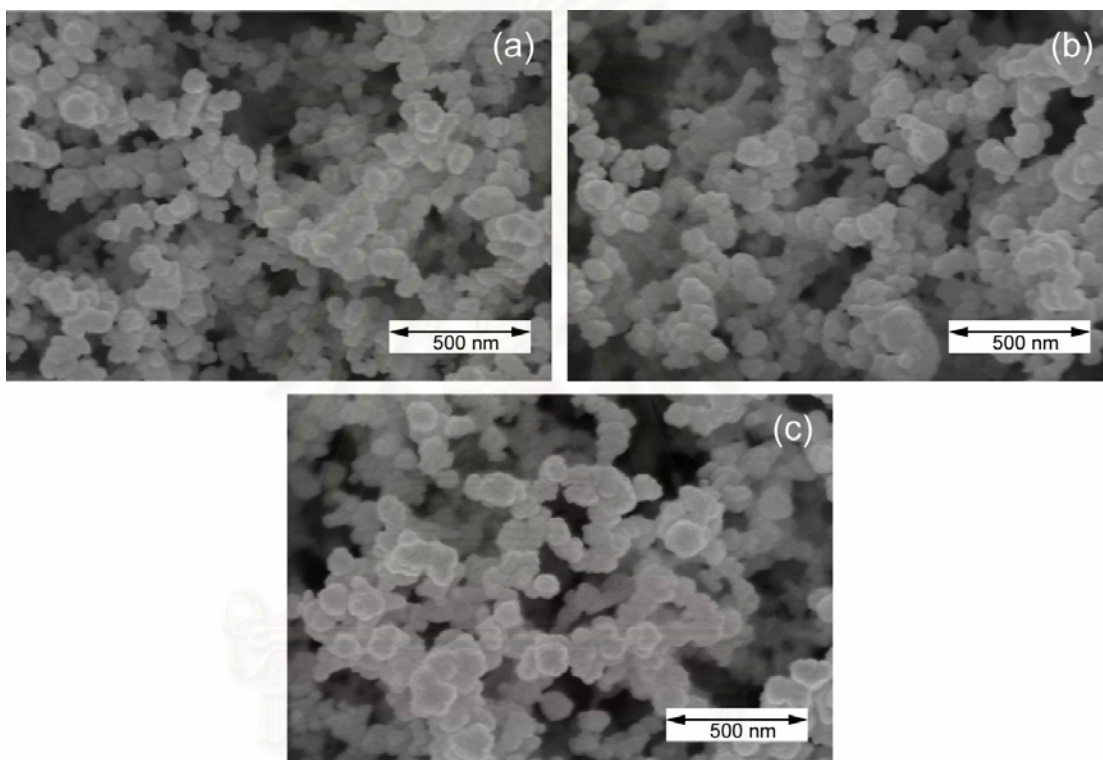


Figure 4.10 SEM micrographs of ZnO nanoparticles with fixed air flow rate at 1 L/min, T_{evp} 600°C and varying nitrogen flow rate (a) 1, (b) 1.5, (c) 2 L/min.

In section 4.1, the morphologies of synthesized ZnO nanoparticles at high evaporation temperature (700 and 800°C) consist of spherical and tetrapod shape. We think the interaction between zinc vapor and oxygen occurred by diffusion force from concentration gradient only. Therefore the oxidation reaction at any cross section inside quartz tube is not same because air was released at the center of quartz tube resulting in high oxygen concentration at the center of quartz tube. Without any mixing control, it is difficult to synthesize uniform size and desired shape of ZnO

nanoparticles. So we should apply mixing device for enhance the mixing between zinc vapor and oxygen.

4.2 Effect of oxidation temperature (T_{oxi}) and mixing device (orifice)

Since primary principal of our research, the reactor was considered and divided into two zones. The first zone is the evaporation zone and we already studied by adjusting evaporation temperature in section 4.1. The second zone is oxidation zone which aim to study about the growth mechanism of synthesized ZnO nanoparticles. Therefore we apply the second furnace into experimental set up as shown in figure 4.11.

4.2.1 Effect of oxidation temperature (T_{oxi}) without mixing device

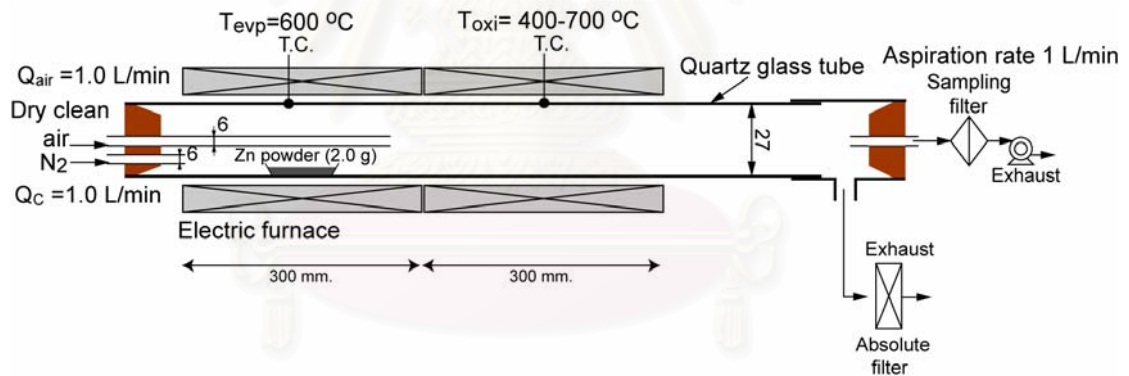


Figure 4.11 Schematic diagram of experimental set up for studying the effect of oxidation temperature without mixing device.

In this section air and nitrogen flow rates were fixed at 1.0 L/min. The evaporation temperature was set at 600°C because the amount of synthesized ZnO at 500 and 500 °C was too small. While the morphology of synthesized ZnO at 700 and 800°C was complicated as could be observed in figure 4.14. The oxidation temperature was varied from 400 to 700°C. Temperature profiles inside the reactor were also measured and mapped using a thermocouple monitoring as shown in figure

4.12. Because of limitation of measurement instrument, temperature profiles were measured from 130 to 730 mm started from first furnace inlet.

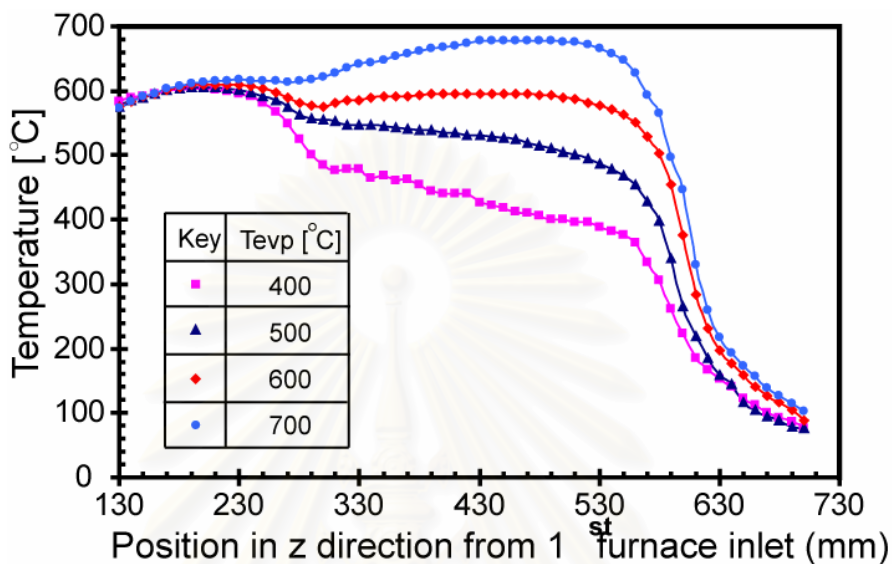


Figure 4.12 Temperature profiles inside reactor by varying oxidation temperature without mixing device.

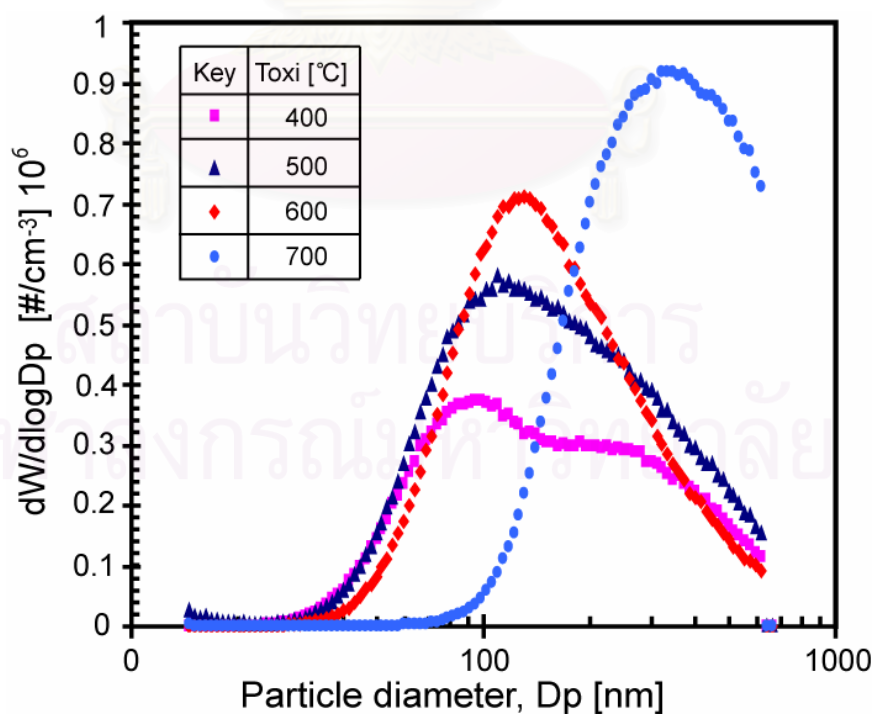


Figure 4.13 Particle size distribution of ZnO nanoparticle by varying oxidation temperature without mixing device.

Synthesized ZnO nanoparticles were collected at the outlet of the reactor by filter. Figure 4.14 shows the morphology of synthesized ZnO nanoparticles on filter. We found that all synthesized ZnO nanoparticles had a spherical shape. From figure 4.13, particle size distribution of ZnO nanoparticles at 400°C was bimodal shape. As we could observe from figure 4.14a that size of ZnO nanoparticles was polydisperse. While other oxidation temperatures, particle size distribution was unimodal shape. At 500 and 600°C, size of ZnO nanoparticles was a little different. However average size of ZnO at 700°C increased from 100 to 320 nm.

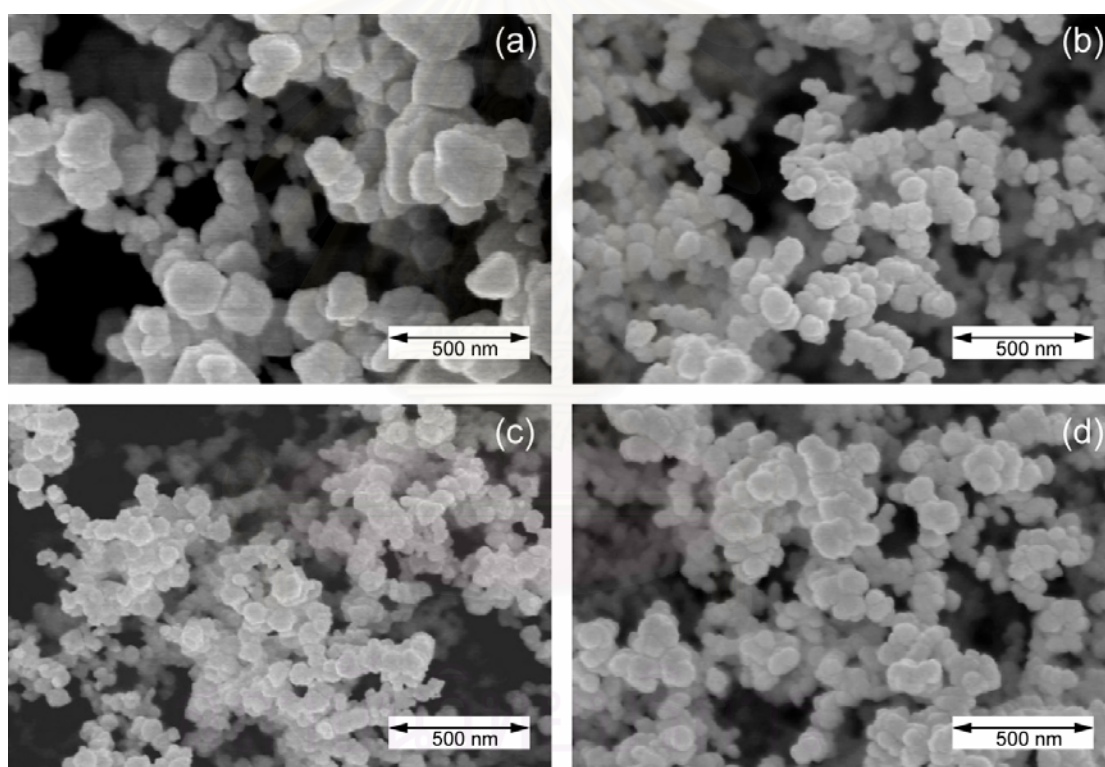


Figure 4.14 SEM micrograph of synthesized ZnO nanoparticles collected by filter (a) T_{oxi} 400 °C, (b) T_{oxi} 500 °C, (c) T_{oxi} 600 °C and (d) T_{oxi} 700 °C, without mixing device.

4.2.2 Effect of oxidation temperature (T_{oxi}) with mixing device

In this part, we used a mixing device for enhance mixing between zinc vapor and oxygen as shown in schematic diagram in figure 4.15. From figure 4.16, we found that temperature profile in the systems without and with orifice were almost same. Therefore orifice did not affect temperature profile inside reactor.

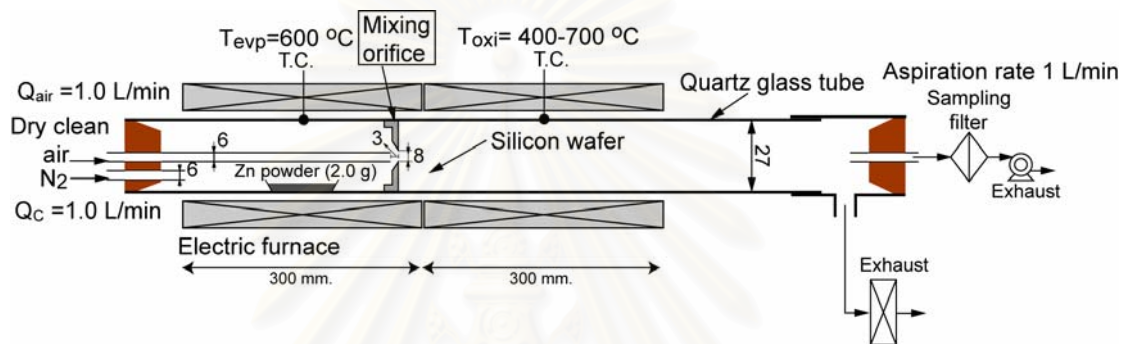


Figure 4.15 Schematic diagram of experimental set up for studying the effect of oxidation temperature with mixing device.

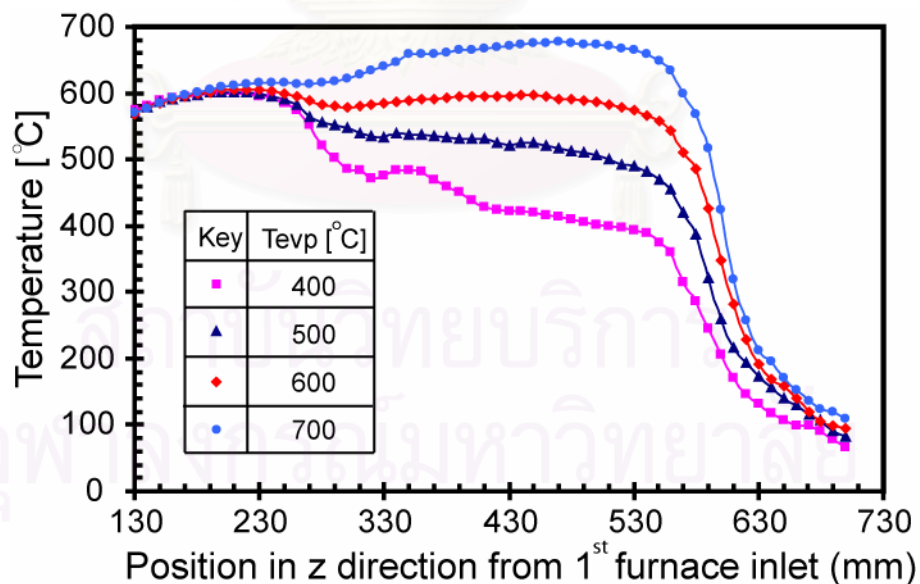


Figure 4.16 Temperature profiles inside reactor by varying oxidation temperature with mixing device.

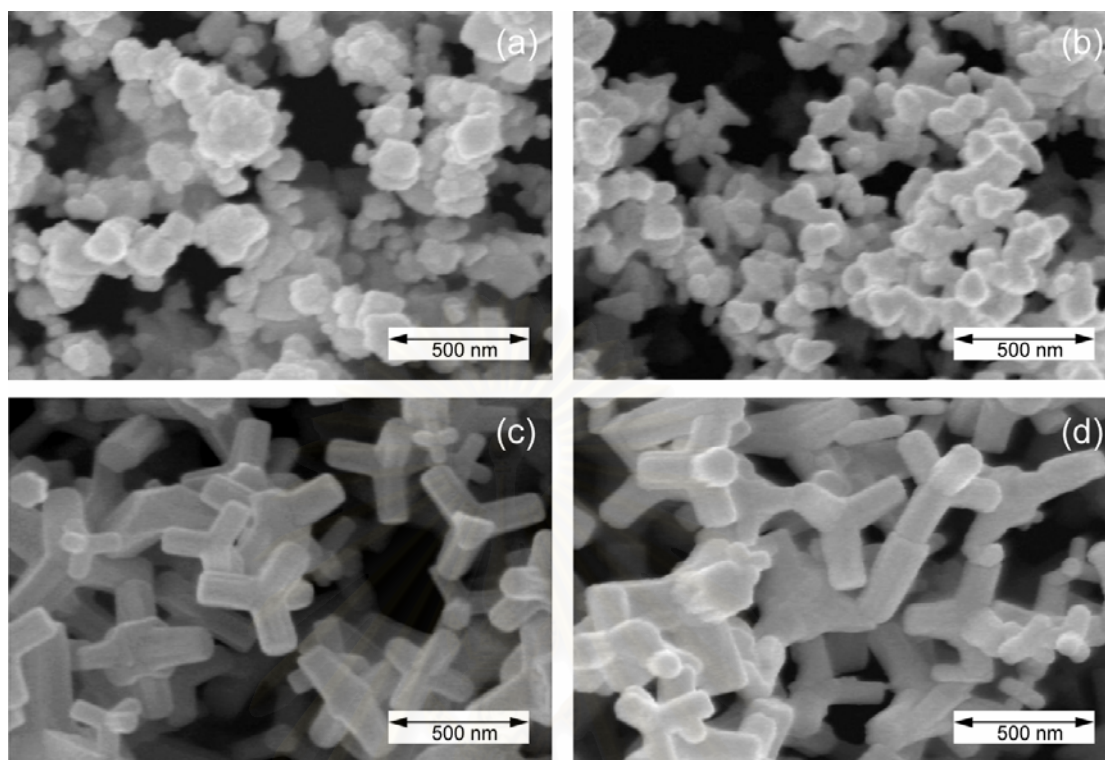


Figure 4.17 SEM micrograph of ZnO nanoparticles collected by filter (a) T_{oxi} 400 °C, (b) T_{oxi} 500 °C, (c) T_{oxi} 600 °C and (d) T_{oxi} 700 °C, with mixing device.

Typical SEM micrographs in figure 4.17 show that morphology of ZnO nanoparticles changed from spherical to tetrapod shape when oxidation temperatures were increased. At oxidation temperature of 400°C, ZnO nanoparticles were spherical shape with 110 nm in diameter. When oxidation temperature increased to 500°C, we could observe both spherical and tetrapod shape. The average particles size was 140 nm. However tetrapod shape had short leg and sharp tip. While at 600 and 700 °C, ZnO nanoparticles exhibited tetrapod shape with uniform diameter leg and hexagonal facet. The size of the legs of tetrapod is about 80-300 nm in diameter and 100-400 nm in length. These results agree with the result from section 4.1 that the morphology of ZnO nanoparticles changed from sphere to tetrapod shape as temperature increased.

4.3 Effect of gas flow rate to the morphologies of ZnO nanoparticles with mixing device and 2nd furnace.

In this part, air and nitrogen flow rate were changed for studying the effect of gas flow rate. Base on the results in part 4.2.2, uniform tetrapod ZnO nanoparticles with hexagonal facet could be synthesized when orifice and 2nd furnace were applied into the experimental set up. Therefore, we also use same experimental set up as shown in figure 4.15. 2nd furnace temperature was fixed at 600°C because this temperature could produce uniform tetrapod ZnO nanoparticles.

4.3.1 Effect of air flow rate

Due to the limitation of experimental apparatus, air flow rate were varied from 0.2 to 2 L/min. As while, nitrogen flow rate was fixed at 1L/min.

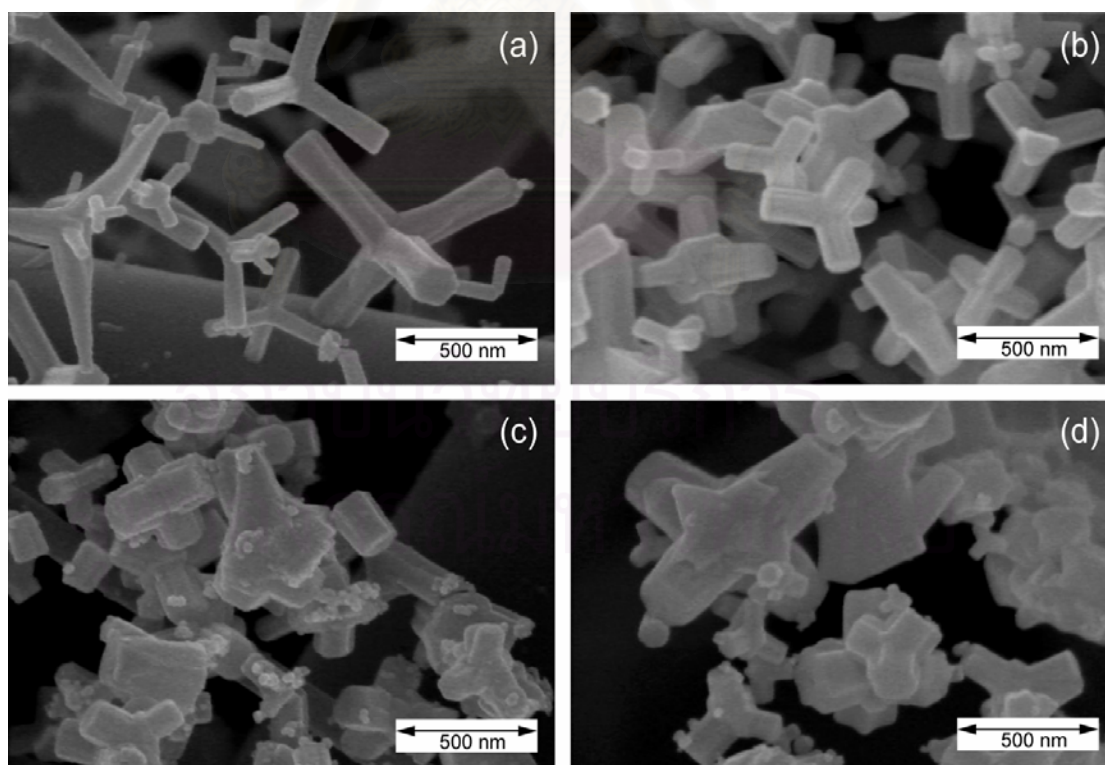


Figure 4.18 SEM micrographs of ZnO nanoparticles by varying air flow rate (a) 0.2, (b) 1, (c) 1.5 and (d) 2 L/min, with nitrogen flow rate 1 L/min.

At air flow rate 0.2 L/min, the lowest air flow rate, synthesized ZnO nanoparticles were tetrapod shape with two types of needles as shown in figure 4.18a. The first one was hexagonal facet with uniform diameter throughout the needle. The other one was sharp needle. Figure 4.18b shows that ZnO nanoparticles were tetrapod shape with hexagonal facet needles when air flow rate was 1 L/min. As while air flow rates were increased to 1.5 and 2 L/min, synthesized ZnO particles were bigger and shape of ZnO nanoparticles was polyhedral shape.

4.3.2 Effect of nitrogen flow rate

Nitrogen flow rate were also investigated by varying from 1 to 2 L/min with air flow rate 0.2 and 1 L/min. From figure 4.19 and 4.20, morphologies of ZnO nanoparticles slightly depend on nitrogen flow rate. On the other hand, when air flow rate was changed from 0.2 to 1 L/min, the morphologies of needle were changed from sharp tip needles to hexagonal facet with uniform diameter throughout the length. Partial pressure of oxygen was also calculated as shown in figure 4.21. We found that the partial pressure of oxygen was between 0.02 and 0.04, needles of tetrapod ZnO nanoparticles were small diameters with sharp tip. As while partial pressure of oxygen were value between 0.07 and 1, needles of tetrapod ZnO nanoparticles were larger diameter with hexagonal facet. When partial pressure was higher than 0.12, ZnO nanoparticles grew to polyhedral shape. Therefore the needles of tetrapod ZnO were smaller diameter and longer length when oxygen partial pressure decreased.

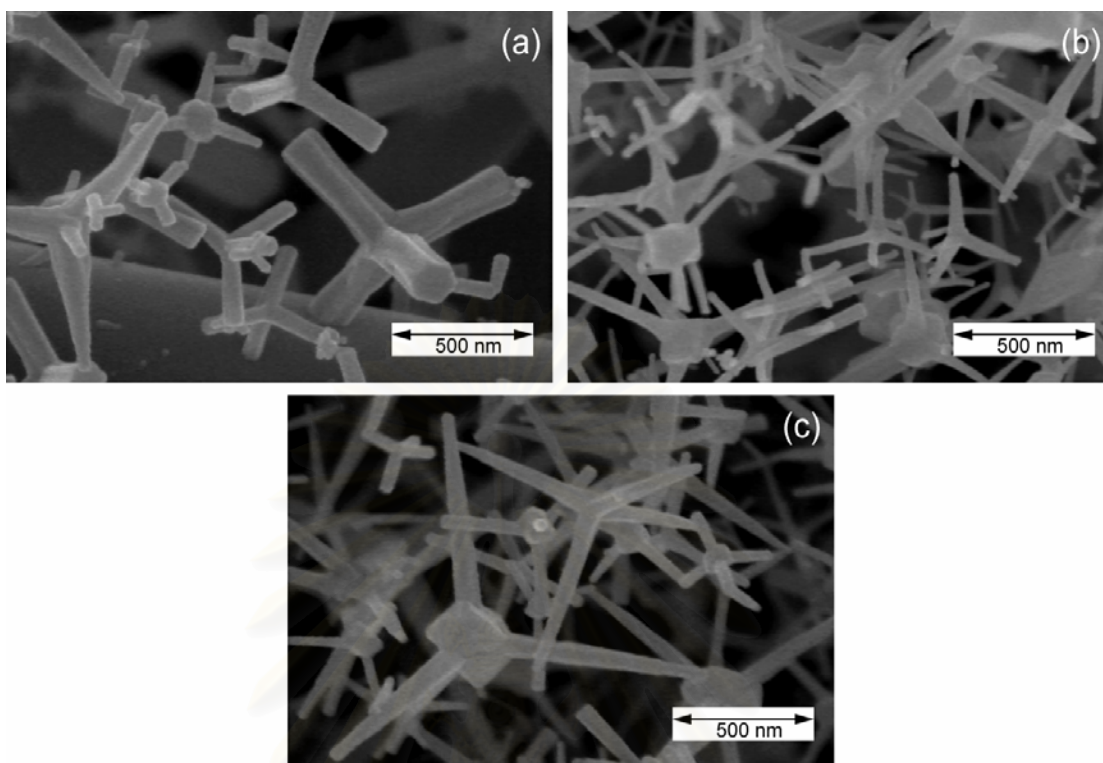


Figure 4.19 SEM micrographs of ZnO nanoparticles by varying nitrogen flow rate (a) 1, (b) 1.5 and (c) 2 L/min, with air flow rate 0.2 L/min.

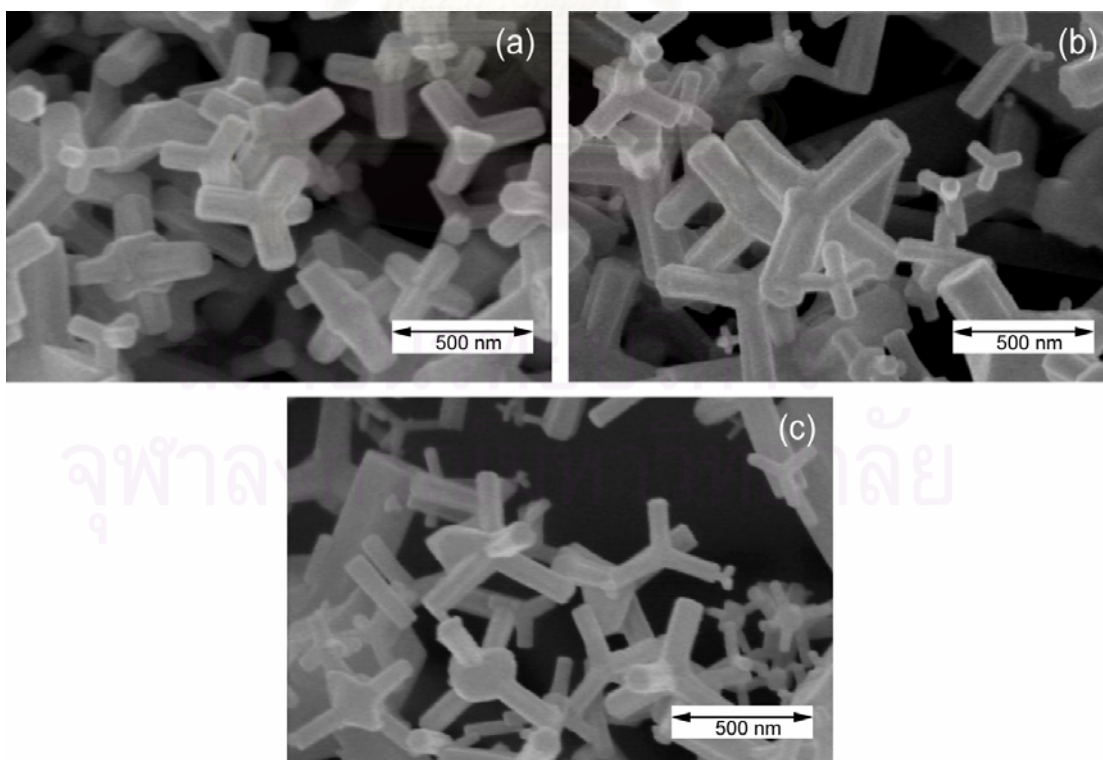


Figure 4.20 SEM micrographs of ZnO nanoparticles by varying nitrogen flow rate (a) 1, (b) 1.5 and (c) 2 L/min, with air flow rate 1 L/min.

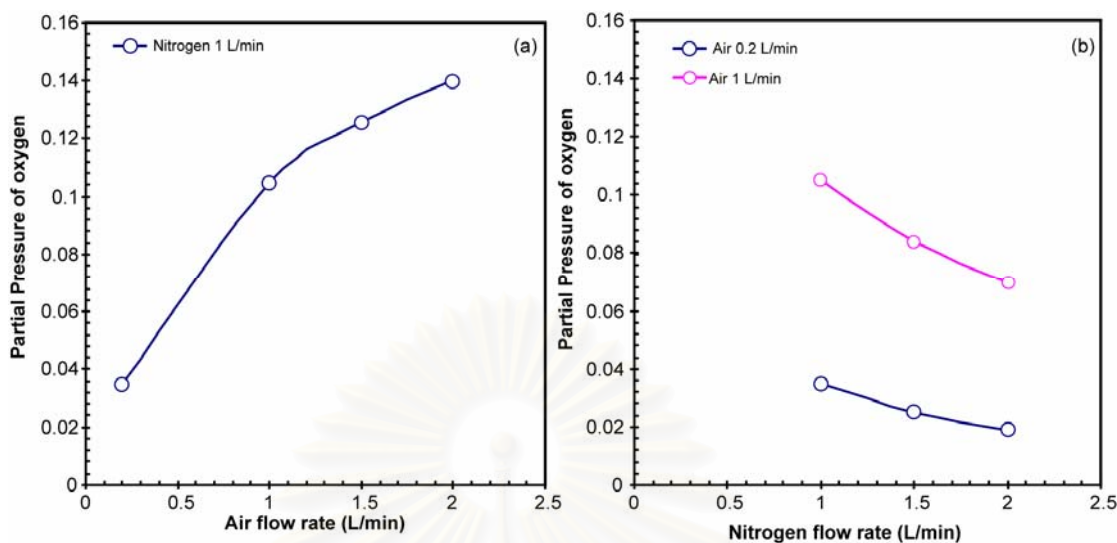


Figure 4.21 Partial pressure of oxygen by varying nitrogen and air flow rate, (a) vary nitrogen flow rate, (b) vary oxygen flow rate.

Based on these results, air flow rate could exert more significant effect on morphology of ZnO nanoparticles than nitrogen flow rate.

4.4 Study growth mechanism of ZnO nanoparticles by gas phase reaction

From literature reviews, many groups studied and proposed about the growth mechanism of ZnO nanoparticles. However the lack of experimental evidence of the earlier nucleation and the formation of the nucleus out of the gas phase, the growth mechanism of ZnO nanoparticles has still been controversial. Therefore we set experimental set up for investigating the growth mechanism of ZnO nanoparticles.

4.4.1 Collecting ZnO nanoparticles by silicon wafer

For studying the growth mechanism of ZnO nanoparticles, we used silicon wafer as substrate for collecting synthesized ZnO nanoparticles at any position inside the reactor. Silicon wafer was put on stainless steel plate as shown in figure 4.22a and then stainless steel plate was inserted into the second furnace. Figure 4.22b shows that we could observe white particle on silicon wafer after the experiment finished.

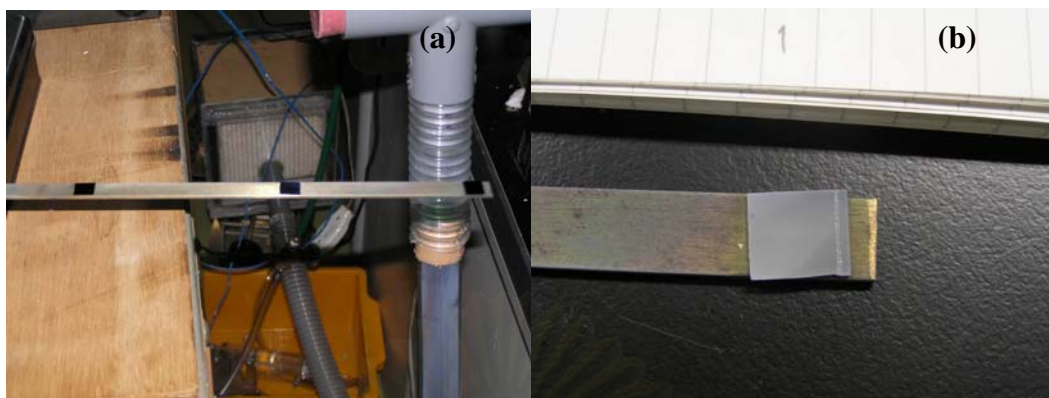


Figure 4.22 Silicon wafer, (a) before experiment (b) after experiment

In this part, evaporation and oxidation temperatures were set at 600°C because temperature inside reactor was almost same throughout the heating zone. Air and nitrogen flow rate were set at 1 L/min. Morphologies of synthesized ZnO nanoparticles on silicon wafer were characterized by SEM as shown in figure 4.23. At 1 and 10 cm, ZnO nanoparticles had rod shape with polyhedral and hexagonal facet. At 20 cm, ZnO nanoparticles exhibited tetrapod and rod shape. We could observe that agglomerations between tetrapod ZnO nanoparticles took place at 30 cm. At 40 cm, few of tetrapod ZnO nanoparticle were deposited on silicon substrate. We think the growth process of ZnO nanoparticles occurred on the surface of substrate at 1, 10 and 20 cm. From figure 4.16, temperature profile from 1 to 20 cm was excessively high. Then oxidation reaction between zinc vapor and oxygen could occur on the surface of substrate resulting in growth of ZnO nanoparticles. However, we wanted to use silicon substrate for collecting generated ZnO from the airborne. Therefore a cooling tip was made for collecting ZnO nanoparticles from airborne as shown in figure 3.6. We think that quenched silicon substrate could enhance the collected efficiency and avoid the growth on silicon substrate.

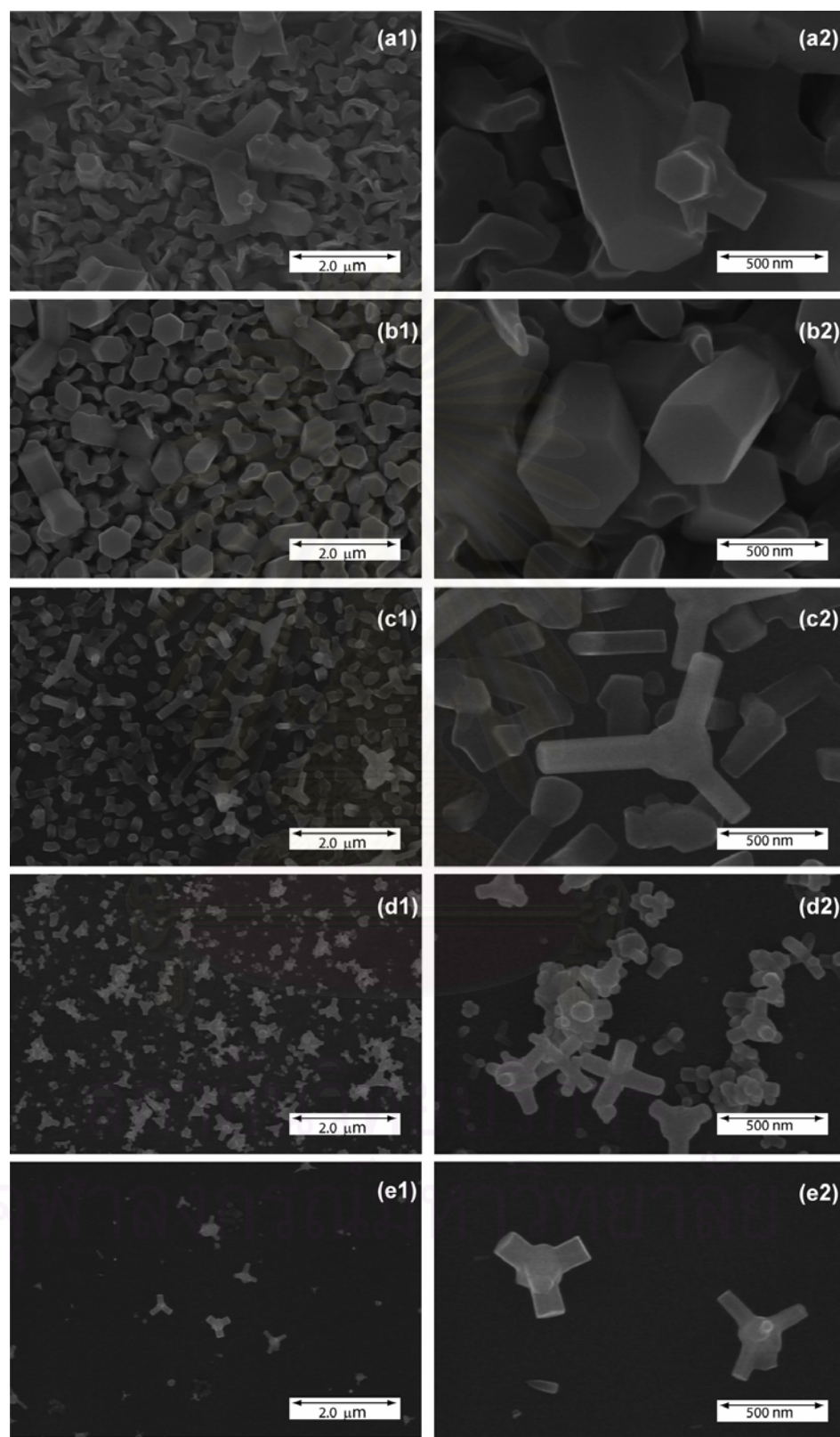


Figure 4.23 SEM images of ZnO nanoparticles in 2nd furnace (a) 1, (b) 10, (c) 20, (d) 30, (e) 40cm.

4.4.2 Effect of orifice on morphologies of ZnO nanoparticles

In this part, we study the effect of orifice by using two set of experimental set up as shown in figure 4.24. Besides we applied cooling tip into our experimental set up. Synthesized ZnO nanoparticles were collected at 1 and 30 cm from the entrance of the 2nd furnace as indicate by red arrow in figure 4.24 for studying growth mechanism of ZnO nanoparticles. Synthesized ZnO nanoparticles were also collected by filter.

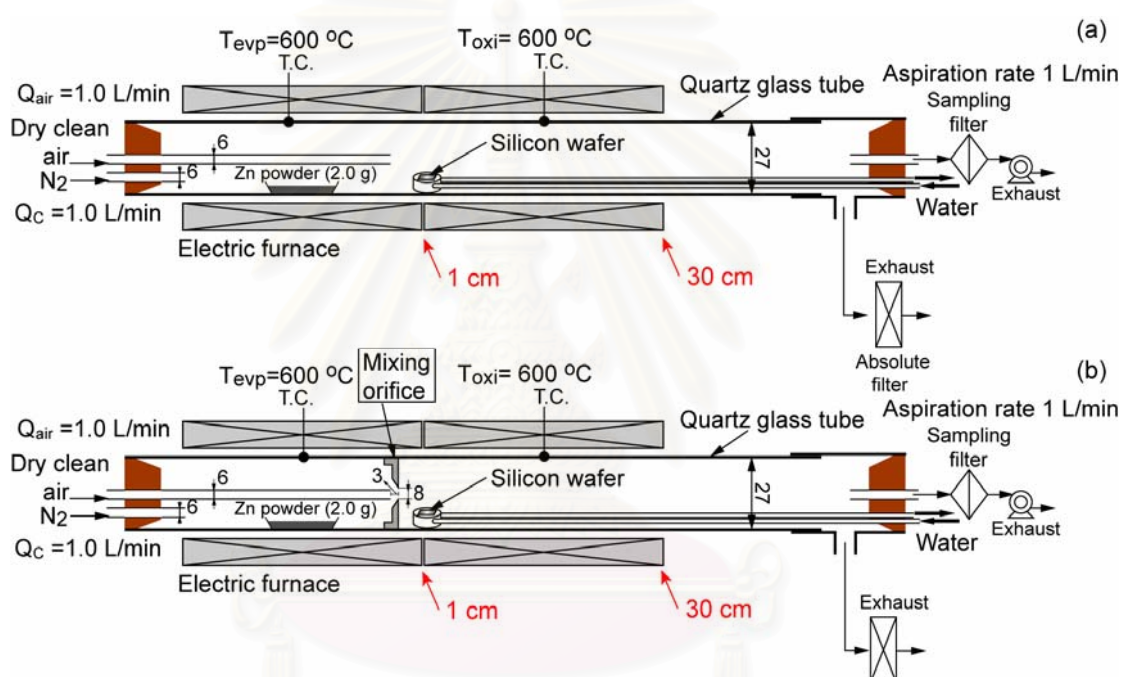


Figure 4.24 Schematic diagram of experimental set-up (a) without orifice and (b) with orifice.

Figures 4.25 and 4.26 show typical SEM micrographs of two different ZnO nanostructures which were collected by quench silicon wafer at 1 and 30 cm from inlet of second furnace. The morphologies of generated ZnO strongly depend on the existent of orifice. It could be observed that when orifice was not used, spherical structures were obtained at all collected position as shown in figure 4.25. The size of spherical particles is about 70-200 nm that was confirmed by particle size distribution in figure 4.27a. However, when orifice was inserted into the system as a mixing device, spherical structures were still obtained at 1 cm as shown in figure 4.26a. As

while tetrapod nanostructures were collected at 30 cm and filter as shown in Figure 4.26b and c. The size of the legs of tetrapod is about 80-300 nm in diameter and 100-400 nm in length. From this result, we claim that the formation process of tetrapod ZnO could divide into two stages. The first stage is the formation of nucleus as collected particles at 1cm and the second stage is the needle crystal growth of tetrapod nanostructures. This process is confirmed by Zhou et al. (2005). Zhou claimed that whole process of tetrapod ZnO generation was divided into two first order reactions as a nucleus formation period for 0.5-1.05 min and the needle crystal growth stage for 2.5-6 min. However, no photo evidence in their work. Thus one key and novel contribution of our work are the presentation of the first direct evidence in support of formation process of tetrapod ZnO where ZnO nucleus are generated at 1 cm then these ZnO nucleus grow to tetrapod ZnO nanostructures by crystallization. The second key contribution of this work is to report the effect of mixing device (orifice), by controlling the initial mixing between zinc vapor and oxygen which affected the morphology of synthesized ZnO nanoparticles, as discussed later.

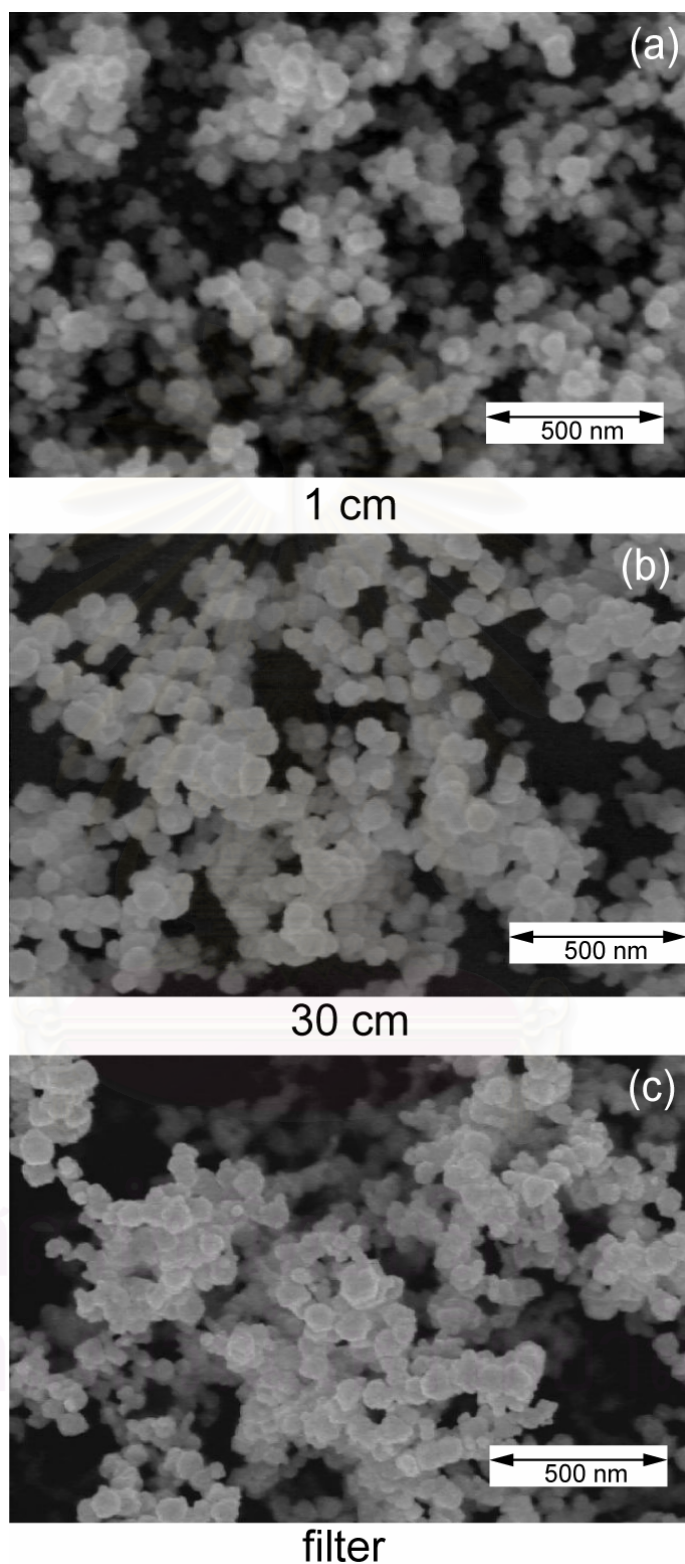


Figure 4.25 SEM micrographs of ZnO nanoparticles collected by quenched silicon wafer under various position from 2nd furnace inlet without mixing device (a) 1, (b) 30 cm and (c) filter.

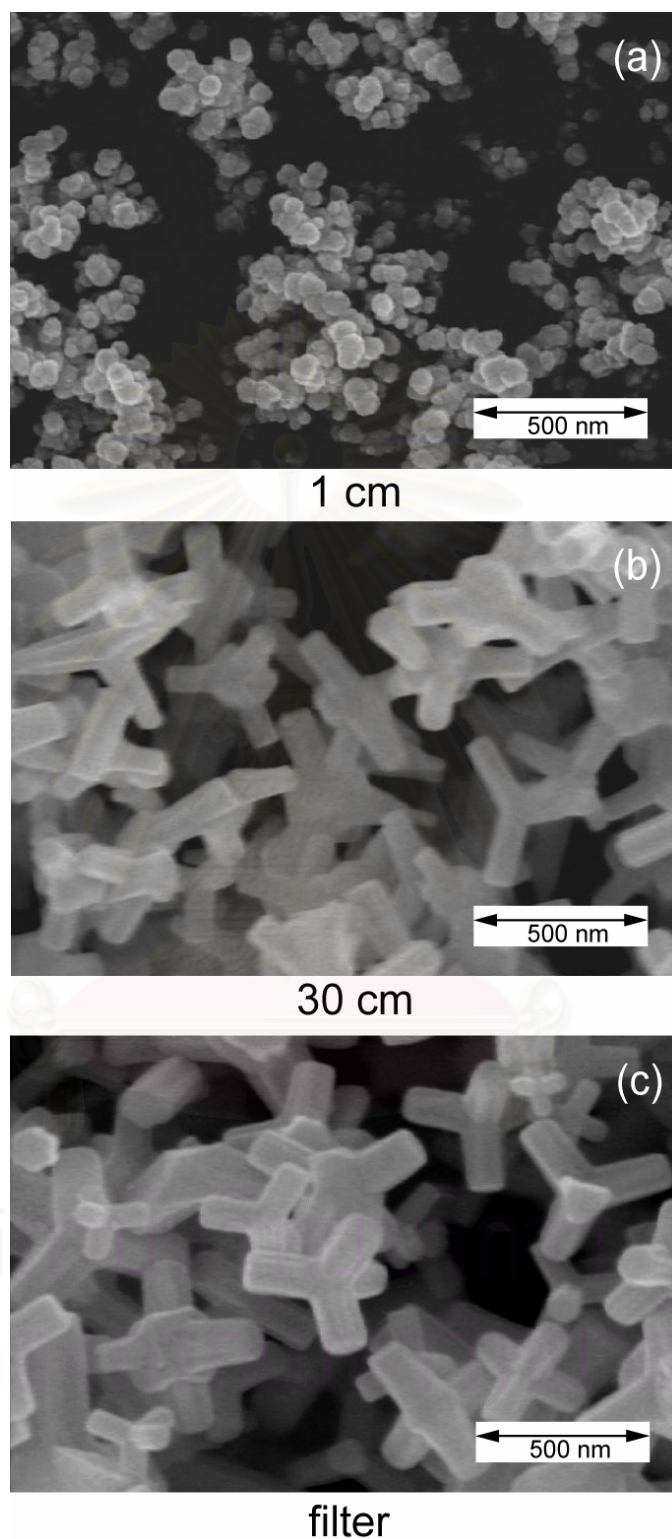


Figure 4.26 SEM micrographs of ZnO nanoparticles collected by quenched silicon wafer under various position from 2nd furnace inlet with mixing device (a) 1, (b) 30 cm and (c) filter.

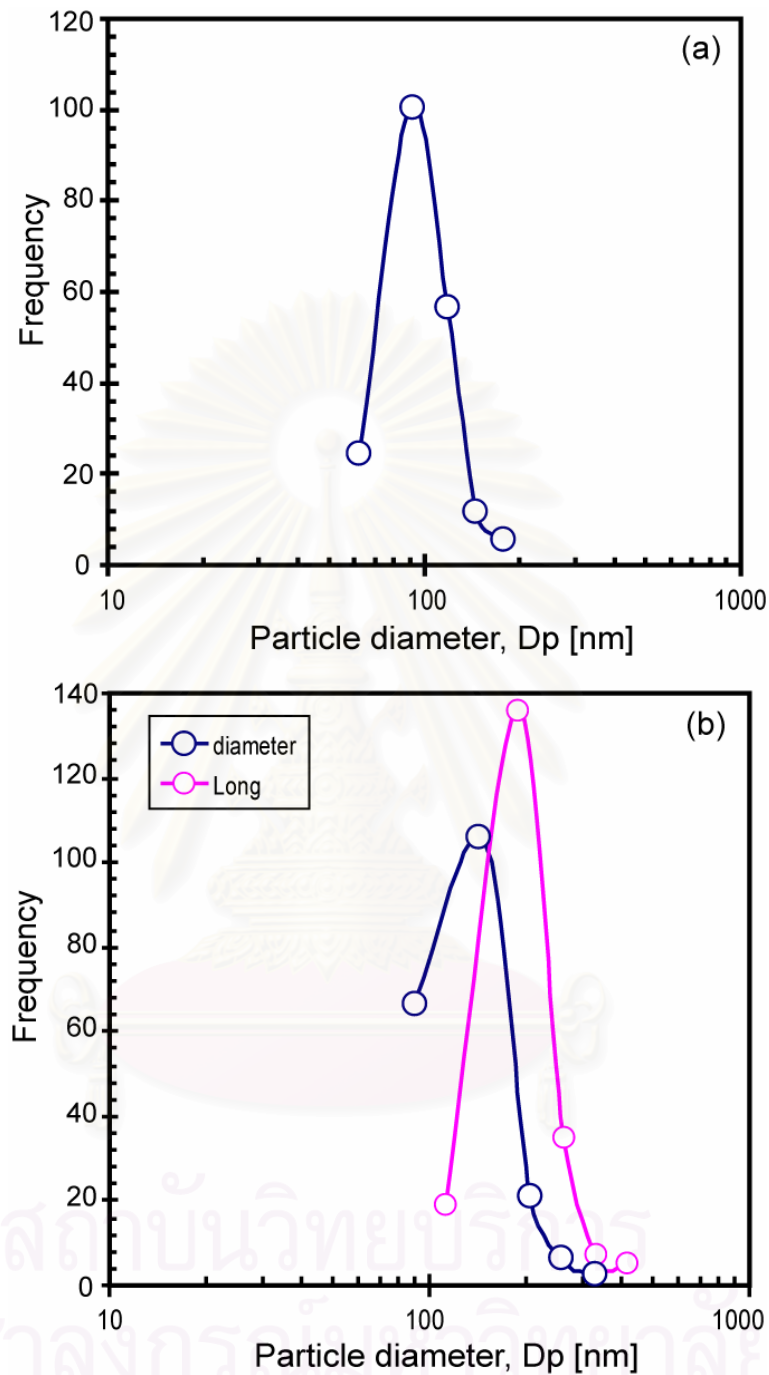


Figure 4.27 Particle size distribution of ZnO nanoparticle, (a) without mixing device, (b) with mixing device

Figure 4.28 shows the XRD pattern of sphere and tetrapod ZnO nanostructures. The main peaks appear at 31.9° , 34.4° and 36.4° that are typical diffraction peaks from hexagonal ZnO planes of (100), (002) and (101), respectively. As indexed in Fig. 4.28, all other peaks also match the hexagonal ZnO structure with lattice constants of $a =$

3.250 Å and $c = 5.207$ Å. This indicates that the spherical and tetrapod ZnO are composed of wurtzite structural ZnO. No diffraction peaks from Zn or other impurity phases are found in any of our samples, confirming that the products are pure ZnO.

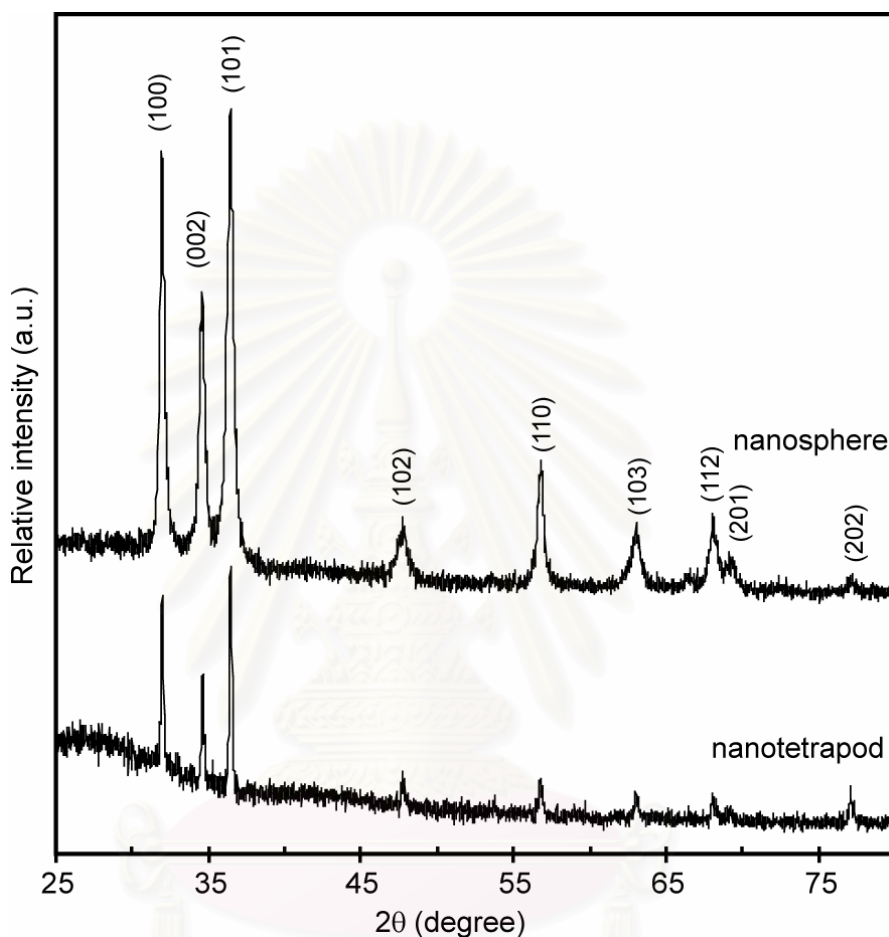


Figure 4.28 XRD patterns of ZnO nanosphere and ZnO nanotetrapod.

For investigating the effect of orifice on generation of ZnO nanostructure, firstly temperature profiles inside the reactor were measured as shown in figure 4.29, the orifice insignificantly affect the temperature profiles inside the reactor. Therefore the dimension of tetrapods is directly linked to a supersaturation of vapor phase rather than the effect of temperature according with Chen et al. (2004). Furthermore the particle size distributions of collected ZnO nanoparticles at 1 cm of both cases were measured. Without orifice, the particle size distribution of collected ZnO nanoparticles has the smaller size range than with using orifice as shown in figure 4.30. The average particle size of collected particle without orifice is 71 nm, while the

average particle size with orifice is 96 nm. Consequently when an orifice was used, the size of ZnO nanoparticles which was generated at initial stage was bigger than that of without orifice. This result is attributed to the growth of generated ZnO nanoparticles at the initial stage at which mixing between Zn vapor and oxygen inside the reactor could play an important role in ZnO formation.

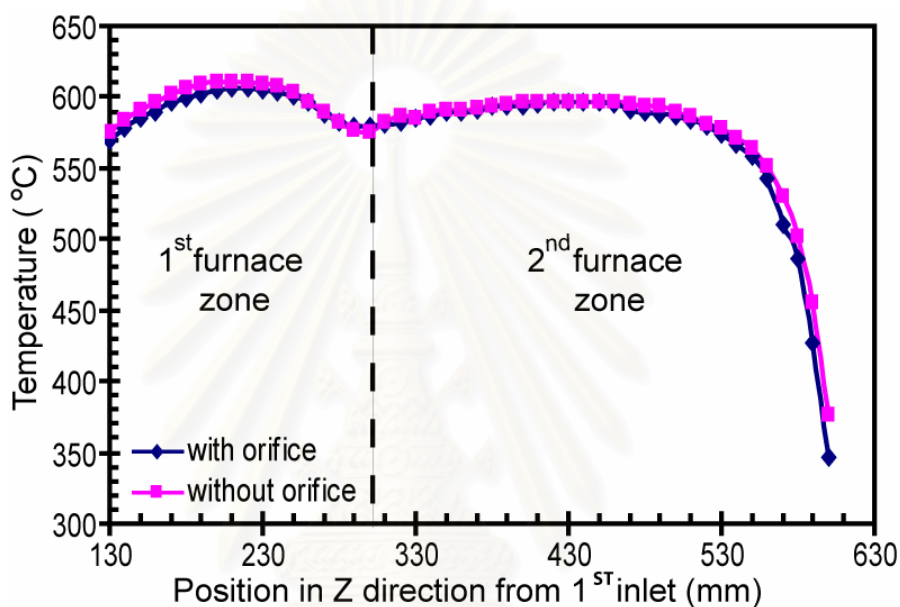


Figure 4.29 Temperature profiles inside reactor.

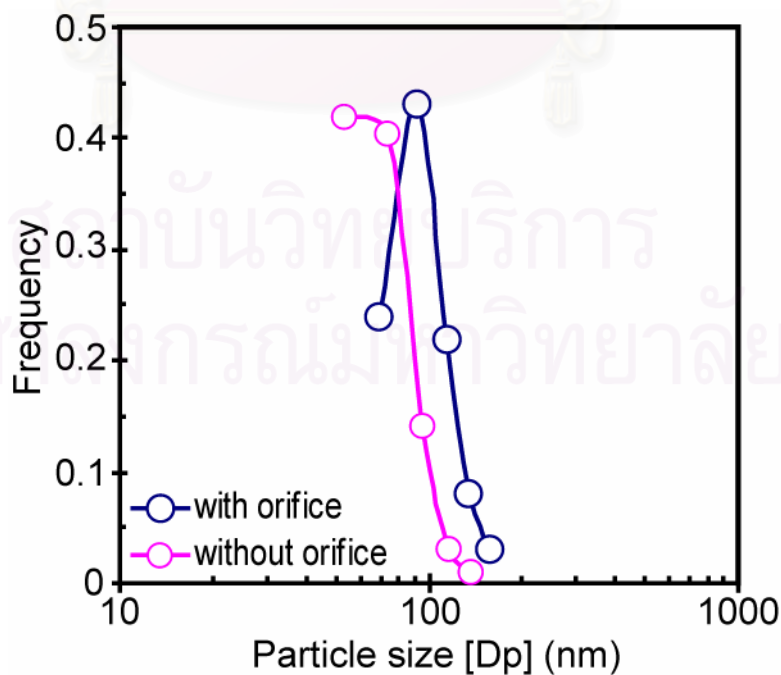


Figure 4.30 Particle size distributions of ZnO nanoparticles at 1cm.

The effect of orifice on mixing between Zn vapor and oxygen was numerically verified by computational fluid dynamic (CFD) technique. In this work, FLUENT[®] was employed for calculating the concentration of zinc vapor and oxygen inside the reactor. However in this numerical resolution method, we assumed that no oxidation reaction occurred throughout the reactor and the temperature at the wall of reactors was fixed at 600°C. Density of gas mixture was computed from the ideal gas law. Diffusion coefficient was a constant at 600°C and was calculated by using theory of diffusion in gas at low density. The related parameters used for the computations obtained from Tena-Zaera et al. (2004). Since we emphasized on the effect of orifice toward mixing between Zn vapor and oxygen inside the reactors, the observed zone was started from the orifice to the end of the first furnace. For easy to understand, the observed zone was also divided into two zones along radius direction. From center of the reactor ($r=0$ mm) to 4 mm in radius direction, we referred this zone as a center zone. And from 4 mm to wall of the reactor ($r=13.5$ mm), this zone was referred as an outer zone as shown in figure 4.31b.

The contours of oxygen and Zn vapor concentration inside the reactor were shown in figure 4.31 and 4.32. In case of without orifice, it is clearly shown that the oxygen and Zn vapor concentration gradient inside the reactor. Figure 4.31a shows that oxygen concentration at the center zone is higher than at the outer zone, whereas Zn vapor concentration at the center zone is lower than the outer zone as indicated in figure 4.32a. In case of with orifice, the different of oxygen concentration and Zn vapor concentration between center zone and outer zone are not obviously observed as displayed in figure 4.31b and 4.32b.

จุฬาลงกรณ์มหาวิทยาลัย

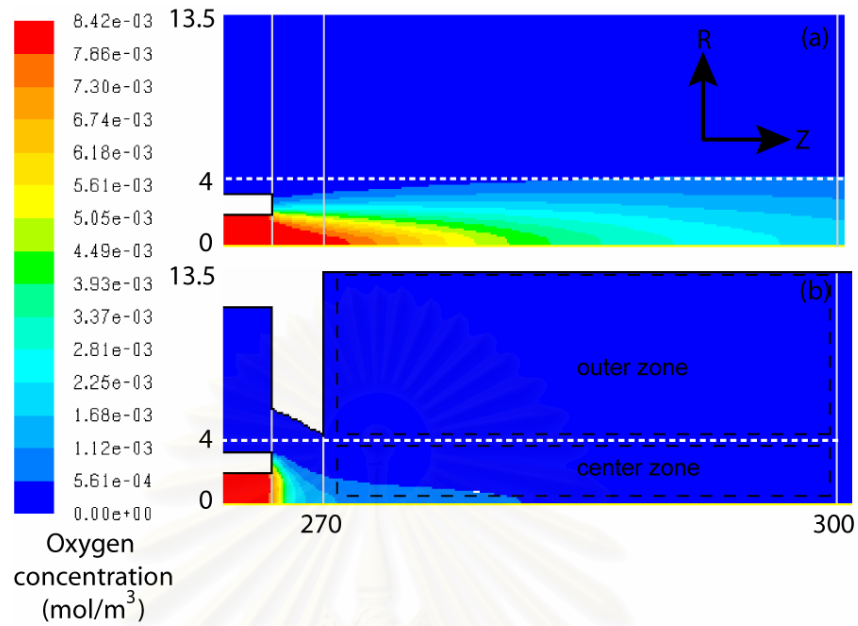


Figure 4.31 Contours of the oxygen concentration inside reactor (a) without orifice and (b) with orifice

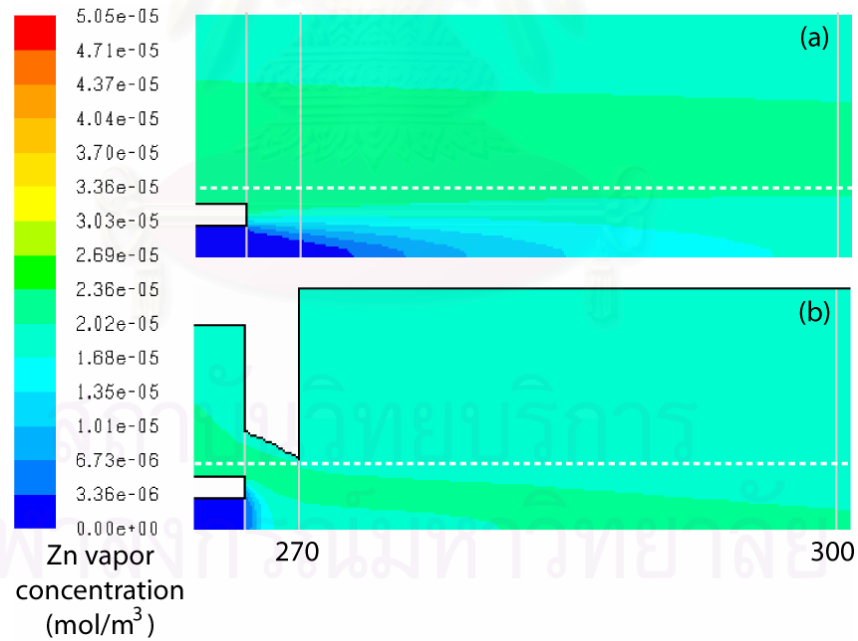


Figure 4.32 Contours of the zinc vapor concentration inside reactor (a) without orifice and (b) with orifice

For further information about the effect of orifice, oxygen and Zn vapor concentration versus distance in radius direction were plotted as displayed in figure 4.33. Without orifice, oxygen concentration at the center zone is higher than with orifice while Zn vapor concentration at the center zone is lower than with orifice. On the other hand, oxygen concentration at the outer zone is lower than with orifice. Moreover, oxygen concentration and Zn vapor concentration without orifice are not uniform throughout the reactor as indicated in dash line in figure 4.33. For example, oxygen concentration (at 270 cm from first furnace inlet) varied from 8.22×10^{-3} (at the center of reactor) to 6.08×10^{-16} mol/m³ (at the wall of reactor). However in downstream direction, oxygen concentrations at the center zone are quietly decreased while at the outer zone are rapidly raised by diffusion. On the contrary, when the orifice was used, oxygen concentration and Zn vapor concentration are uniform throughout the reactor.



สถาบันวิทยบริการ
จุฬาลงกรณ์มหาวิทยาลัย

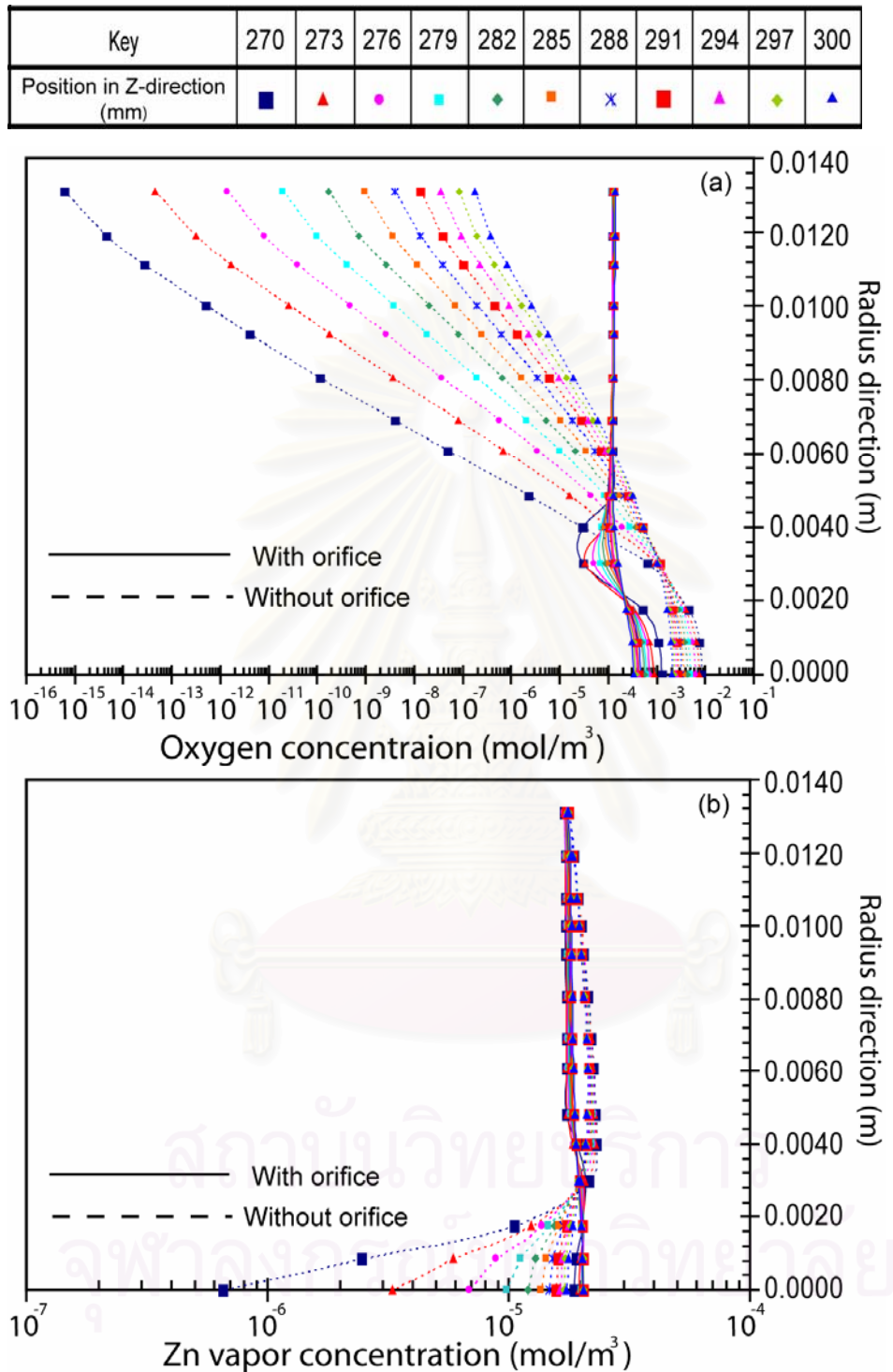


Figure 4.33 Relation between reactant concentration inside the reactor and radius direction, (a) oxygen concentration, (b) zinc vapor concentration.

In addition, we computed the chemical reaction rate by multiplication between oxygen and zinc vapor from figure 4.33. Additionally we supposed that chemical

reaction rate of ZnO depends on first order of oxygen and zinc vapor concentration. However we have to consider chemical rate constant as a constant value. Therefore the multiplication of these two values could refer to chemical reaction rate of ZnO as shown in equation (1).

$$r_{\text{ZnO}} \propto [\text{Zn}][\text{O}_2] \quad (1)$$

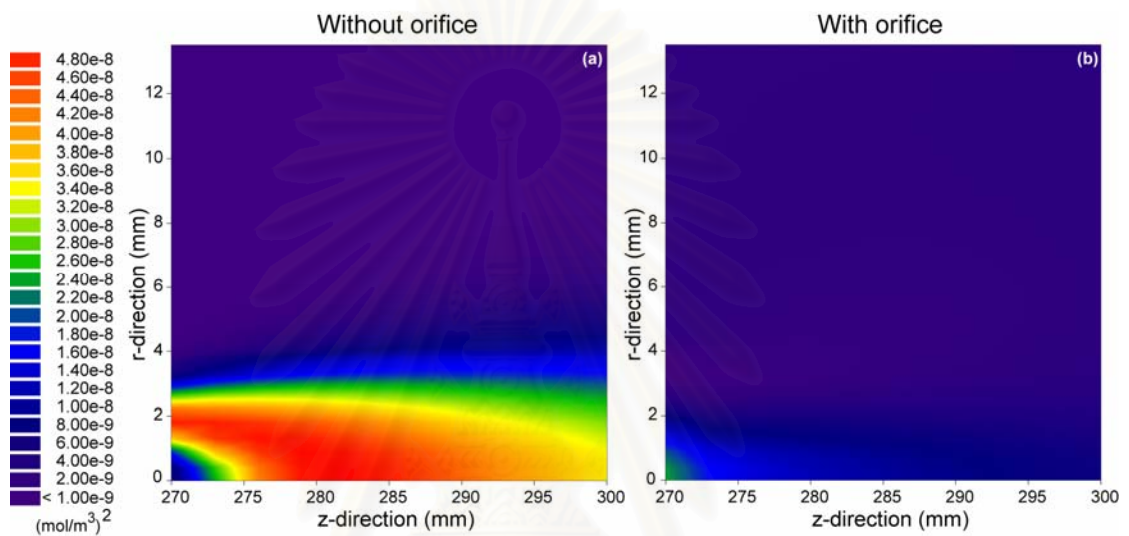


Figure 4.34 Contours of multiplication between oxygen and zinc vapor inside the reactor, (a) without orifice and (b) with orifice.

Figure 4.34 shows the contours of multiplication between oxygen and zinc vapor concentration inside the reactor. It shows that the reaction zones (in case of without using orifice) are around the center zone. Therefore the reaction between zinc vapor and oxygen slowly took place. While with using orifice reaction zone is widened throughout the reactor because of rapid mixing resulting in supersaturation of ZnO.

In addition, Reynolds numbers inside the reactor were calculated as shown in appendix B. Without orifice, flow regimes are transition flow because Reynolds numbers vary about from 2,000 to 4,400. While with orifice, flow regimes consist of laminar, transition and turbulent flow. At the center zone of the reactor, flow regimes are turbulent flow because Reynolds numbers vary from 13,000 to 38,500 along z-direction and r-direction. While at the outer zone, flow regimes are laminar flow from 270 mm to 279 mm in z-direction and change to transition flow when fluids pass through 282 in z-direction. From these results, when orifice was used, gas flows

inside the reactor are more turbulent resulting in enhance the mixing between zinc vapor and oxygen.

From FLUENT[®] results, we summarized the effect of orifice toward mixing between oxygen and Zn vapor. In case of the system without orifice, the mixing between oxygen and Zn vapor slowly occurred by diffusion force from concentration gradient. Therefore the reaction zones locally occurred around the interface between center zone and outer zone and the chemical reaction rate at any zone inside the reactor are different. On the other hand, the mixing between oxygen and Zn vapor with orifice are rapidly took place resulting in uniform concentration all over the reactor. Therefore the reaction zone between oxygen and Zn vapor broaden throughout the reactor and the chemical reaction rates are similarly occurred all over the reactor. Consequently, installation of the orifice could enhance mixing between oxygen and Zn vapor resulting in higher growth rate of generated particles at the initial stage. This result according to the size of collected particles at 1 cm which collected particles with orifice is bigger than without orifice.

4.4.3 Growth mechanism of ZnO nanoparticles in gas phase reaction

From SEM and FLUENT[®] analyse, the growth mechanism of ZnO nanoparticles in gas phase reaction is proposed as shown in figure 4.35. Without orifice, the mixing between oxygen and Zn vapor occur purely from diffusion force from concentration gradient. Then the reaction zone occurs locally around the interface between center and outer zone of reactor. Therefore smaller ZnO cluster are generated at the initial stage as displayed in figure 4.25a. We refer these ZnO cluster as the ZnO primary particles. Since these smaller primary particles have low surface, therefore they do not have appropriate crystal plane for absorb Zn vapor on the surface for growing to tetrapod shape. In addition the remaining precursors around ZnO primary particles in the crystal growth stage are high concentration because the mixing between oxygen and Zn vapor in the initial stage are poorly. Consequently, the crystal growths on the surface of ZnO primary particles take place in all direction. Therefore these ZnO primary particles grow to larger sphere ZnO nanoparticles with unclear boundary condition.

Conversely, the mixing between oxygen and Zn vapor with orifice occur rapidly. Then the chemical reaction can take place all over the region of reactor because oxygen and Zn vapor concentration are uniformly throughout the reactor. Consequently, larger ZnO primary particles were formed at the initial stage. These ZnO primary particles acted as a nucleus, as the collected particles on silicon wafer at 1 cm as shown in figure 4.26a. Since the sizes of these ZnO primary particle were larger than the appropriate critical size for growing to tetrapod shape. Moreover, the large ZnO primary particles have more surfaces which are sufficiently large for absorbed Zn vapor on the surface M. Kitano (1991). Then oxygen and Zn vapor oxidize on the surface of ZnO primary particles by surface reaction resulting in crystal growth of tetrapod ZnO, C.X. Xu (2005). Furthermore, it has been reported that tetrapod ZnO nanostructures can be synthesized under limiting condition of low oxidation rate, M. Kitano (1991). Since the mixing between oxygen and Zn vapor is enhanced by orifice at the nucleus formation stage, therefore the remaining oxygen and Zn vapor are low concentration at the crystal growth stage. Consequently, these also promote the crystal growth of tetrapod ZnO nanoparticles.

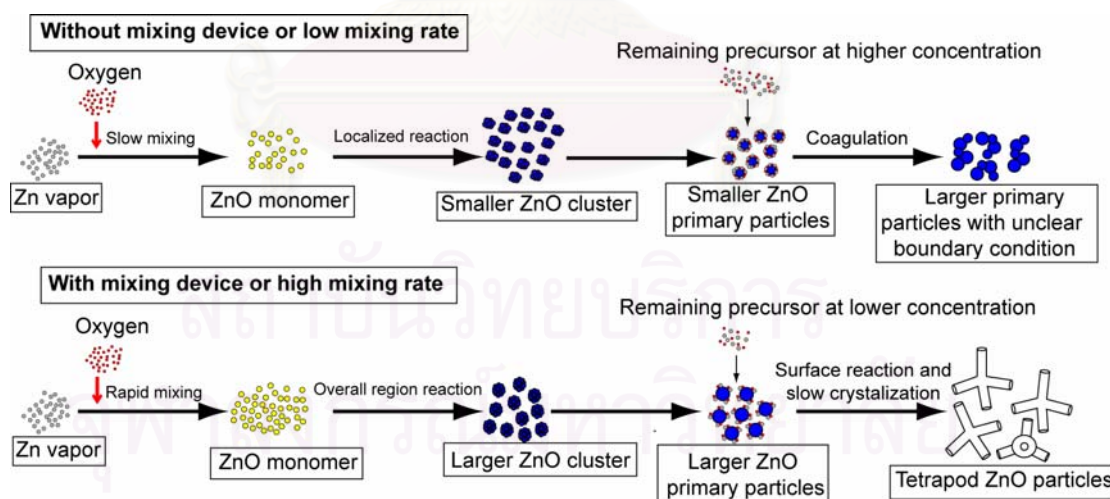


Figure 4.35 Possible growth mechanism of ZnO nanoparticles in gas phase reaction.

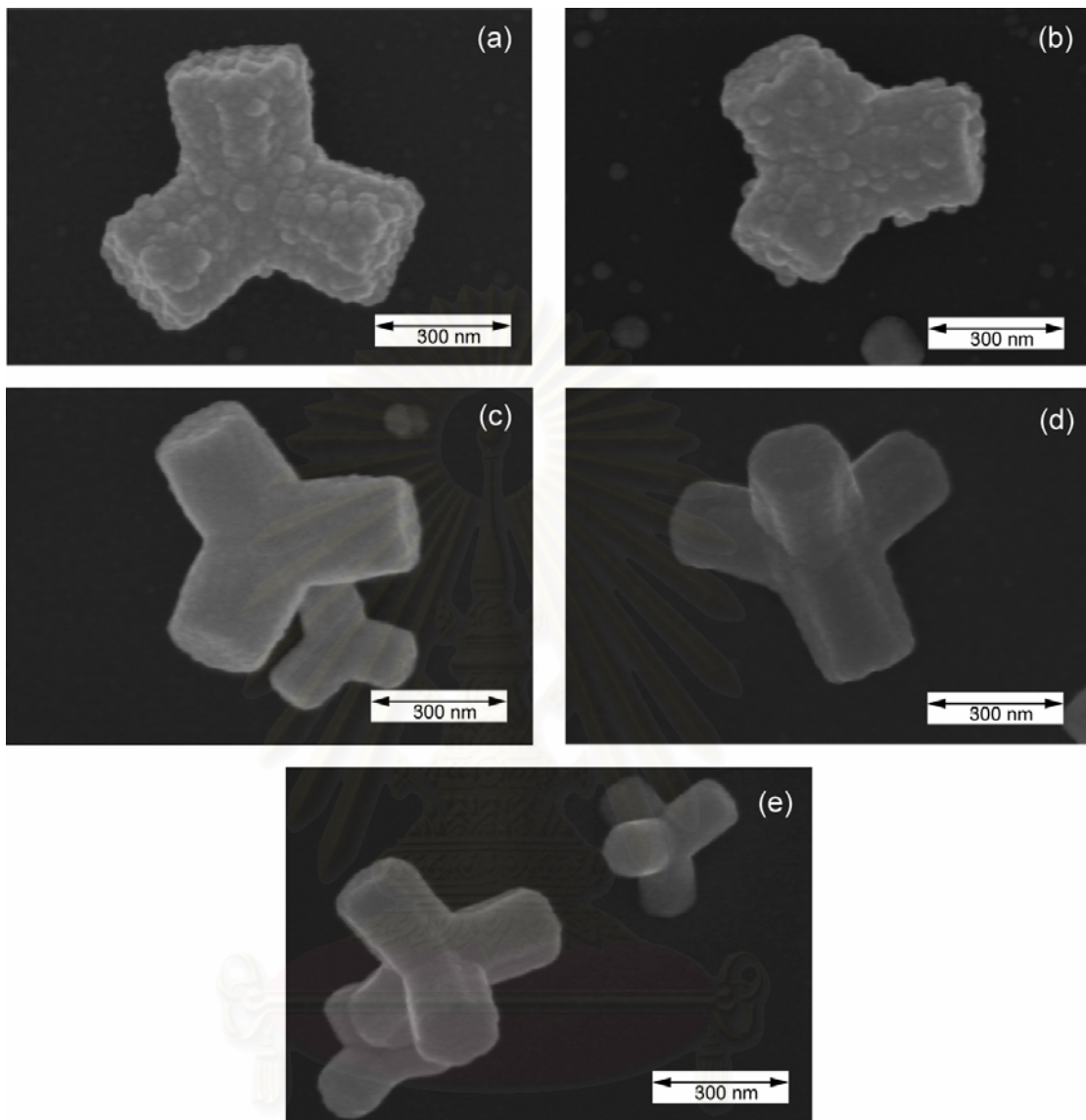


Figure 4.36 SEM micrographs of ZnO nanoparticles collected by quenched silicon wafer under any positions from 2nd furnace inlet with mixing device (a) 5, (b) 10, (c) 15, (d) 20 and (e) 25cm

In addition, growth mechanism of tetrapod ZnO was investigated by collecting ZnO nanoparticles synthesized at any position in 2nd furnace. From previous results, spherical ZnO nucleus formed at 1 cm from 2nd furnace inlet. Typical SEM image in figure 4.36 shows that morphology of ZnO nanoparticles changed from sphere to tetrapod shape when ZnO nanoparticles were collected after 5 cm from 2nd furnace inlet. The growth of ZnO from nucleus to tetrapod occurred rapidly in narrow zone. We think that supersaturation is the driving force for both the initial nucleation step

and the following crystal growth, both of which could not occur in saturated or undersaturated conditions. From figure 4.36a and b, at 5 and 10 cm, tetrapod ZnO nanoparticles were rough surface. While ZnO nanoparticles which were collected after 15 cm from 2nd furnace inlet were smooth surface as shown in figure 4.36 c-e. We think that the crystallization occurred in the growth process of tetrapod ZnO nanoparticles and it had to occur in high temperature zone. This result was confirmed by treating collected ZnO nanoparticles. ZnO nanoparticles collected on silicon substrate were treated in closed system by using electrical furnace at 600°C for one hour.

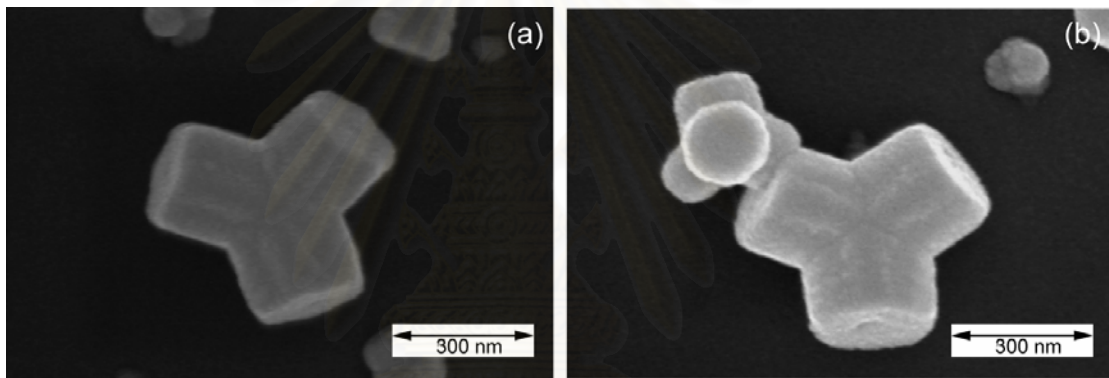


Figure 4.37 SEM images of ZnO nanostructures treated at 600 C for one hour, (a) at 5cm, (b) at 10cm.

SEM images in figure 4.37 shows that surface of ZnO nanoparticles changed from rough to smooth surface after they were treated at high temperature. Therefore temperature affected to the crystallization of ZnO nanoparticles.

CHAPTER V

CONCLUSION AND RECOMMENDATION

5.1 Conclusions

In this work, uniform ZnO nanoparticles could be synthesized by using the oxidation between zinc vapor and oxygen in gas phase reaction technique. The main purpose of this research is to investigate the effect of evaporation temperature, oxidation temperature, mixing device, and gas flow rate on characteristic of synthesized ZnO nanoparticles. According to above mentioned experimental results, it can be concluded as follows.

5.1.1 Effect of evaporation temperature (T_{evp})

From experimental results, it could be clearly observed that the size and morphologies of synthesized ZnO nanoparticles are dependent on the evaporation temperature. The uniform small spherical shape of synthesized ZnO nanoparticles was achieved when evaporation temperatures were 500 and 600°C. With relatively high evaporation temperature for example 700 and 800°C, the morphologies of ZnO nanoparticles consisted of spherical and tetrapod shape.

5.1.2 Effect of oxidation temperature (T_{oxi})

The effects of oxidation temperature were experimentally studied together with using of an orifice as a mixing device. From the experimental results, the oxidation temperature can greatly affect the morphology of synthesized ZnO nanoparticles. Without using the orifice, the morphologies of synthesized ZnO were only spherical shape regardless of oxidation temperature. However, when the oxidation temperature was increased from 400 to 700°C using the mixing device could result in change of the morphologies of synthesized ZnO from spherical to tetrapod

shape. The crystal growth of tetrapod ZnO nanoparticles could be supposed to enhance under the high temperature condition.

5.1.3 Effect of gas flow rate

The effect of gas flow rate was studied because it is related to the partial pressure of oxygen inside the reactor. From experimental results, the partial pressure of oxygen could affect the morphology of synthesized ZnO nanoparticles. The tetrapod ZnO nanoparticles with small diameter and long legs were synthesized when partial pressure of oxygen was lower than 0.04. It was found that the legs of these small tetrapod ZnO nanoparticles were sharp tip. When partial pressure of oxygen was between 0.07 and 1, the synthesized tetrapod ZnO nanoparticles exhibited uniform diameter and the shape of legs was hexagonal facet. When partial pressure of oxygen was more than 0.12, the morphology of synthesized ZnO was polyhedral shape.

5.1.4 Effect of gas mixing apparatus (orifice)

In this work, an orifice was used to enhance the interaction between zinc vapor and oxygen. With relatively high interaction between these two reactants, the synthesized ZnO nanoparticles were uniform size and morphology as reported in chapter 4. Two types of uniform in their ZnO nanostructures, spherical and tetrapod particles were synthesized with and without using mixing device, respectively. These two morphologies strongly depend on existent of orifice which in turn affects size of synthesized particles at the initial stage. However the mixing device did not affect the temperature inside the reactor. Therefore the interaction between zinc vapor and oxygen was an important factor for controlled the morphologies of synthesized ZnO nanoparticles.

Furthermore, quenched silicon substrate with cooling was used for investigation the growth mechanism of ZnO nanoparticles. We have successfully demonstrated for the first time that generation of tetrapod ZnO, by gas phase reaction, could divide into two stages. The first stage is the formation of nucleus and the second

stage is the crystal growth of tetrapod. Beside we reported that, installation of orifice could enhance the mixing between Zn vapor and oxygen which was confirmed by FLUENT simulation.

5.2 Recommendation for future work

From the experimental results in this work, we proposed that the growth mechanism of tetrapod ZnO nanoparticle can divide into two stages. The first one is nucleation stage. The second one is crystal growth stage. We think that the important factor for growing to tetrapod shape was the critical size of nucleus. For confirm our result, we should study further about the effect critical size of nucleus.

In addition, the morphology of synthesized ZnO nanoparticles depends on the mixing between zinc vapor and oxygen which was controlled by mixing device. Therefore we should investigate more about mixing device by changing the shape of orifice for example by varying hole diameter of the orifice. Furthermore, the chemical reaction of ZnO should be add in FLUENT for calculating the concentration of zinc vapor and oxygen inside reactor.

REFERENCES

- A. Umar, E.-K. Suh and Y.B. Hahn, *Non-catalytic growth of high aspect-ratio ZnO nanowires by thermal evaporation*, Solid State Communications **139** (2006): 447-451
- A. Umar, S.H. Kim, Y.-S. Lee, K.S. Nahm and Y.B. Hahn, *Catalyst-free large-quantity synthesis of ZnO nanorods by a vapor–solid growth mechanism: Structural and optical properties*, Journal of Crystal Growth **282** (2005): 131-136
- B.H. Kong, D.C. Kim and H.K. Cho, *Shape control and characterization of one-dimensional ZnO nanostructures through the synthesis procedure*, Physica B **376** (2006): 726–730
- C.X. Xu, X.W. Sun, Z.L. Dong and M.B. Yu, *Self-organized nanocomb of ZnO fabricated by Au-catalyzed vapor-phase transport*, Journal of Crystal Growth **270** (2004): 498-504
- G. Shen, J. H. Cho and C. Jin Lee, *Morphology-controlled synthesis, growth mechanism and optical properties of ZnO nanonails*, Chemical Physics Letters **401** (2005): 414–419
- H. Iwanaga, M. Fujii and S. Takeuchi, *Growth model of tetrapod Zinc Oxide particles*, Journal of Crystal Growth **134** (1993): 275-280
- J. Park, H.H Choi, K. Siebian and R. K. Singh, *Two-step evaporation process for formation of aligned zinc oxide nanowires*, Journal of Crystal Growth **258** (2003): 342–348

- J. Zhang, Y. Yang, F. Jiang and J. Li, *Fabrication, structural characterization and the photoluminescence properties of ZnO nanoneedle arrays*, Physica E27 (2005): 302-307
- K. Nakaso, K. Okuyama, M. Shimada and S.E. Prasinis, *Effect of reaction temperature on CVD-made TiO₂ primary particle diameter*, Chemical Engineering Science 58 (2003): 3327-3335
- K. Nishio, T. Isshiki, M. Kitano and M. Shiojiri, *Structure and growth mechanism of tetrapod-like ZnO particles*, Philosophical Magazine A 76 (1997): 889-904
- M.H. Huang, S. Mao, H. Feick, H.Q. Yan, Y.Y. Wu, H. Kind, E. Weber, R. Russo and P.D. Yang, *Room-temperature Ultraviolet Nanowire Nanolasers*, Science 292 (2001): 1897-1899
- M. Kitano, T. Hamabe and S. Maeda, *Growth of large tetrapod-like ZnO crystals II. Morphological considerations on growth mechanism*, Journal of Crystal Growth 108 (1991): 277-284
- M. Shiojiri and C. Kaito, *Structure and growth of ZnO smoke particles prepared by gas evaporation technique*, Journal of Crystal Growth 52 (1981): 173-177
- R.B. Bird, W.E. Stewart and E.N. Lighfoot, *Transport phenomena*, J. Wiley 2002 2nd edition
- R. Tena-Zaera, M.C. Martinez-Tomas, S. Hassani, R. Triboulet and V. Munoz-Sanjose, *Study of the ZnO crystal growth by vapour transport methods*, Journal of Crystal Growth 270 (2004): 711-721
- R. Wu and C. Xie, *Formation of tetrapod nanowhiskers and its optical properties*, Material Research Bulletin 39 (2004): 637-645

- R. Wu, J. Wu, C.S. Xie, J. Zhang and A.H. Wang, *Morphological characteristic of Zn/ZnO nanopowders and the optical properties*, Materials Science and Engineering A328 (2002): 196–200
- R. Yang and Z.L. Wang, *Interpenetrative and transverse growth process of self-catalyzed ZnO nanorods*, Solid State Communications 134 (2005): 741-745
- V.A.L. Roy, A.B. Djurisic, W.K. Chan, J. Gao, H.F. Lui and S. Surya, *Luminescent and structural properties of ZnO nanorods prepared under different conditions*, Applied Physics Letters 83 (2003): 141-143
- W. Cheng, P. Wu, Z. Zou and T. Xiao, *Study on synthesis and blue emission mechanism of ZnO tetrapodlike nanostructures*, Journal of Applied Physics 100 (2006): 54311
- X. Wang, Y. Ding, C.J. Summers and Z.L. Wang, *Large-Scale Synthesis of Six-Nanometer-Wide ZnO Nanobelts*, Journal of Physics Chemistry B 108(2004): 8773-8777
- Y. Dai, Y. Zhang, Z.L. Wang, *The octa-twin tetraleg ZnO nanostructures*, Solid State Communications 126 (2003): 629-633
- Y. Dai, Y. Zhang, Q.K. Li and C.W. Nan, *Synthesis and optical properties of tetrapod-like zinc oxide nanorods*, Chemical Physics Letters 358 (2002): 83–86
- Y.H. Leung, K.H. Tam, A.B. Djurisic, M.H. Xie, W.K. Chan, D. Lu and W.K. Ge, *Zno nanoshells: Synthesis, structure, and optical properties*, Journal of Crystal Growth 283(2005): 134-140

- Y. Li, G.S. Cheng and L.D. Zhang, *Fabrication of highly ordered ZnO nanowire arrays in anodic alumina membranes*, Journal of Material Research **15** (2000): 2305-2308
- Z. Chen, Z. Shan, S. Li, M.S. Cao and S.X. Mao, *Zinc oxide nanotetrapods*, Nanotechnology **15** (2004): 365-369
- Z. Chen, Z. Shan, S. Li, C.B. Liang and S.X. Mao, *A novel and simple growth route towards ultra-fine ZnO nanowires*, Journal of Crystal Growth **265** (2004): 482-486
- Z.G. Chen, A. Ni, F. Li, H. Cong, H.-M. Cheng and G.Q. Lu, *Synthesis and photoluminescence of tetrapod ZnO nanostructures*, Chemical Physics Letters **434** (2007): 301-305
- Z. Miao, D. Xu, J. Ouyang, G. Guo, X. Zhao and Y. Tang, *Electrochemically Induced Sol-Gel Preparation of Single-Crystalline TiO₂ Nanowires*, Nano Letters **2** (2002): 717-720
- Z. Zhou, J. Liu and S. Hu, *Studies on the kinetics process of tetra-needle-like ZnO whisker growth*, Journal of Crystal Growth **276** (2005): 317-320



APPENDICES

สถาบันวิทยบริการ
จุฬาลงกรณ์มหาวิทยาลัย

APPENDIX A

Calculation of partial pressure

Partial pressure of zinc vapor and oxygen was calculated by using ideal gas mixtures. The mole fraction of an individual gas component in an ideal gas mixture can be expressed in terms of the component's partial pressure or the moles of the component:

$$x_A = n_A/n \quad (A1)$$

$$p_A = x_A \times p, \quad (A2)$$

where :

- n = total moles of the gas mixture
- p_A = partial pressure of gas component A in gas mixture
- n_A = moles of gas component A in gas mixture
- x_A = moles fraction of gas component A in gas mixture
- p = pressure of gas mixture

For example, in case of 1 L/min of air and nitrogen flow rate

$$\begin{aligned} \text{Mole of oxygen, } n_{O_2} &= \frac{1[L/\text{min}] \times 0.21 \times 1.429[g/L]}{32[g/mole]} \\ &= 9.38 \times 10^{-3} \text{ mole/min} \end{aligned}$$

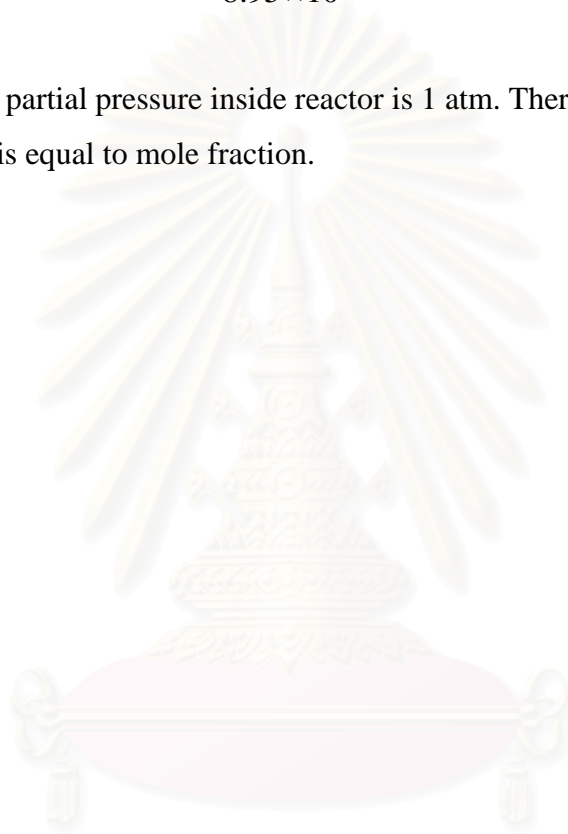
$$\begin{aligned} \text{Mole of nitrogen, } n_{N_2} &= \frac{1[L/\text{min}] \times 0.79 \times 1.251[g/L]}{28[g/mole]} + \frac{1[L/\text{min}] \times 1.251[g/L]}{28[g/mole]} \\ &= 8 \times 10^{-2} \text{ mole/min} \end{aligned}$$

$$\text{Total mole} = 8.938 \times 10^{-2} \text{ mole/min}$$

$$\begin{aligned}\text{Mole fraction of oxygen, } x_{O_2} &= \frac{9.38 \times 10^{-3}}{8.938 \times 10^{-2}} \\ &= 1.05 \times 10^{-1}\end{aligned}$$

$$\begin{aligned}\text{Mole fraction of nitrogen, } x_{N_2} &= \frac{8 \times 10^{-2}}{8.938 \times 10^{-2}} \\ &= 8.95 \times 10^{-1}\end{aligned}$$

We assume that partial pressure inside reactor is 1 atm. Therefore, partial pressure of gas component is equal to mole fraction.



สถาบันวิทยบริการ
จุฬาลงกรณ์มหาวิทยาลัย

APPENDIX B

Expeimental Results

In this work, zinc vapor and oxygen inside reactor were calculated from FLUENT simulation. Figure B1 shows simulation model for calculation.

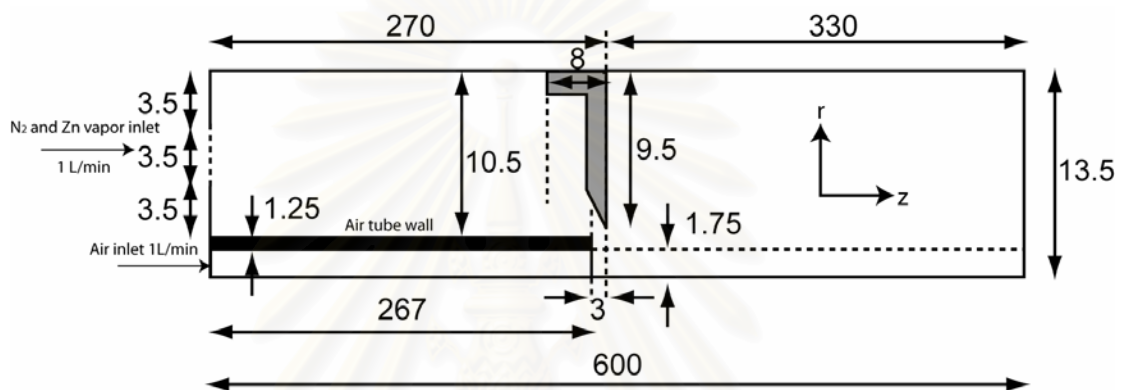


Figure B1 Simulation model for FLUENT

Assumption

- No oxidation reaction occur inside reactor
- Zinc vapor diffuse in nitrogen gas by using theory of diffusion in gas at low density and diffusion coefficient is constant (at $T = 873$ K)
- Temperature at wall tube of quartz reactor in both furnaces is 873 K
- Nitrogen and air flow rate was calculated at $T 298$ K and 1 atm
- Zinc vapor are introduced into reactor at the inlet with nitrogen gas (It don't generated at the center of 1st furnace)

B.1 Oxygen concentration

Table B1 Oxygen concentration from 270 to 279 in z-direction (mol/dm³)

z-direction	270		273		276		279	
r-direction	with ori	wo ori	with ori	wo ori	with ori	wo ori	with ori	wo ori
0.0131	1.21E-04	6.08E-16	1.22E-04	4.45E-14	1.22E-04	1.36E-12	1.23E-04	1.95E-11
0.0119	1.22E-04	4.54E-15	1.23E-04	3.10E-13	1.23E-04	8.16E-12	1.25E-04	1.00E-10
0.0111	1.23E-04	2.76E-14	1.23E-04	1.70E-12	1.24E-04	3.88E-11	1.25E-04	4.12E-10
0.0100	1.23E-04	5.12E-13	1.23E-04	2.62E-11	1.24E-04	4.64E-10	1.25E-04	3.87E-09
0.0092	1.23E-04	4.10E-12	1.23E-04	1.79E-10	1.24E-04	2.61E-09	1.24E-04	1.82E-08
0.0081	1.23E-04	1.13E-10	1.23E-04	3.61E-09	1.24E-04	3.75E-08	1.23E-04	1.94E-07
0.0069	1.23E-04	3.95E-09	1.23E-04	8.19E-08	1.23E-04	5.63E-07	1.21E-04	2.07E-06
0.0061	1.23E-04	4.86E-08	1.23E-04	6.89E-07	1.21E-04	3.43E-06	1.16E-04	9.84E-06
0.0048	1.22E-04	2.28E-06	1.16E-04	1.57E-05	1.04E-04	4.48E-05	9.64E-05	8.53E-05
0.0040	3.07E-05	2.84E-05	7.63E-05	1.02E-04	7.28E-05	1.95E-04	7.44E-05	2.85E-04
0.0030	3.07E-05	6.49E-04	3.31E-05	9.18E-04	4.98E-05	1.08E-03	6.85E-05	1.17E-03
0.0018	5.08E-04	4.57E-03	3.33E-04	3.89E-03	3.16E-04	3.46E-03	3.10E-04	3.10E-03
0.0009	1.06E-03	7.59E-03	7.10E-04	6.38E-03	6.03E-04	5.32E-03	5.37E-04	4.48E-03
0.0000	1.29E-03	8.22E-03	8.77E-04	7.35E-03	7.19E-04	6.12E-03	6.24E-04	5.03E-03

Table B2 Oxygen concentration from 282 to 291 in z-direction (mol/dm³)

z-direction	282		285		288		291	
r-direction	with ori	wo ori	with ori	wo ori	with ori	wo ori	with ori	wo ori
0.0131	1.24E-04	1.68E-10	1.26E-04	9.49E-10	1.27E-04	3.98E-09	1.29E-04	1.31E-08
0.0119	1.26E-04	7.32E-10	1.27E-04	3.58E-09	1.28E-04	1.31E-08	1.30E-04	3.82E-08
0.0111	1.26E-04	2.64E-09	1.27E-04	1.15E-08	1.28E-04	3.79E-08	1.30E-04	1.01E-07
0.0100	1.25E-04	1.99E-08	1.26E-04	7.13E-08	1.27E-04	1.99E-07	1.28E-04	4.57E-07
0.0092	1.25E-04	7.94E-08	1.25E-04	2.48E-07	1.25E-04	6.14E-07	1.26E-04	1.27E-06
0.0081	1.23E-04	6.52E-07	1.22E-04	1.64E-06	1.21E-04	3.37E-06	1.22E-04	5.97E-06
0.0069	1.18E-04	5.28E-06	1.16E-04	1.06E-05	1.16E-04	1.80E-05	1.17E-04	2.71E-05
0.0061	1.12E-04	2.06E-05	1.10E-04	3.51E-05	1.10E-04	5.22E-05	1.12E-04	7.05E-05
0.0048	9.42E-05	1.31E-04	9.59E-05	1.76E-04	1.00E-04	2.16E-04	1.06E-04	2.51E-04
0.0040	8.02E-05	3.63E-04	8.85E-05	4.25E-04	9.80E-05	4.72E-04	1.08E-04	5.04E-04
0.0030	8.69E-05	1.21E-03	1.04E-04	1.21E-03	1.19E-04	1.19E-03	1.32E-04	1.15E-03
0.0018	3.01E-04	2.78E-03	2.90E-04	2.51E-03	2.77E-04	2.27E-03	2.63E-04	2.07E-03
0.0009	4.88E-04	3.82E-03	4.50E-04	3.31E-03	4.17E-04	2.90E-03	3.87E-04	2.58E-03
0.0000	5.56E-04	4.21E-03	5.05E-04	3.59E-03	4.64E-04	3.12E-03	4.30E-04	2.76E-03

Table B3 Oxygen concentration from 294 to 300 in z-direction (mol/dm³)

z-direction	294		297		300	
r-direction	with ori	wo ori	with ori	wo ori	with ori	wo ori
0.0131	1.31E-04	3.56E-08	1.34E-04	8.35E-08	1.36E-04	1.74E-07
0.0119	1.32E-04	9.35E-08	1.35E-04	1.99E-07	1.38E-04	3.80E-07
0.0111	1.32E-04	2.27E-07	1.34E-04	4.49E-07	1.37E-04	8.01E-07
0.0100	1.30E-04	9.07E-07	1.32E-04	1.61E-06	1.35E-04	2.60E-06
0.0092	1.28E-04	2.32E-06	1.30E-04	3.80E-06	1.33E-04	5.75E-06
0.0081	1.24E-04	9.47E-06	1.27E-04	1.38E-05	1.30E-04	1.88E-05
0.0069	1.19E-04	3.74E-05	1.23E-04	4.84E-05	1.27E-04	5.96E-05
0.0061	1.16E-04	8.89E-05	1.20E-04	1.06E-04	1.26E-04	1.23E-04
0.0048	1.13E-04	2.80E-04	1.21E-04	3.02E-04	1.28E-04	3.20E-04
0.0040	1.18E-04	5.26E-04	1.27E-04	5.38E-04	1.35E-04	5.44E-04
0.0030	1.42E-04	1.11E-03	1.51E-04	1.07E-03	1.58E-04	1.02E-03
0.0018	2.50E-04	1.89E-03	2.39E-04	1.74E-03	2.28E-04	1.61E-03
0.0009	3.59E-04	2.32E-03	3.32E-04	2.10E-03	3.06E-04	1.92E-03
0.0000	3.99E-04	2.46E-03	3.69E-04	2.22E-03	3.39E-04	2.02E-03


 สถาบันวิทยบริการ
 จุฬาลงกรณ์มหาวิทยาลัย

B2. Zinc concentration**Table B4** Zinc concentration from 270 to 279 in z-direction (mol/dm³)

z-direction	270		273		276		279	
	with ori	wo ori	with ori	wo ori	with ori	wo ori	with ori	wo ori
0.0131	1.70E-05	1.77E-05	1.70E-05	1.77E-05	1.70E-05	1.77E-05	1.71E-05	1.77E-05
0.0119	1.71E-05	1.87E-05	1.72E-05	1.86E-05	1.72E-05	1.86E-05	1.74E-05	1.86E-05
0.0108	1.72E-05	1.95E-05	1.72E-05	1.94E-05	1.74E-05	1.94E-05	1.75E-05	1.93E-05
0.0100	1.72E-05	2.00E-05	1.73E-05	1.99E-05	1.74E-05	1.98E-05	1.75E-05	1.98E-05
0.0092	1.72E-05	2.05E-05	1.73E-05	2.04E-05	1.75E-05	2.03E-05	1.76E-05	2.03E-05
0.0081	1.73E-05	2.12E-05	1.74E-05	2.11E-05	1.75E-05	2.10E-05	1.76E-05	2.10E-05
0.0069	1.73E-05	2.19E-05	1.74E-05	2.18E-05	1.75E-05	2.17E-05	1.77E-05	2.16E-05
0.0061	1.73E-05	2.24E-05	1.74E-05	2.22E-05	1.76E-05	2.21E-05	1.78E-05	2.20E-05
0.0048	1.74E-05	2.29E-05	1.76E-05	2.27E-05	1.79E-05	2.25E-05	1.81E-05	2.23E-05
0.0040	1.93E-05	2.31E-05	1.84E-05	2.27E-05	1.86E-05	2.24E-05	1.88E-05	2.20E-05
0.0030	2.08E-05	2.15E-05	2.04E-05	2.06E-05	2.01E-05	2.01E-05	2.00E-05	1.97E-05
0.0018	2.03E-05	1.06E-05	2.05E-05	1.24E-05	2.05E-05	1.36E-05	2.05E-05	1.46E-05
0.0009	1.91E-05	2.45E-06	1.99E-05	5.92E-06	2.01E-05	8.86E-06	2.02E-05	1.12E-05
0.0000	1.86E-05	6.52E-07	1.96E-05	3.31E-06	1.99E-05	6.84E-06	2.01E-05	9.79E-06

Table B5 Zinc concentration from 282 to 291 in z-direction (mol/dm³)

z-direction	282		285		288		291	
	with ori	wo ori	with ori	wo ori	with ori	wo ori	with ori	wo ori
0.0131	1.71E-05	1.77E-05	1.72E-05	1.77E-05	1.73E-05	1.77E-05	1.73E-05	1.77E-05
0.0119	1.75E-05	1.86E-05	1.76E-05	1.85E-05	1.77E-05	1.85E-05	1.78E-05	1.85E-05
0.0108	1.76E-05	1.93E-05	1.77E-05	1.93E-05	1.78E-05	1.92E-05	1.79E-05	1.92E-05
0.0100	1.77E-05	1.97E-05	1.78E-05	1.97E-05	1.79E-05	1.97E-05	1.80E-05	1.96E-05
0.0092	1.77E-05	2.02E-05	1.78E-05	2.02E-05	1.79E-05	2.01E-05	1.80E-05	2.01E-05
0.0081	1.78E-05	2.09E-05	1.79E-05	2.08E-05	1.80E-05	2.07E-05	1.81E-05	2.07E-05
0.0069	1.78E-05	2.15E-05	1.80E-05	2.14E-05	1.81E-05	2.13E-05	1.82E-05	2.13E-05
0.0061	1.79E-05	2.19E-05	1.81E-05	2.18E-05	1.82E-05	2.17E-05	1.83E-05	2.15E-05
0.0048	1.83E-05	2.21E-05	1.85E-05	2.19E-05	1.86E-05	2.17E-05	1.87E-05	2.15E-05
0.0040	1.89E-05	2.17E-05	1.89E-05	2.15E-05	1.90E-05	2.13E-05	1.90E-05	2.11E-05
0.0030	1.98E-05	1.96E-05	1.97E-05	1.95E-05	1.96E-05	1.95E-05	1.96E-05	1.96E-05
0.0018	2.04E-05	1.55E-05	2.04E-05	1.62E-05	2.03E-05	1.68E-05	2.03E-05	1.73E-05
0.0009	2.03E-05	1.29E-05	2.03E-05	1.42E-05	2.04E-05	1.52E-05	2.04E-05	1.60E-05
0.0000	2.02E-05	1.20E-05	2.03E-05	1.35E-05	2.03E-05	1.47E-05	2.04E-05	1.56E-05

Table B6 Zinc concentration from 294 to 300 in z-direction (mol/dm³)

z-direction	294		297		300	
r-direction	with ori	wo ori	with ori	wo ori	with ori	wo ori
0.0131	1.74E-05	1.77E-05	1.75E-05	1.77E-05	1.75E-05	1.77E-05
0.0119	1.79E-05	1.85E-05	1.79E-05	1.85E-05	1.80E-05	1.85E-05
0.0108	1.80E-05	1.92E-05	1.81E-05	1.92E-05	1.81E-05	1.91E-05
0.0100	1.81E-05	1.96E-05	1.81E-05	1.96E-05	1.82E-05	1.95E-05
0.0092	1.81E-05	2.00E-05	1.82E-05	2.00E-05	1.83E-05	1.99E-05
0.0081	1.82E-05	2.06E-05	1.83E-05	2.06E-05	1.84E-05	2.05E-05
0.0069	1.83E-05	2.12E-05	1.84E-05	2.11E-05	1.85E-05	2.10E-05
0.0061	1.84E-05	2.14E-05	1.85E-05	2.13E-05	1.86E-05	2.12E-05
0.0048	1.87E-05	2.14E-05	1.88E-05	2.13E-05	1.88E-05	2.11E-05
0.0040	1.90E-05	2.10E-05	1.90E-05	2.09E-05	1.91E-05	2.08E-05
0.0030	1.95E-05	1.96E-05	1.95E-05	1.97E-05	1.94E-05	1.97E-05
0.0018	2.02E-05	1.77E-05	2.01E-05	1.81E-05	2.00E-05	1.84E-05
0.0009	2.04E-05	1.67E-05	2.03E-05	1.72E-05	2.03E-05	1.76E-05
0.0000	2.04E-05	1.63E-05	2.04E-05	1.69E-05	2.04E-05	1.74E-05



สถาบันวิทยบริการ
จุฬาลงกรณ์มหาวิทยาลัย

B.3 Reynolds number

Table B7 Reynolds number from 270 to 279 in z-direction (m/s)

z-direction	270		273		276		279	
r-direction	with ori	wo ori	with ori	wo ori	with ori	wo ori	with ori	wo ori
0.0135	0	0	0	0	0	0	0	0
0.0119	0	2127	292	2086	754	2056	1357	2038
0.0108	0	2829	566	2785	1077	2750	1650	2725
0.0100	0	3139	744	3098	1233	3065	1728	3041
0.0092	0	3362	933	3323	1361	3295	1749	3275
0.0081	0	3555	1234	3521	1506	3504	1687	3493
0.0069	0	3579	1557	3555	1593	3553	1449	3555
0.0061	0	3486	1779	3476	1522	3489	1400	3503
0.0048	0	3136	1937	3165	4119	3209	7261	3248
0.0040	0	2690	13004	2784	15827	2882	17857	2964
0.0030	36288	1609	38432	2085	36778	2379	34723	2579
0.0018	25234	2133	36187	2475	37928	2672	38088	2786
0.0009	16945	3745	31354	3503	34537	3339	35412	3220
0.0000	13914	4365	29494	4024	33210	3687	34365	3432

Table B8 Reynolds number from 282 to 291 in z-direction (m/s)

z-direction	282		285		288		291	
r-direction	with ori	wo ori	with ori	wo ori	with ori	wo ori	with ori	wo ori
0.0135	0	0	0	0	0	0	0	0
0.0119	2061	2029	2767	2025	3390	2024	3887	2024
0.0108	2208	2709	2679	2698	3032	2691	3269	2687
0.0100	2150	3024	2441	3011	2595	3001	2636	2994
0.0092	2007	3260	2082	3248	1993	3239	1792	3231
0.0081	1633	3486	1328	3479	926	3473	727	3468
0.0069	1181	3558	1498	3560	2365	3561	3310	3561
0.0061	2362	3513	3873	3522	5310	3528	6513	3535
0.0048	9817	3280	11686	3309	13006	3336	13880	3363
0.0040	19076	3033	19796	3093	20184	3147	20315	3195
0.0030	33033	2724	31598	2834	30355	2921	29243	2992
0.0018	37989	2856	37735	2905	37281	2944	36592	2980
0.0009	35873	3139	36195	3088	36412	3060	36508	3051
0.0000	35019	3268	35495	3169	35854	3112	36104	3083

Table B9 Reynolds number from 294 to 300 in z-direction (m/s)

z-direction	294		297		300	
	with ori	wo ori	with ori	wo ori	with ori	wo ori
0.0135	0	0	0	0	0	0
0.0119	4244	2024	4457	2024	4528	2023
0.0108	3401	2684	3436	2681	3376	2680
0.0100	2595	2989	2489	2985	2329	2981
0.0092	1533	3224	1250	3219	971	3214
0.0081	872	3463	1273	3458	1698	3454
0.0069	4150	3561	4830	3562	5309	3563
0.0061	7449	3542	8094	3549	8487	3556
0.0048	14407	3388	14648	3414	14653	3438
0.0040	20236	3240	19972	3281	19544	3319
0.0030	28193	3054	27154	3109	26089	3159
0.0018	35674	3015	34559	3051	33286	3087
0.0009	36452	3054	36190	3067	35666	3087
0.0000	36236	3074	36226	3078	36020	3092



สถาบันวิทยบริการ
จุฬาลงกรณ์มหาวิทยาลัย

APPENDIX C

International conference

Title	Controlled synthesizes of ZnO nanoparticles in gas-phase reaction
Conference	The 5 th Asian Aerosol Conference
Session	Oral presentation
Place	Tuntex sky tower, Kaohsiung, Taiwan
Date	28 August 2007



สถาบันวิทยบริการ
จุฬาลงกรณ์มหาวิทยาลัย



*The 5th
Asian
Aerosol
Conference*

ABSTRACT BOOK
Volume I

**ORAL
PRESENTATION**



CONTROLLED SYNTHESSES OF ZnO NANOPARTICLES IN GAS-PHASE REACTION

P. Nartpochananon^{a*}, T. Fujimoto^b, T. Charinpanitkul^a, Y. Otani^b

^a Center of Excellence in Particle Technology, Department of Chemical Engineering,
Faculty of Engineering, Chulalongkorn University, Thailand

^b Particle Processing Lab, Department of Chemical Engineering,
Graduate School of Natural Science and Technology, Kanazawa University, Japan

*Corresponding author. Tel.: +81-80-6360-7763 Fax: +81-76-264-6239

Email: p_nartpochananon@yahoo.co.th

ABSTRACT

Gas-phase reaction is applied to synthesize ZnO nanoparticles by using two heating zone tube furnace equipped with an orifice for enhancing the mixing between zinc vapor and air. SEM analyses show that two types of ZnO nanoparticles form as a result of oxidation of zinc vapor. The crystalline structure and the particle size distribution have been investigated by XRD and ELPI, respectively. The effects of mixing on the growth mechanism are also discussed.

Keyword: ZnO nanoparticles, oxidation, mixing, orifice

INTRODUCTION

Research and development on the synthesis of nanoparticles have attracted a great attention because of the promising characteristics of nanoparticles which cannot be found in bulk materials. ZnO nanoparticles have been of great interest because they have a wide band gap of 3.37 eV and a high exciton binding energy of 60 MeV. These properties of ZnO lead to several advantages in the fabricating various electronic and photonic devices. Various methods including metal vapor deposition (MVD) [1], non-catalytic growth by thermal evaporation [2] and oxidation reaction between zinc vapor and oxygen in gas-phase [3] have been developed for ZnO nanoparticle syntheses. Gas-phase reaction is commonly employed since synthesized particles contain less impurities [3].

In the present work, two tube furnace reactors equipped with an orifice are employed for enhancing the mixing between zinc vapor and oxygen. The effects of synthesizing parameters on characteristics of synthesized ZnO nanoparticles has been mixing on the characteristics of synthesized ZnO nanoparticles were investigated using SEM, ELPI, TEM and XRD analyses.

EXPERIMENTAL

ZnO nanoparticles are synthesized in two tube furnace reactors. 2 g of Zn powder (Sigma Aldrich) are loaded into an alumina boat placed at the center of the heating zone in the first heating zone in the furnace. An orifice is placed about 10 cm downstream of the alumina boat in order to enhance the mixing between Zn vapor and air. Zn vapor reacts with oxygen to form ZnO particles in the second heating zone. Silicon wafer quenched with cold water is used as a deposition substrate in order to enhance the deposition flux by thermophoresis as well as avoiding the growth of collected particles on the substrate. The Si wafer is placed 1 to 40 cm downstream

of the orifice. Prior to the heating, the quartz tube is purged with nitrogen for 10 min. The temperature of the first heating zone is set to 550°C what that of the second heating zone is varied between 300-700°C. The volumetric flow rates of nitrogen and air are set at 0.2 to 2 L/min.

RESULTS AND DISCUSSIONS

Typical SEM micrographs of ZnO nanoparticles which are synthesized at the second heating zone temperature of 600 °C and collected on the Si substrate placed at 1 and 20 cm downstream of the orifice are shown in Fig 1(a) and (b). The ZnO nanoparticles collected 1 cm downstream of the orifice have a spherical shape while those collected at 20 cm downstream exhibits tetra-pod morphology. These results suggest that amorphous ZnO particles are first formed via nucleation and then grow into crystalline ZnO particles.

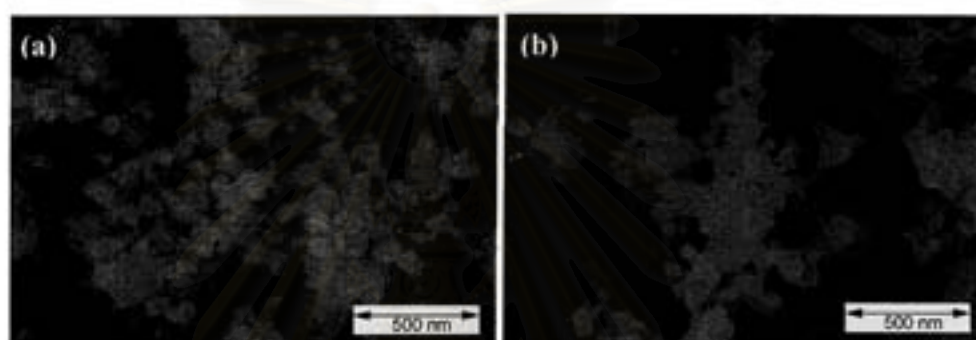


Fig.1 SEM images of synthesized ZnO nanoparticles deposited on Si substrate at (a) 1cm and (b) 20 cm downstream of the mixing orifice

CONCLUSION

ZnO nanoparticles were synthesized by a gas-phase oxidation of Zn vapor and successfully sampled on Si wafer substrates by using thermophoresis. Two types of ZnO nanoparticles were found on Si substrates at different positions in the furnace.

ACKNOWLEDGEMENT

The authors thanks for the financial support of National Nanotechnology Center, NSTDA, Thailand. P.N. also acknowledges support from JASSO for his one-year fellowship at Kanazawa University.

REFERENCES

- [1] G. Shen, Y. Bando, D. Chen, B. Liu, C. Zhi, and D. Golberg, *Journal of Physical Chemistry B*, vol. 110, pp. 3973-3978, 2006
- [2] A. Umar, E.-K. Suh, and Y.B. Hahn, *Solid State Communications*, vol. 139, pp. 447-451, 2006
- [3] R. Wu, and C. Xie, *Materials Research Bulletin*, vol. 39, pp. 637-645, 2004.

VITA

Mr. Pat Nartpochananon was born in Bangkok, Thailand, on May 29, 1983. He studied in primary and secondary educations at Demonstrative School of Ramkamheang University. In 2005, he graduated Bachelor Degree of Engineering (Chemical Engineering) from Chulalongkorn University. After that, he continued to study in Master degree in Center of Excellence in Particle Technology at Chemical Engineering Department, Faculty of Engineering, Chulalongkorn University with the master thesis entitled “Controlled synthesises of ZnO nanoparticles using gas phase reaction”.



สถาบันวิทยบริการ
จุฬาลงกรณ์มหาวิทยาลัย